University of California
Los Angeles

Order and disorder in superconducting systems

A dissertation submitted in partial satisfaction
of the requirements for the degree
Doctor of Philosophy in Physics

by

Antonio Enrico Russo

2016

Abstract of the Dissertation

Order and disorder in superconducting systems

by

Antonio Enrico Russo

Doctor of Philosophy in Physics

University of California, Los Angeles, 2016

Professor Sudip Chakravarty, Chair

An analysis of three kinds of physical systems exhibiting superconducting properties is presented: the pseudogap regime of the cuprates, chiral p-wave superconductors, and chiral d-wave superconductors, following a brief overview of superconductivity. The effect of disorder on a $\mathbb{Z}_2$ symmetry breaking order parameter is examined in the aforementioned psuedogap regime. Majorana modes in p-wave superconductors are examined. Finally, currents in both p and d-superconductors are calculated numerically.

In the pseudogap regime of the cuprates, commensurate charge order breaks a $\mathbb{Z}_2$ symmetry, reflecting a broken translational symmetry. Therefore, the interaction of charge order and quenched disorder due to potential scattering, can, in principle, be treated as a random field Ising model. A numerical analysis of the ground state of such a random field Ising model reveals local, glassy dynamics in both $2D$ and $3D$. The dynamics are treated in the glassy limit as a heat bath which couple to the itinerant electrons, leading to an unusual electronic non-Fermi liquid. If the dynamics are strong enough, the electron spectral function has no quasiparticle peak and the effective mass diverges at the Fermi surface, precluding quantum oscillations. In contrast to charge density, d-density wave order (reflecting staggered circulating currents) does not directly couple to potential disorder, allowing it to support quantum oscillations. At fourth order in Landau theory,

there is a term consisting of the square of the d-density wave order parameter, and the square of the charge order. This coupling could induce parasitic charge order, which may be weak enough for the Fermi liquid behavior to remain uncorrupted. This distinction must be made clear, as one interprets quantum oscillations in cuprates.

A chiral $p_x + ip_y$ superconductor on a square lattice with nearest and next-nearest hopping and pairing terms is considered. Gap closures, as various parameters of the system are varied, are found analytically and used to identify the topological phases. The phases are characterized by Chern numbers (ranging from -3 to 3), and (numerically) by response to introduction of weak disorder, edges, and magnetic fields in an extreme type-II limit, focusing on the low-energy modes (which presumably become zero-energy Majorana modes for large lattices and separations). Several phases are found, including a phase with Chern number 3 that cannot be thought of in terms of a single range of interaction, and phase with Chern number 2 that may host an additional, disorder resistant, Majorana mode. The energies of the vortex quasiparticle modes were found to oscillate as vortex position varied. The spatial length scale of these oscillations was found for various points in the Chern number 3 phase which increased as criticality was approached.

Finally, currents in chiral $p_x + ip_y$ and $d_{x^2-y^2} + id_{xy}$ superconductors are examined in a cylindrical configuration, self-consistently. Edge currents, while localized at the boundary as expected, are highly parameter dependent but generically non-vanishing. Preliminary results are presented, and the techniques employed are explained. In particular, the calculation of the correlators and currents in both the p and d wave cases, and the numerical techniques used to find the self-consistent Hamiltonian are overviewed.

The dissertation of Antonio Enrico Russo is approved.

Rahul Roy

Terence Chi-Shen Tao

Sudip Chakravarty, Committee Chair

University of California, Los Angeles

2016

To my family and my friends.

Table of Contents

List of Figures

Vita

2003–2008 B.S. (Mathematics) and B.S. (Physics), Carnegie Mellon University, Pittsburgh, Pennsylvania.

2008–2011 M.S. (Physics), University of California at Los Angeles, California.

Publications

Phases in two dimensional $p_x + ip_y$ superconducting systems with next-nearest-neighbor interactions Antonio Russo and Sudip Chakravarty. Phys. Rev. B. 88, pp. 184513—Published 25 November 2013

Random field disorder and charge order driven quantum oscillations in cuprates Antonio Russo and Sudip Chakravarty. Phys. Rev. B. 93, pp. 094504—Published 3 March 2016

Edge currents in 2D p_x+ip_y and $d_{x^2-y^2}+id_{xy}$ chiral superconductors on the lattice Antonio Russo and Sudip Chakravarty *(work in progress)*

CHAPTER 1

Introduction

The unifying theme in the development of physics has been the distillation of complex phenomena into the simple, essential underlying themes. When Newton simultaneously introduced calculus and universal gravitation, a wide diversity of experimental phenomena suddenly became simple consequences of these underlying principles. Similarly, the development of Bloch waves and electronic band theory led to a systematic treatment of crystalline atomic solids. One might say that physics is the study of beauty in nature.

This dissertation will examine order of select systems, and especially the response to disorder. The focus will be on angular momentum $\ell = 1$ and $\ell = 2$ superconducting order, as well as the response of d-density-wave pairing to disorder, for example in the pseudo-gap regime of the cuprates. The discussion begins with a general description of order, and then proceeds to the specifics of the cases considered. Details are left to the appendix, for completeness.

1.1 A Microscopic Picture of Superconductivity

A microscopic explanation of conventional superconductivity was famously discovered in 1957 by Bardeen, Cooper and Schrieffer [BCS57]. Very briefly, the motion of an electron through a periodic lattice excites an oscillation of that lattice. An electron with equal and opposite momentum interacts coherently with this oscillation. It becomes energetically favorable, therefore, for electrons to cre-

ate "Cooper pairs" of oppositely moving electrons, which have lower energy than independently moving ones. At low enough temperature, the Fermi surface is destroyed by this so-called "Cooper instability."

This chapter will gives a brief development of the mean-field approach to handling condensates, especially the particle-particle condensates of a superconducting order parameter. Not only relevant to the s-wave superconductivity, and higher angular momentum superconductivity of direct interest in this dissertation, the techniques presented here generalize well to other materials described by order parameters other than the superconducting gap (such as charge density). The end result will be a quadratic Hamiltonian which can be diagonalized [Bog58, Val58]. This technique is reviewed in Appendix A, which also includes a few significant numerical simplifications, which I have been unable to find referenced in the literature.

Although the bulk of the work will be performed on a lattice, the specific lattice symmetry introduces a number of complication that can interfere with an otherwise simple explanation. For this reason, we will try to avoid any such details in this section. Begin with a uniform system, with only a single band. Consider the noninteracting Hamiltonian, already Fourier transformed:

$$H_0 = \sum_{\mathbf{k},s} \xi_{\mathbf{k}} a^\dagger_{\mathbf{k},s} a_{\mathbf{k},s} \tag{1.1}$$

The fermionic operators $a_{\mathbf{k}}$ are normalized to satisfy

$$\{a_{k,s}, a_{k',s'}\} = 0 \quad \text{and} \quad \left\{a^\dagger_{k,ss}, a_{k',s'}\right\} = \delta_{kk'}\delta_{s,s'} \tag{1.2}$$

(details are in Appendix A). Consider an interaction

$$H_{\mathrm{I}} = \frac{1}{2} \sum_{\mathbf{k}',\mathbf{k},s'_2,s'_1,s_2,s_1} V_{\mathbf{k}',\mathbf{k},s'_1,s'_2,s_1,s_2} a^\dagger_{\mathbf{k}',s'_1} a^\dagger_{-\mathbf{k}',s'_2} a_{-\mathbf{k},s_2} a_{\mathbf{k},s_1} \tag{1.3}$$

Finding the true solutions to fully interacting Hamiltonian $H_0 + H_{\mathrm{I}}$ is a very delicate and challenging problem. Instead, certain properties of the system, typically

expressed as a correlator, e.g. the density

$$n_s(\mathbf{k}) = \left\langle c^\dagger_{\mathbf{k},s} c_{\mathbf{k},\mathbf{s}} \right\rangle_{\psi_G} \tag{1.4}$$

at the ground state $|\psi_G\rangle$, are assumed to be very nearly constant. In this approximation, the system is bathed in this "mean field." The Hamiltonian is then expressed in terms of this mean field, and fluctuations about the mean-field are neglected. More generally, the mean field created by

$$n_{ss'}(\mathbf{k}) = \left\langle c^\dagger_{\mathbf{k}+Q,s} c_{\mathbf{k},s'} \right\rangle_{\psi_G} \tag{1.5}$$

produces a particle-hole condensation, or a density-wave [Nay00]. Depending on how $n(\mathbf{k})$ depends on $\mathbf{k}$, the condensate will have an associated angular momentum.

If $s = s'$, and $n(\mathbf{k})$ is independent of $\mathbf{k}$, the state has no angular momentum (s-wave) and is called a charge density wave (CDW). If the vector Q is a rational multiple of 2π, the order is commensurate with the underlying lattice, if irrational it is incommensurate with the lattice. In Chapter 2, some important features of these two kinds of order parameters are discussed.

The BCS ground state is found by expanding around a mean field, of not the density mentioned above, but rather

$$b_{\mathbf{k},s_1,s_2} = \langle a_{-\mathbf{k},s_2} a_{\mathbf{k},s_1} \rangle_{\psi_G} \tag{1.6}$$

which corresponds to a particle-particle (or hole-hole) condensation. Explicitly, the fluctuations are neglected by assuming that the quantity

$$\delta b_{\mathbf{k},s_1,s_2} = a_{-\mathbf{k},s_2} a_{\mathbf{k},s_1} - b_{\mathbf{k},s_1,s_2} \tag{1.7}$$

is small, i.e., assume that $|\delta b_{\mathbf{k},s_1,s_2}|^2 \ll 1$, and substitute into Eqn. 1.3 to get

$$H_{\mathrm{I}} = \frac{1}{2} \sum V_{\mathbf{k}',\mathbf{k},s'_1,s'_2,s_1,s_2} \Big[-\bar{b}_{\mathbf{k}',s'_1,s'_2} b_{\mathbf{k},s_1,s_2} + \delta b^\dagger_{\mathbf{k}',s'_1,s'_2} \delta b_{\mathbf{k},s_2,s_1} + b_{\mathbf{k},s_1,s_2} a^\dagger_{\mathbf{k}',s'_1} a^\dagger_{-\mathbf{k}',s'_2} + \bar{b}_{\mathbf{k}',s'_1,s'_2} a_{-\mathbf{k},s_2} a_{\mathbf{k},s_1} \Big] \tag{1.8}$$

The first term is a constant, the second term is neglected, and the last two terms are simplified by defining the superconducting order parameter

$$\Delta_{\mathbf{k}',s_1',s_2'} = \sum_{\mathbf{k},s_2,s_1} V_{\mathbf{k}',\mathbf{k},s_1',s_2',s_1,s_2} \left\langle a_{-\mathbf{k},s_2} a_{\mathbf{k},s_1} \right\rangle_{\psi_G} \tag{1.9}$$

and, therefore

$$H_{\mathrm{I}} \doteq K_{\mathrm{int}} + \frac{1}{2} \sum_{\mathbf{k},s_1,s_2} \left[\Delta_{\mathbf{k},s_2,s_1} a^\dagger_{\mathbf{k},s_1} a^\dagger_{-\mathbf{k},s_2} + \bar{\Delta}_{\mathbf{k},s_1,s_2} a_{-\mathbf{k},s_2} a_{\mathbf{k},s_1} \right] \tag{1.10}$$

where

$$K_{\mathrm{int}} = -\frac{1}{2} \sum V_{\mathbf{k}',\mathbf{k},s_1',s_2',s_1,s_2} \left\langle a_{\mathbf{k}',s_1'} a_{-\mathbf{k}',s_2'} \right\rangle \left\langle a_{-\mathbf{k},s_2} a_{\mathbf{k},s_1} \right\rangle \tag{1.11}$$

The full hamiltonian $H_0 + H_{\mathrm{I}}$ can be expressed compactly in terms of Nambu spinors: collect constants, and use the commutation relations:

$$H_0 + H_{\mathrm{I}} = K + \frac{1}{2} \sum_{\mathbf{k}} \begin{bmatrix} (\hat{a}^\dagger_{\mathbf{k}})^\top & (\hat{a}_{-\mathbf{k}})^\top \end{bmatrix} \hat{\mathcal{H}}_{\mathbf{k}} \begin{bmatrix} \hat{a}_{\mathbf{k}} \\ \hat{a}^\dagger_{-\mathbf{k}} \end{bmatrix} \tag{1.12}$$

where

$$\hat{\mathcal{H}}_{\mathbf{k}} = \begin{bmatrix} \xi_{\mathbf{k}} I_{2\times 2} & \hat{\Delta}_{\mathbf{k}} \\ \bar{\hat{\Delta}}^\top_{\mathbf{k}} & -\xi_{\mathbf{k}} I_{2\times 2} \end{bmatrix} \tag{1.13}$$

$I_{2\times 2}$ is the two-dimensional identity matrix,

$$\hat{a}_{\mathbf{k}} = \begin{bmatrix} a_{\mathbf{k},+} \\ a_{\mathbf{k},-} \end{bmatrix} \tag{1.14}$$

where the $\top$ operator is taken to only act on the matrix portion of the $a_{\mathbf{k}}$ operator, i.e.,

$$(\hat{a}_{\mathbf{k}})^\top = \begin{bmatrix} a_{\mathbf{k},+} & a_{\mathbf{k},-} \end{bmatrix} \tag{1.15}$$

and

$$\hat{\Delta}_{\mathbf{k}} = \begin{bmatrix} \Delta_{\mathbf{k},+,+} & \Delta_{\mathbf{k},+,-} \\ \Delta_{\mathbf{k},-,+} & \Delta_{\mathbf{k},-,-} \end{bmatrix} \tag{1.16}$$

Provided that the self-consistency condition Eqn. 1.9 is satisfied, and the fluctuations of Eqn. 1.7 are indeed small, the solutions to this quadratic Hamiltonian

should be a good approximation of an eigenstate of the true Hamiltonian. As is the typical trend in mean-field theories, the higher the dimension, the better the approximation. The fluctuations in three dimensional superconductors is small enough that the BCS theory works, but, in one and two dimensions, fluctuations can destroy superconductivity [GK77, Tin96]. In realistic layered quasi two-dimensional systems, interlayer interactions are sufficient to stabilize superconductivity.

1.2 Symmetries of the Order Parameter

A great deal of the modern "art" of modern theoretical superconductor physics is in the careful choice of a mean-field to expand around. The coarsest classification of order parameters is on their transformation properties. Because Δ enters as a coefficient of an operator that creates a *pair* of fermions, it therefore transforms as such: under spatial inversion, Eqn. 1.9 leads to

$$\hat{\Delta}_{-\mathbf{k}} = -\begin{bmatrix} \Delta_{\mathbf{k},+,+} & \Delta_{\mathbf{k},-,+} \\ \Delta_{\mathbf{k},+,-} & \Delta_{\mathbf{k},-,-} \end{bmatrix} \tag{1.17}$$

This relationship is opaque, but can be made more clear by first separating Δ into the triplet and singlet spin states:

$$\hat{\Delta}_{\mathbf{k}} = \Delta_{\mathbf{k},+,+} \overbrace{\begin{bmatrix} 1 & 0 \\ 0 & 0 \end{bmatrix}}^{\hat{\chi}^{(1)}_{1}} + \Delta_{\mathbf{k},-,-} \overbrace{\begin{bmatrix} 0 & 0 \\ 0 & 1 \end{bmatrix}}^{\hat{\chi}^{(1)}_{-1}} + \frac{1}{2}\left(\Delta_{\mathbf{k},+,-} + \Delta_{\mathbf{k},-,+}\right) \overbrace{\begin{bmatrix} 0 & 1 \\ 1 & 0 \end{bmatrix}}^{\hat{\chi}^{(1)}_{0}} + \frac{i}{2}\left(\Delta_{\mathbf{k},+,-} - \Delta_{\mathbf{k},-,+}\right) \overbrace{\begin{bmatrix} 0 & -i \\ i & 0 \end{bmatrix}}^{\hat{\chi}^{(0)}} \tag{1.18}$$

The $\chi^{(l)}_m$ matrix captures the spin-sector pairing, giving the spin angular momentum. Triplet pairing comprises the first three states $\hat{\chi}^{(1)}_{\pm 1}$ and $\hat{\chi}^{(1)}_0$, which have a symmetric spin part and consequentially antisymmetric spatial part. The last

state is the singlet, with an antisymmetric spin, and symmetric spatial wavefunction. Generally, Δ may have contributions from all such pairings, and moreover this combination could depend on the momentum $\mathbf{k}$. Indeed, for Helium-3, a very rich topology emerges [Leg75] when all forms of pairing play a role, and are allowed to vary with momentum. For the cases considered here—superconductivity and density order—the focus will be on pairing of the form

$$\hat{\Delta}_{\mathbf{k}} = \Delta_{\mathbf{k}}\hat{\chi} = |\Delta_{\mathbf{k}}|e^{i\phi_{\mathbf{k}}}\hat{\chi} \tag{1.19}$$

where χ describes the spin channel pairing, and is independent of $\mathbf{k}$ and moreover is entirely spin-singlet or spin-triplet. Furthermore, the spatial part of the wavefunction can be decomposed into angular momentum eigenstates, i.e., $\phi_{\mathbf{k}}$ goes from 0 to $2\pi\ell_{\text{orbital}}$ as $\mathbf{k}$ goes around the origin, where ℓ_{s} is an integer, and describes the orbital angular momentum of the Cooper pair. Notice that the orbital and spin angular momentum have to add to an even integer to maintain the correct exchange symmetry. Therefore, e.g., s-wave ($\ell_{\text{orbital}} = 0$) and d-wave ($\ell_{\text{orbital}} = 2$) pairing is only possible for spin-singlet states. Similarly, p-wave ($\ell_{\text{orbital}} = 1$) orbital pairing is only possible for spin-triplet pairing.

The solutions of Eqn. 1.12 can be expressed in terms of the eigenvectors of χ. The details are worked out in Appendix A.1, but roughly: working with either of these eigenvectors, the spectrum can be stated in terms of eigenvectors of

$$\mathcal{H}_{\mathbf{k},m} = \begin{bmatrix} \xi_{\mathbf{k}} & \Delta_{\mathbf{k}}\chi_m \\ \bar{\Delta}_{\mathbf{k}}\chi_m & -\xi_{\mathbf{k}} \end{bmatrix} \tag{1.20}$$

where χ_m is an eigenvalue of $\hat{\chi}$. Generically, $\mathcal{H}_{\mathbf{k},m}$ has positive eigenvalue $\epsilon_{\mathbf{k},m} = \sqrt{\xi_{\mathbf{k}}^2 + \chi_m^2|\Delta_{\mathbf{k}}|^2}$ and eigenvector

$$\begin{bmatrix} u_{\mathbf{k},m} \\ v_{\mathbf{k},m} \end{bmatrix} = \begin{bmatrix} \chi_m \frac{e^{i\phi_{\mathbf{k}}/2}}{\sqrt{2}}\sqrt{1 - \frac{\xi_{\mathbf{k}}}{\sqrt{\xi_{\mathbf{k}}^2+\chi_m^2|\Delta_{\mathbf{k}}|^2}}} \\ \frac{e^{-i\phi_{\mathbf{k}}/2}}{\sqrt{2}}\sqrt{1 + \frac{\xi_{\mathbf{k}}}{\sqrt{\xi_{\mathbf{k}}^2+\chi_m^2|\Delta_{\mathbf{k}}|^2}}} \end{bmatrix} \tag{1.21}$$

The operator

$$\Psi^\dagger_{\mathbf{k},m} = u_{\mathbf{k}}(\hat{a}_{\mathbf{k}})^\top\hat{\chi}_m + v_{\mathbf{k}}(\hat{a}^\dagger_{-\mathbf{k}})^\top\hat{\chi}_m \tag{1.22}$$

(where $\hat{\chi}_m$ is the *eigenvector* of $\hat{\chi}$ of eigenvalue χ_m) becomes the quasiparticle operator, and the Hamiltonian takes the form

$$H_0 + H_{\mathrm{I}} = C + \sum_{\mathbf{k},m} \epsilon_{\mathbf{k},m} \Psi^\dagger_{\mathbf{k},m} \Psi_{\mathbf{k},m} \tag{1.23}$$

The subscript m captures the z component of the spin angular momentum of the Cooper pairs. For the "spin-polarized" triplet cases, $\chi_m = 0, 1$, the $\chi_m = 0$ case contributes trivially—superconducting pairing occurs for only one of the spins—and can be ignored entirely. A linear combination of $\hat{\chi}^{(1)}_{\pm 1}$ corresponds to pairing of both spin-up and spin-down fermions; this can lead to interesting effects where currents may cancel, but spin currents will not. A more general combination of $\chi^{(1)}_m$ is out of the scope of this discussion (and is in general more difficult to address, since $\hat{\chi}$ may not be diagonalizable). For the most part, we'll assume we're in the spin-polarized case, and moreover mostly ignore the nonpairing fermions. This is equivalent to starting from the perspective of working with spinless fermions. For the singlet case, $\chi_m = \pm 1$ and each case contributes essentially the same. For much of what is done here, the m subscript can be safely ignored.

1.3 Topology of the Order Parameter

Further classification of order parameters can be made based on the topological features over the complete Brillouin zone [TKN82, HK10, AZ97]. For one of the m branches,

$$\mathcal{H}_{\mathbf{k}} = \begin{bmatrix} \xi_{\mathbf{k}} & |\Delta_{\mathbf{k}}| e^{i\phi_{\mathbf{k}}} \\ |\Delta_{\mathbf{k}}| e^{-i\phi_{\mathbf{k}}} & -\xi_{\mathbf{k}} \end{bmatrix} = \xi_{\mathbf{k}} \sigma_z + \sigma_x |\Delta_{\mathbf{k}}| \cos\phi_k - \sigma_y |\Delta_{\mathbf{k}}| \sin\phi_k = \mathbf{h}(\mathbf{k}) \cdot \sigma \tag{1.24}$$

where σ is the formal vector $\begin{bmatrix}\sigma_x & \sigma_y & \sigma_z\end{bmatrix}^\top$, and the Anderson pseudospin vector

$$\mathbf{h}(\mathbf{k}) = \begin{bmatrix} \operatorname{Re}\Delta_{\mathbf{k}} \\ -\operatorname{Im}\Delta_{\mathbf{k}} \\ \xi_k \end{bmatrix} \tag{1.25}$$

gives the very pretty expression for the excitation energies: $\epsilon_{\mathbf{k}} = |\mathbf{h}(\mathbf{k})|$. Provided that the gap does not collapse, i.e. $\epsilon_{\mathbf{k}} \neq 0$, the function $\hat{\mathbf{h}}(\mathbf{k}) = \mathbf{h}(\mathbf{k})/\epsilon(\mathbf{k})$ maps the Brillouin zone, the 2-torus, to the unit sphere [Ber84, Nak03]. Much as a curve has a winding number when mapped onto the unit circle, an analogous integer characterizes the number of times the torus is wrapped around the sphere:

$$n_{\text{Chern}} = \frac{1}{4\pi}\int d^2\mathbf{k}\left(\partial_{k_x}\hat{\mathbf{h}} \times \partial_{k_y}\hat{\mathbf{h}}\right)\cdot\hat{\mathbf{h}} \tag{1.26}$$

which is the integral of the Berry curvature,

$$\left[\frac{1}{2\pi}\nabla_k \times \langle G|\,\Psi_k i\nabla_k\Psi_k^\dagger\,|G\rangle\right]_z = \left[\frac{1}{4\pi}(\nabla_k\phi)\times(\nabla_k\mathbf{h})\right]_z = \frac{1}{4\pi}\hat{\mathbf{h}}\cdot\frac{\partial\hat{\mathbf{h}}}{\partial k_x}\times\frac{\partial\hat{\mathbf{h}}}{\partial k_y} \tag{1.27}$$

(notice that all other components of the first two expressions vanish) which is (almost, there are continuity issues) the curl of the Berry connection,

$$\langle G|\,\Psi_k i\nabla_k\Psi_k^\dagger\,|G\rangle = \frac{1}{2}\hat{\mathbf{h}}_z\nabla_k\phi_k \tag{1.28}$$

Recognizing the cross product as the surface normal, the integral is some (signed) area that the vector $\hat{\mathbf{h}}$ maps out. Provided the mapping is smooth, it must be some integer multiple of 4π, ensuring that the Chern invariant n_{Chern} is, in fact, an integer, the degree of the map $\hat{\mathbf{n}}$. According to the Hopf classification, the degree characterizes the mapping $\hat{\mathbf{n}}$ topologically, i.e. up to homotopy. We emphasize here that we have so far said nothing about the presence of zero-energy modes or sublattices: only the topologically invariant Chern number.

One can do slightly better. A first attempt might be to try to apply Stokes theorem and just calculate the loop integral. This can easily fail spectacularly

because the gradient term $\nabla_k \phi_k$ is definitely not smooth. Instead, a topological argument will make this calculation much easier.

Choose a particular region of the Brillouin zone bounded by a region where $\mathbf{h_k} = 0$ (which can be colorfully described as the Fermi surface of the parent system). Inside this region, $\hat{\mathbf{h}_z} \neq 0$. It is (at least visually) clear that a smooth deformation can make $\hat{\mathbf{h}} = \pm\hat{z}$ except when $\mathbf{h_k} = 0$ vanishes (or, more correctly, when k is within some small distance to the region where $\mathbf{h_k} = 0$). The Chern number must therefore depend only on the winding of the phase of the superconducting order parameter around the Fermi surface (of the parent state, i.e., where $\mathbf{h_k} = 0$). Because such a smooth deformation will not close the band gap, the topological invariant is unchanged. The integral over the Brillouin zone therefore becomes a line integral over the $\mathbf{h_k} = 0$ surface, which is sensitive only to the winding of the superconducting order parameter's phase ϕ.

The winding of ϕ can only occur around zeros of Δ, and always in multiples of 2π. Neglecting higher-order zeros of Δ, one simply counts the number of zeros enclosed by the Fermi surface, and note whether their winding is clockwise or counterclockwise to get the Chern number. To get the sign of the answer correct, "enclosed" is taken to mean the particle-like side of the Fermi surface. We emphasize now that we are dealing with a quadratic, *single-band* Hamiltonian. Analogous results for multi-band Hamiltonians would be more complicated.

1.4 Defects and Boundaries

As mentioned above, the topology of a system cannot change unless the gap closes. In the quasiclassical approximation that the physical system changes gradually from one topology to another—and therefore that the momentum space picture presented above is valid everywhere—the gap *must* close at some point, creating a topological edge state of zero energy. Of course, this quasiclassical limit is not

exact, and there are caveats. Nonetheless, zero energy modes are indeed required to exist at the edges of topological phases in a variety of situations. If some state $\epsilon_n = 0$,

$$H\Psi_n^\dagger |G\rangle = 0 \tag{1.29}$$

The basis can be chosen such that

$$\Psi_n^\dagger = \Psi_n \tag{1.30}$$

Such an operator creates a "Majorana" fermion, one which is its own antiparticle, since the operator is self-adjoint. The edges of physical systems, vortices within superconductors, and defects can all produce a region of a different phase than the surrounding topologically nontrivial system. Therefore, any such inhomogeneity might conceivably harbor a Majorana mode. On the other hand, not every defect will produce a Majorana mode—care must be taken to distinguish mere defect modes from truly zero energy Majorana modes. This subtle question is compounded by the fact that, in finite systems, the finite localization of Majorana fermions allows them to interact with each other—causing them to hybridize and acquire a finite energy. Separating one effect from another is a subtle task, and one that is addressed in the present work, in part, via numerical techniques.

CHAPTER 2

Charge Density Waves, Disorder, and Quantum Oscillations

Before delving deep into the superconducting state and investigating the topological properties of the superconducting order parameter, we'll examine the properties of a few particle-hole condensates often closely associated with superconductivity, especially in the cuprates. A comparison is made of commensurate and incommensurate charge density wave, and a d-density wave. From symmetry grounds, we find that the charge density wave can interfere with the formation of a Fermi surface. Coupled with the evidence of quantum oscillations in the underdoped cuprates, our result brings into question the conventional wisdom as to the role the charge density wave plays, e.g., in the pseudogap regime.

2.1 Introduction

Experiments have observed an incommensurate charge density wave order (ICDW) in the underdoped regime of the cuprates [WMK11, LKH12, GLM12, CBH12, Hof02, KTF07, ASM12, CBH12, TLT14, GLD15], inspiring an explanation for the underlying order in underdoped cuprates. However, one should note the distinction between the low-field regime and the high-field regime where quantum oscillations are observed. Here, we take a critical view of CDW as the underlying order in terms of its ability to support quantum oscillations, which are generally agreed to reflect a Fermi surface reconstruction [DPL07, LDL07, JVA08], and

therefore a Fermi liquid ground state, at least in the sense of continuity [Cha08]. To date, there is no general agreement as to the precise nature of this reconstruction.

Because strict ICDW does not have a sharply defined Fermi surface [ZMK15], there can be no quantum oscillations that are truly a periodic function of $1/B$ (where B is the magnetic field). The central result of the paper is a proof of principle argument that even commensurate charge density wave (CDW) order—chosen for simplicity to be of period-2—in the presence of disorder may not be able to explain a Fermi surface reconstruction and consequently quantum oscillations. In short, ubiquitous potential disorder necessarily couples to CDW order, leading to a non-Fermi liquid electron spectral function without quasiparticles. Unless disorder is weak and the CDW order very long ranged [GJN15], the principal order that leads to quantum oscillations could not be CDW.

Another possibility for quantum oscillations is the d-density wave (DDW) proposed previously [CK08]. This order, illustrated in Fig. 2.1 in its period-8 version, reflects staggered, circulating currents, making it impervious to direct potential scattering. To the extent that period-8 DDW can induce period-4 CDW, the DDW can be affected by potential disorder—but only at 4th order in Landau theory. Experimentally, the situation is unclear: some neutron scattering results [MDH02, MDH04] are consistent with DDW order, but nuclear magnetic resonance (NMR) measurements find no circulating currents [SGM11] (see, however, [HMV14] for a dissenting opinion). The period-8 DDW has one electron pocket and two smaller hole pockets in the reduced Brillouin zone, thus providing an explanation of the quantum oscillations of the Hall coefficients [EWC12].

The paper's approach is to first introduce the random field Ising model, and derive its behaviors when exposed to $\mathbb{Z}_2$ symmetry breaking disorder, in particular the dynamic susceptibility $\chi(\omega)$, in Section 2.2. Next, this dynamic susceptibility is used to calculate the imaginary part of the skeleton graph perturbative

Figure 2.1: Current pattern for period-8 DDW.

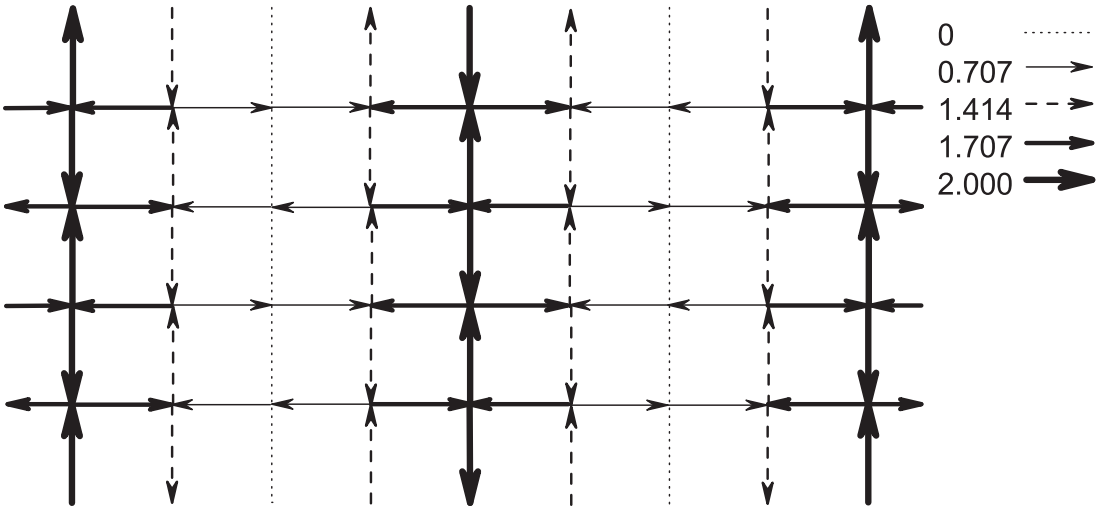

d-density wave with ordering wave vector $\mathbf{Q} = (\frac{3\pi}{4a}, \frac{\pi}{a})$, where a is the lattice constant (reproduced from [EWC12]; also see [DGJ08]). In Landau theory, it can couple to CDW with ordering vector $2\mathbf{Q}$. The relative magnitudes of the currents are depicted by the thickness of the arrows in the legend. Note the antiphase domain wall structure.

correction to the electronic self energy $\mathrm{Im}\,\Sigma(\omega)$ in Section 2.3. The results are related back to the more realistic case of an anisotropic system with a mean-field theory argument interpolating between two- and three-dimensional systems in Section 2.4. Concluding remarks are made in Section 2.5.

2.2 Random Field Ising Model

For simplicity, we focus on period-2 CDW, which breaks $\mathbb{Z}_2$ symmetry and necessarily couples to potential disorder. On symmetry grounds, the effective Hamiltonian is modeled by a random field Ising model (RFIM), [You98]

$$H_0 = -J \sum_{\langle ij \rangle} s_i^z s_j^z - \sum_i h_i^z s_i^z, \tag{2.1}$$

where J is the coupling between the Ising spins, and $\{h_i^z\}$ is a set of uncorrelated, uniformly distributed (rectangular distribution) random variables with zero mean and variance σ^2. The notation $\langle ij \rangle$ denotes nearest neighbors. It is not clear that doping immediately destroys commensurability, but if it does, by the Imry-Ma argument, ICDWs can only be more susceptible to disorder because of the continuous symmetry implied by the ICDW. If one wishes, the Ising variable can be thought of as $s_i^z = n_i - \frac{1}{2}$, where $n_i = 0, 1$ is the charge density at site i. Double occupancy is naturally forbidden in the underdoped, high-T_c cuprates because of large U. The model is controlled by a single dimensionless number, $\zeta = \frac{J}{\sigma}$, which we treat as a phenomenological parameter.

The disorder in a RFIM drives fluctuations on many length scales, and consequently many time scales, producing glassy dynamics and a frequency-dependent susceptibility [SC09] $\chi(\omega)$. This result is recapitulated, with improved precision here for the two-dimensional ($2D$) case and extended to the essential three-dimensional ($3D$) case. Analogous to the thermally driven fluctuation of an Ising system at finite temperature, the RFIM has disorder driven fluctuations at zero temperature. A distribution $p(L)$ (defined below more precisely) of domain walls of scale L arises from the domains in the ground state of the RFIM, playing a crucial role in our work, and is new.

The appearance of domain walls in RFIM is identified numerically by converting the RFIM to a network flow model, explained in Appendix B. Briefly, by careful choice of the parameters of the flow-network and the addition of two fictional source and sink nodes, each cut is made to correspond to a spin configuration such that the minimal cut corresponds to the RFIM ground state configuration. The probability that a domain wall of linear dimension L exists in the ground state, $P_{\rm dw}(L)$, is determined by averaging over many disorder realizations. To help understand the meaning of this quantity, notice that, in the $1D$ case, a domain wall is just a spin flip. In the disorder-free case, creating a single spin flip costs energy

Figure 2.2: Scaling of $P_{\rm dw}$ in the one-dimensional case.

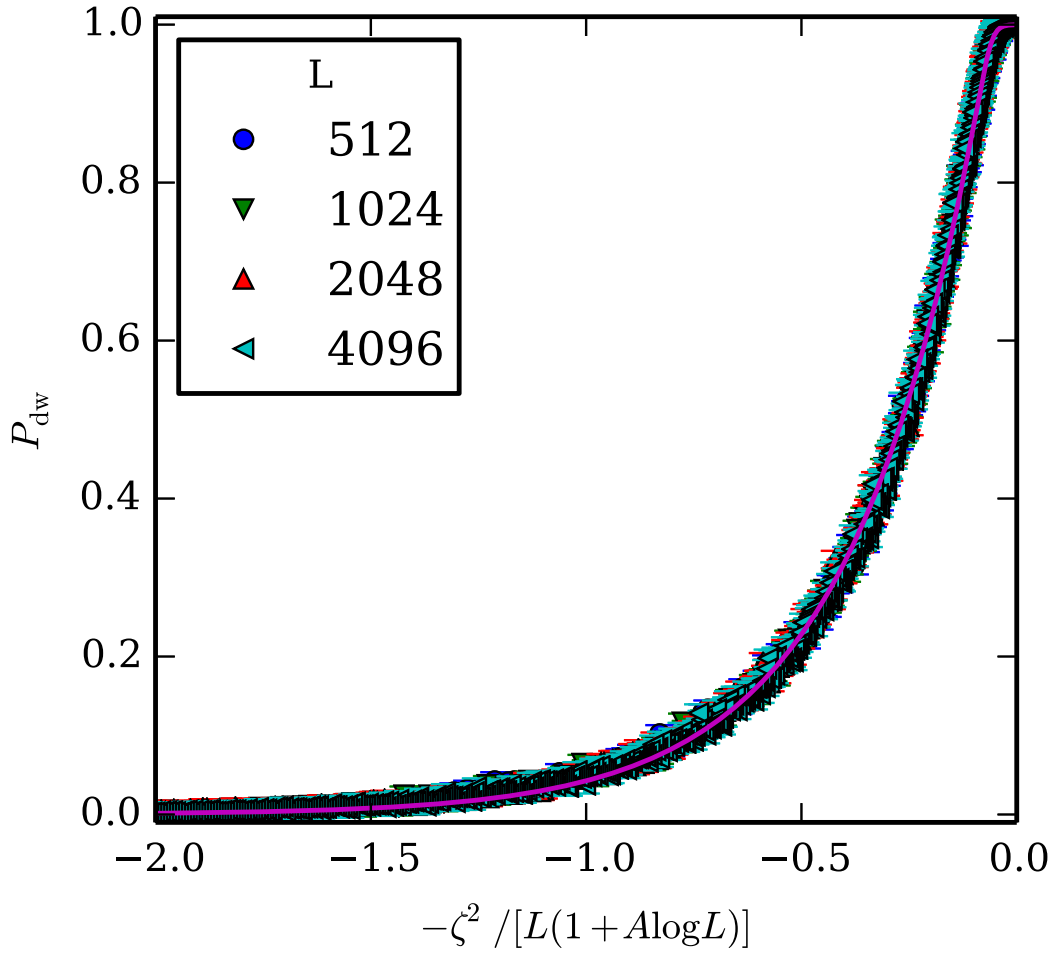

The collapse works as expected for $x = (J/\sigma)^2/L = \zeta^2/L$; the logarithmic correction factor $(1 + A \log L)$ is found to have little effect: $A = 0 \pm 0.3$. The best fit parameters to Eqn. 2.3 are $x_0 = 0.0596 \pm 0.0007$, $\lambda = -0.0103 \pm 0.0005$ and $\theta = 0.034 \pm 0.002$. All points correspond to averages performed over 2048 disorder realizations.

$\sim 2J$, an energy that, by Jordan-Wigner transformation, can be thought of as a fermion gap. The spin flip can move throughout the system at no energy cost. In the $1D$ case, the Imry-Ma argument shows that the ordered domains scale like $L \sim (J/\sigma)^2$, presented numerically in Fig. 2.2.

In higher dimensions, the analogy is less precise, but the presence of a domain wall results in the collapse of the gap in the Ising system. Most importantly, the size of the domains is controlled by locations of these domain walls. In particular, P_{dw} is the cumulative distribution function of the ordered domains or "clusters" of linear dimension L, and therefore

$$p(L) = \frac{dP_{\mathrm{dw}}}{dL}. \tag{2.2}$$

P_{dw} is found to lie on a universal curve [SC09] which is an asymmetric sigmoid,

$$P_{\mathrm{dw}} \approx f(x) = \frac{1}{\left(1 + \exp\left[\frac{x_0 - x}{\lambda}\right]\right)^{\theta}} \tag{2.3}$$

where $x = \log L - (\zeta/\zeta_0)^k$ and ζ_0 is numerically fit, and sets a scale for the strength of the disorder. In $2D$, k is set to 2 as in [SC09], in agreement with the analytical result [Bin83] for the special case $P_{\mathrm{dw}} = 1/2$. In $3D$, k is numerically fit. The sigmoid's best fit parameters x_0 and λ control its center and width, respectively, while θ controls the asymmetry. Physically, x_0 determines the onset of the occurrence of domain walls, and λ how quickly the regime is dominated by the existence of at least one domain wall. The numerical results are summarized in Fig. 2.2 and Fig. 2.3 and Table 2.1.

The distribution $p(L)$ is important because, in the limit of glassy RFIM dynamics in which we work, it controls the (necessarily local) susceptibility [Sac11, SC09]

$$\operatorname{Im} \chi(\omega) \sim \int dL\, p(L) \delta\left(\omega - \omega_0 e^{-cL^{\alpha}}\right) \tag{2.4}$$

This phenomenological argument for the susceptibility captures the essential glassy characteristics resulting from $p(L)$. In principle, the attempt frequency ω_0, the

D	x_0	λ	θ	ζ_0	k
2	1.41(4)	0.28(2)	0.31(2)	0.75(2)	2
3	0.2(1)	0.33(1)	0.137(6)	0.47(9)	5.6(1)

Table 2.1: Best fit parameters for P_{dw} in Fig. 2.2 and Fig. 2.3 and Eqn. 2.3.

fractal dimension α, and the length scale c are microscopic parameters, which are left undetermined. Notice that the fractal dimension $\alpha \leq D$, where D is the ambient spatial dimension. For $2D$ and $3D$, the integral simplifies in the small ω limit to

$$\operatorname{Im}\chi(\omega) \to \chi_0 \frac{\omega_0}{\omega} \Omega^{\psi}, \tag{2.5}$$

We have put $\Omega = 1/\left(\log \frac{\omega_0}{\omega}\right)$ for clarity and compactness; $\Omega(\omega)$ is strictly increasing for $0 < \omega < \omega_0$, and vanishes as $\omega \to 0$. The exponent

$$\psi = 1 + 1/(\lambda\alpha) > 1 \tag{2.6}$$

depends only on the fractal dimension of the domains α and on their distribution of sizes via the parameter λ. Moreover, in both $2D$ and $3D$, the numerical value of λ was found to lead to $\psi > 2$ (see Table 2.1).

2.3 The Electron Self Energy

We now focus on the interaction of the itinerant electrons with the emergent glassy CDW order, assumed to enter as a heat bath of fluctuations of the RFIM. The self energy Σ of the electrons is calculated to leading order in perturbation theory (see Fig. 2.5), assuming some coupling γ of the RFIM fluctuations to the electrons, from the form of χ in Eqn. 2.5 in a reduced graph expansion [ASW14]. It is unnecessary to use the matrix formalism corresponding to the charge order, because, as we shall see, there are no quasiparticles, and hence no possible Fermi

Figure 2.3: Scaling of P_{dw} in $2D$.

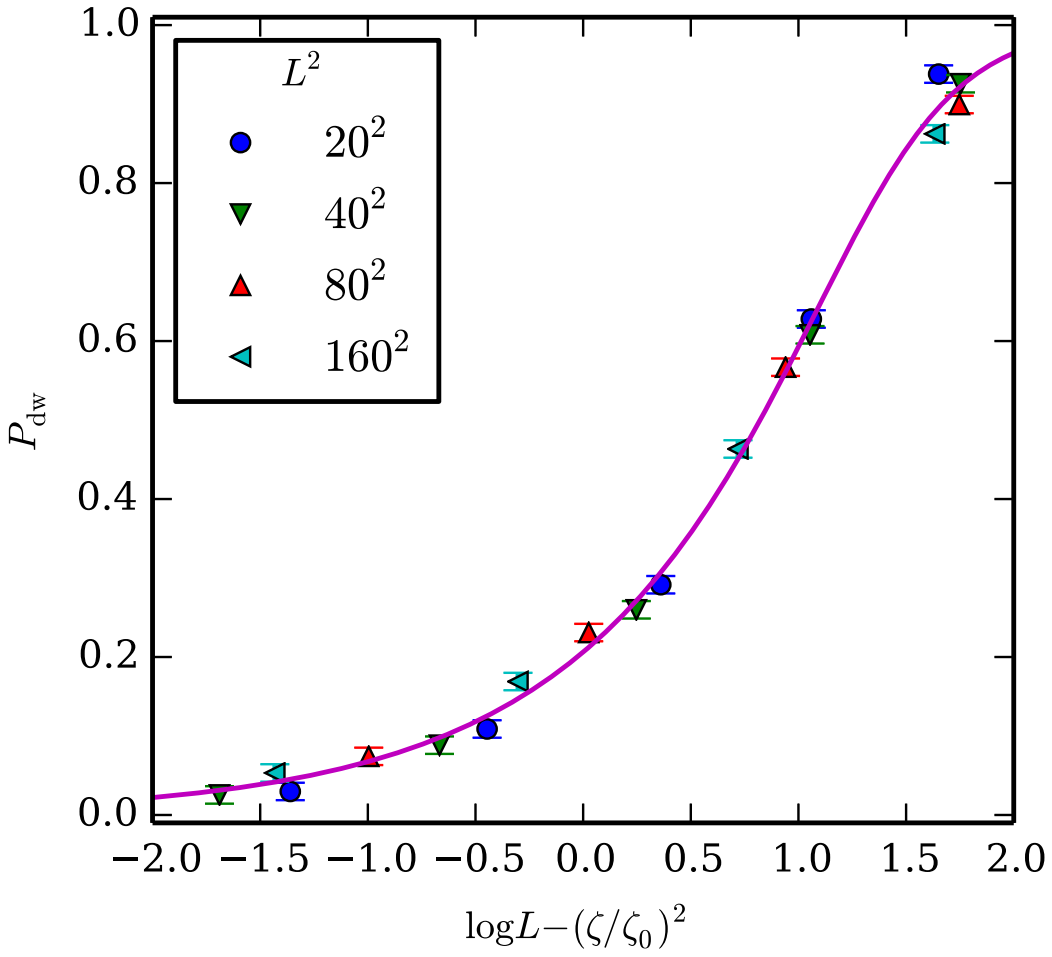

All points are averages over 2048 disorder realizations.

Figure 2.4: Scaling of P_{dw} in $3D$.

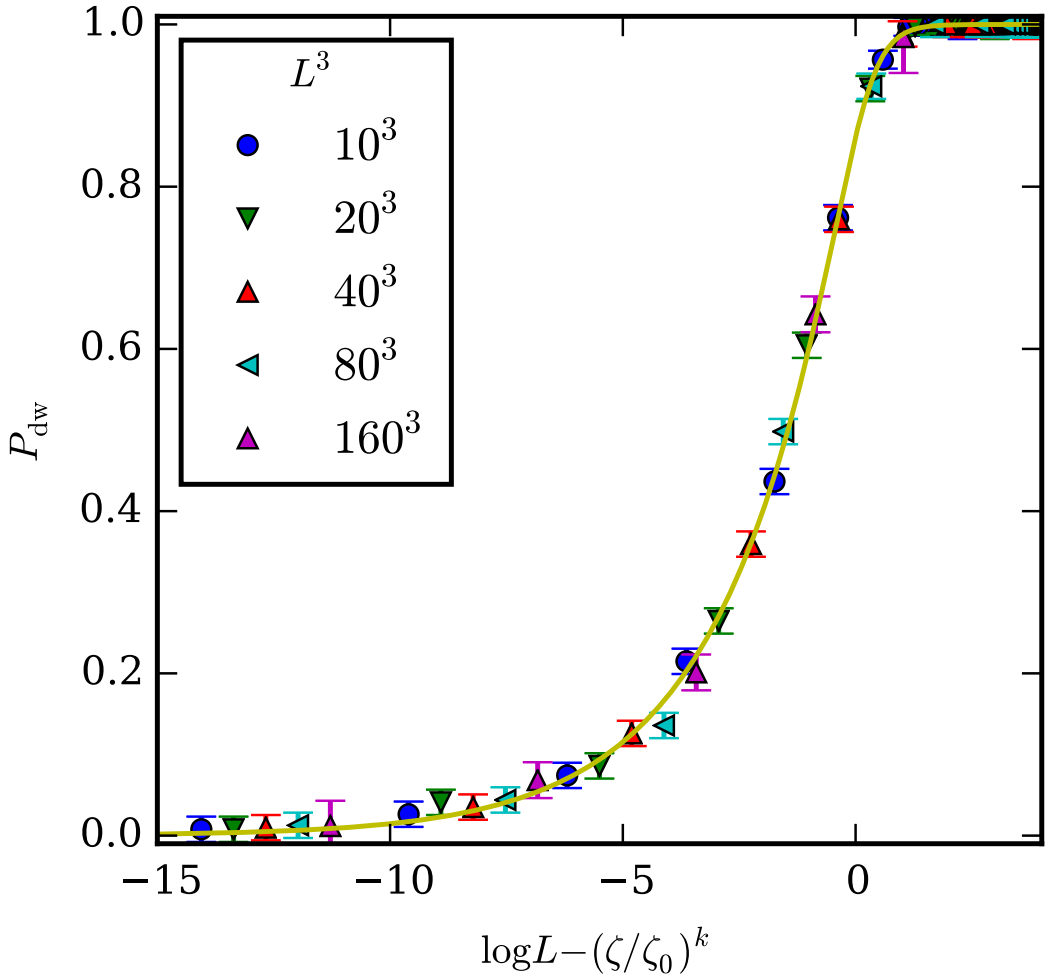

Points represent averages over many disorder realizations: for $L = 20$, with 2048 realizations, for $L = 40$ and $L = 80$, with 1024 realizations, and for $L = 160$, with 512 realizations.

surface reconstruction. In terms of the energy of quasiparticles ω,

$$\mathrm{Im}\,\Sigma(\omega) = -\gamma^2 \int \frac{d\omega'}{\pi} \sum_{\mathbf{q}} \mathrm{Im}\,G(\mathbf{k}-\mathbf{q}, \omega-\omega')\mathrm{Im}\,\chi(\mathbf{q},\omega') \times [b(\omega') + f(\omega-\omega')] \tag{2.7}$$

The Fermi and Bose functions $f(\omega)$ and $b(\omega)$ restrict the ω' integration to $[0,\omega]$ in the zero-temperature limit we are considering, making the integral vanish for $\omega < 0$. Because the susceptibility is local, the self energy is also local, and the sum over $\mathbf{q}$ reduces to the density of states at the Fermi surface, ν:

$$\mathrm{Im}\,\Sigma(\omega) = -\gamma^2\nu \int_0^{\omega} \mathrm{Im}\,\chi(\omega')\,d\omega' = -\frac{\Sigma_0}{\psi-1}\Omega^{\psi-1}$$

where $\Sigma_0 = \gamma^2\nu\chi_0\omega_0$, and $\omega > 0$. From the Kramers-Kronig relations:

$$\begin{aligned}\mathrm{Re}\,\Sigma(\omega) &= \frac{2}{\pi}P\int_0^{\infty} \frac{\omega'\mathrm{Im}\Sigma(\omega')}{\omega'^2-\omega^2}\,d\omega' \\ &= -\frac{2\Sigma_0}{\pi(\psi-1)}P\int_0^{\Lambda} \frac{\omega'}{\omega'^2-\omega^2}\Omega^{\psi-1}\,d\omega'\end{aligned} \tag{2.8}$$

where we have introduced a cutoff Λ. Because Ω is slowly varying, we approximate it as a constant with $\omega' = \omega$:

$$\mathrm{Re}\,\Sigma(\omega) \approx \frac{2\mathrm{Im}\Sigma(\omega)}{\pi}\ln\frac{\omega_0}{\omega} = -\frac{2\Sigma_0}{\pi(\psi-1)}\Omega^{\psi-2} \tag{2.9}$$

where we have taken the largest possible value of the cutoff, $\Lambda \to \omega_0$, and discarded the subdominant terms in the limit $\omega \to 0$. Because $\psi > 2$, as $\omega \to 0$, both the real and the imaginary part of the self energy vanish.

The spectral function $A(k = k_F, \omega)$ is plotted in Fig. 2.6 for several values of ψ. The emergent behavior is of an unusual non-Fermi liquid; for $k = k_F$ and in the $\omega \to 0$ limit,

$$A(k_F,\omega) \to \frac{\pi}{4}\frac{\psi-1}{\Sigma_0}\Omega^{3-\psi}. \tag{2.10}$$

Provided that $\psi < 3$ or equivalently[1] $\alpha > (2\lambda)^{-1}$, the spectral function vanishes as $\omega \to 0$. The falloff is extremely slow, behaving as a fractional power of a

[1]Although we have no lower bound on α, the condition $\alpha > (2\lambda)^{-1}$ is rather mild $\alpha \gtrsim 1$ and $\alpha \gtrsim 1.5$ in $2D$ and $3D$, respectively.

Figure 2.5: Leading order (one-loop) self energy graph.

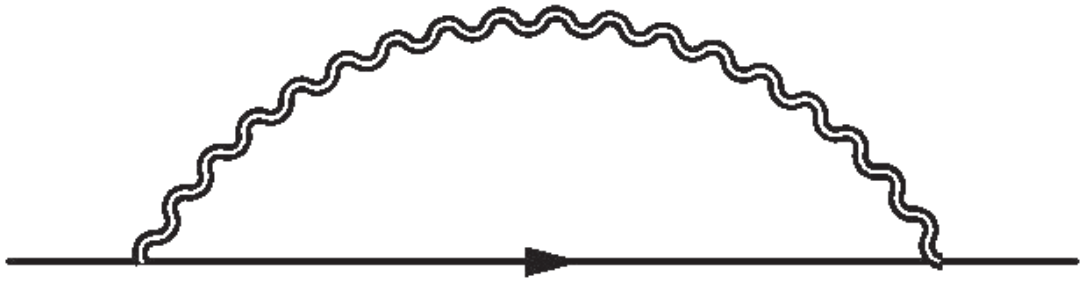

The fermion couples to the bath of RFIM fluctuations

logarithm. Furthermore, and despite the slow falloff, the quasiparticle weight always vanishes, and equivalently the effective mass diverges, as $\omega \to 0$:

$$Z^{-1} = 1 - \mathrm{Re}\frac{\partial \Sigma}{\partial \omega} = 1 + \frac{2\Sigma_0}{\pi\omega}\frac{\psi - 2}{\psi - 1}\Omega^{\psi - 1} \tag{2.11}$$

2.4 Stacks of Two Dimensional Layers

Cuprates are reasonably modeled as weakly coupled stacks of $2D$ layers [NTK14]. The above work addresses isotropic coupling; we now argue that anisotropy will not materially affect the results. Consider the Hamiltonian

$$H_{\text{stacked}} = -J_{\|} \sum_{\langle ij \rangle_{xy}} s_i^z s_j^z - J_z \sum_{\langle ij \rangle_z} s_i^z s_j^z - \sum_i h_i^z s_i^z \tag{2.12}$$

where $J_{\|}$ is the in-plane coupling and J_z the inter-plane coupling. $\langle ij \rangle_z$ denotes nearest neighbors in the z direction, and $\langle ij \rangle_{xy}$ the neighbors in the xy plane. The random fields h_i^z are as before.

Unlike $2D$, in $3D$ there is a order-disorder phase transition. In the isotropic case, i.e., $J = J_z = J_{\|}$, the zero temperature phase transition occurs at a finite $\zeta = \frac{J}{\sigma}$, found numerically to be $\zeta_c = 0.446 \pm 0.001$, in good agreement with previous results [MF02].

Figure 2.6: Spectral density after coupling to RFIM

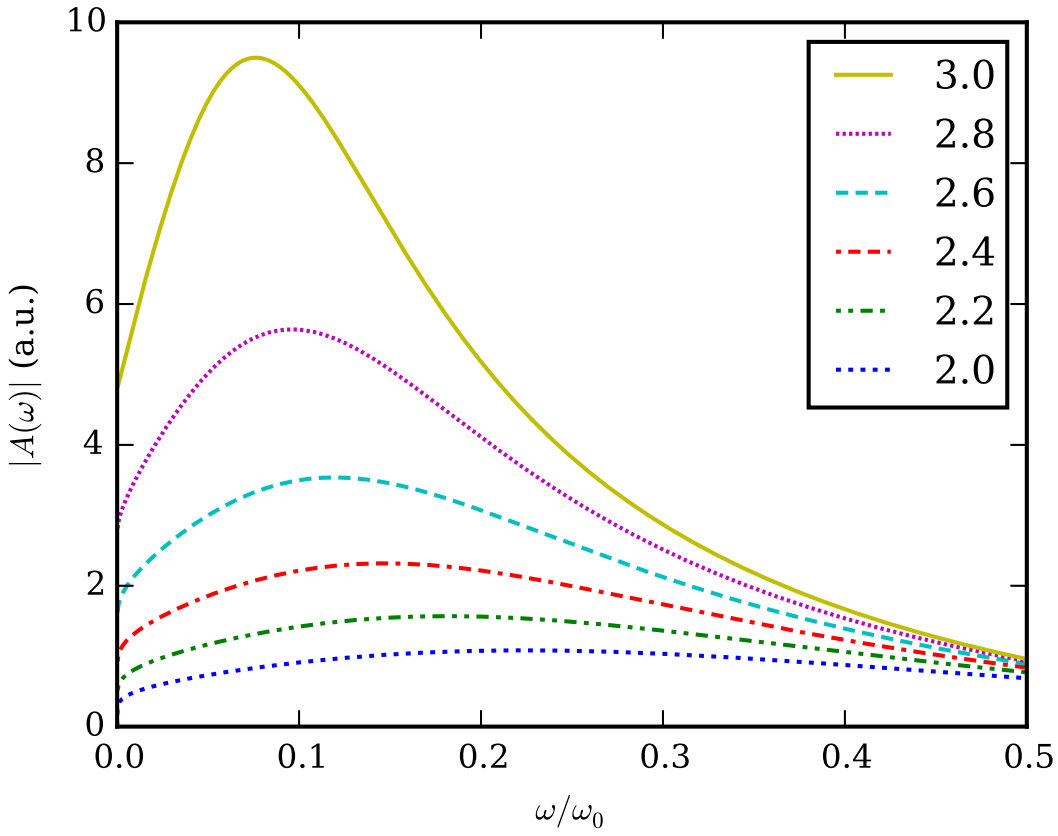

Plotted as a function of frequency relative to the chemical potential, with wave vector $k = k_F$, for several values of the exponent ψ. The relative scale of each curve is arbitrary: the unspecified prefactor Σ_0 is not included.

The anisotropic case (with $J_z \neq J_\parallel$) is illustrated in Fig. 2.7. Numerically, a particular value of J_z is fixed, and $J_\parallel$ is varied to identify the phase boundary in the J_z-$J_\parallel$ plane. A simple mean field theory result is also illustrated: as shown earlier [SC09], in $2D$ the correlation length

$$\xi_{2\mathrm{D}}[J/\sigma] \sim \exp\left[\left(\frac{J/\sigma}{\zeta_0}\right)^2\right] \tag{2.13}$$

with $\zeta_0 \approx 0.75$. Treating the $3D$ system as a stack of coupled $2D$ planes, a mean field theory argument suggests the crossover from purely $2D$ (at weak enough J_z) to $3D$ occurs for

$$J_z \gtrsim J_\parallel/\xi_{2\mathrm{D}}^2. \tag{2.14}$$

The qualitative features are readily understood. When $J_\parallel \to 0$, the system decouples as a $1D$ RFIM, which cannot order (a scenario irrelevant to the cuprates). On the other hand, when $J_z \to 0$, the case simplifies to the $2D$ RFIM, which while it also cannot order, has an exponentially large crossover scale. It is in the latter regime that the fully $3D$ and stacked $2D$ results overlap. For weak J_z, the system is disordered and the total energetic contribution from the J_z coupling can be made small relative to the in-plane $J_\parallel$ terms. An interpolation between the $2D$ and $3D$ cases is expected in the anisotropic case, which should always result in the suppression of a quasiparticle peak.

2.5 Conclusion

In conclusion, random field disorder is significant even in the apparently well ordered materials of high temperature superconductors, but its effect is quite different for the two orders, CDW and DDW. Because the $\mathbb{Z}_2$ symmetry is broken for period-2 CDW, it is susceptible to random field disorder, destroying the Fermi surface, as we have found here by treating it as a RFIM. The disorder results in the glassy susceptibility $\mathrm{Im}\,\chi(\omega)$ of Eqn. 2.5, producing a quite unusual non-Fermi

Figure 2.7: Phase diagram in the anisotropic case

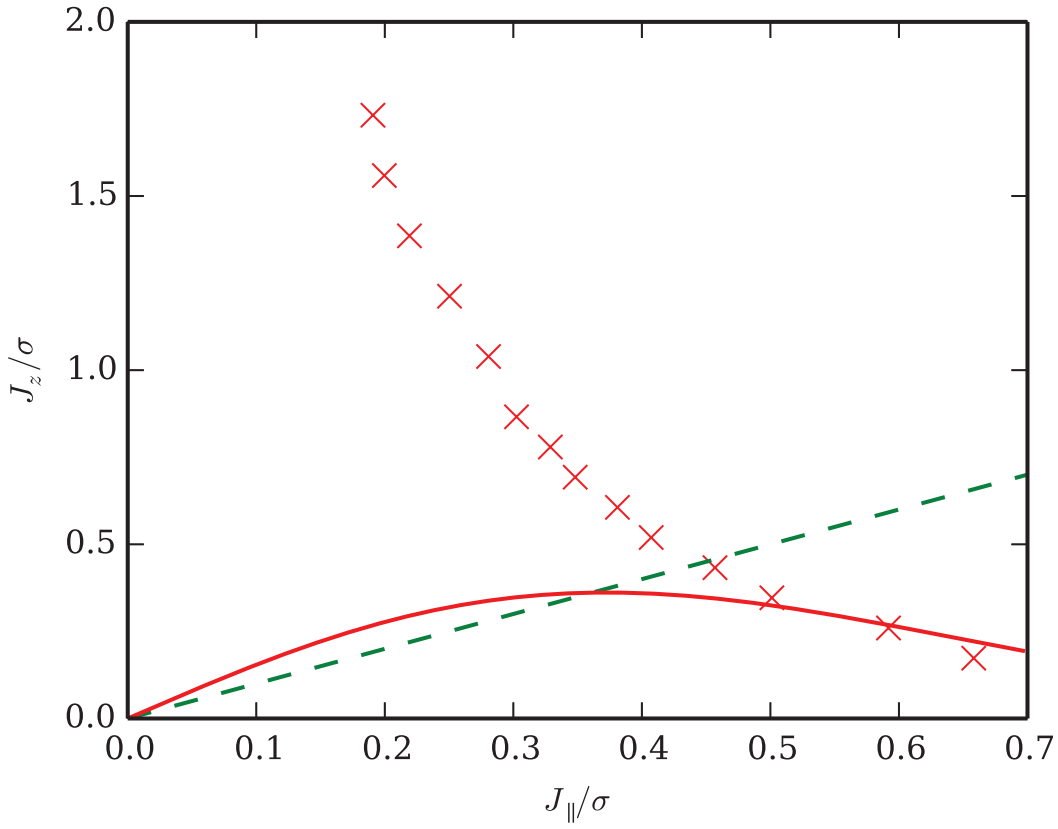

The $3D$ isotropic case corresponds to the dashed diagonal line $J_z = J_\parallel$. For each value of J_z considered, the numerically identified phase transition is a red $\times$. The mean field result, Eqn. 2.14, is the red line (including an approximate scale factor). The ordered phase is above the $\times$ symbols.

liquid. Physically, the glassy dynamics are due to the wide range of scales over which domain walls exist in the ground states of the $2D$ and $3D$ RFIM and are characterized by the parameter ψ, which controls susceptibility and in turn the non-Fermi liquid behavior. No Fermi-surface reconstruction can in principle occur, precluding quantum oscillations, up to some important caveats: the coupling parameter Σ_0 must not be too small, and the CDW correlation length cannot be too large relative to the cyclotron radius (see [THZ15]). Truly incommensurate order in the presence of disorder is far too complex a problem and was not addressed in the present work. In any case, ICDW destroys strict quantum oscillations [ZMK15] even without disorder, only making the situation worse.

In contrast, DDW modulates bond currents—a Hartree-Fock calculation of DDW is given by Laughlin [Lau14]—which cannot directly couple to potential disorder, even though the order breaks translational symmetry. No non-Fermi liquid behavior is expected. Higher periodicity DDW (for example, period-8) can induce parasitic charge order that can couple to disorder. Being a higher order effect in Landau theory, this coupling may be weak. However, the observed weak CDW involves such a small motion of the atoms, it is hard to believe that it could be the cause of a large magnitude pseudogap. In any case, the short range nature of the CDW order [GJN15] combined with RFIM disorder cannot explain quantum oscillations, at least if the resulting electronic state is a non-Fermi liquid. As a third option, if we neglect disorder and assume very long-ranged CDW, (perhaps infinitely long-ranged), Fermi surface reconstruction and quantum oscillation have been shown to be possible [MHR14, SHB14, ACS14, DBC15]. The current experiments, however, do not support long-ranged order, nor is there any reason to neglect disorder.

CHAPTER 3

Chiral Superconductor with Next-Nearest-Neighbor Terms

In this chapter, a number of chiral superconductors with up to next-nearest-neighbor terms are introduced. Using the techniques described in the introduction, the phases and Chern numbers are identified. Both p_x+ip_y and $d_{x^2-y^2}+id_{xy}$ order parameters are considered.

3.1 Terms

Both nearest and next-nearest neighbor hopping terms are considered, illustrated in Fig. 3.1, and explicitly:

$$\begin{aligned} t_{ij} = -\mu\delta_{ij} + t_1\left[\delta_{i-a\hat{x},j} + \delta_{i+a\hat{x},j} + \delta_{i-a\hat{y},j} + \delta_{i+a\hat{y},j}\right] \\ + t_2\left[\delta_{i-a(\hat{x}-\hat{y}),j} + \delta_{i+a(\hat{x}-\hat{y}),j} + \delta_{i-a(\hat{x}+\hat{y}),j} + \delta_{i+a(\hat{x}+\hat{y}),j}\right] \end{aligned} \quad (3.1)$$

Where a chemical potential has also been included. Taking a Fourier transform,

$$\begin{aligned} &\sum t_{ij}c_i^\dagger c_j \\ &\quad = \sum_k \left[-\mu + 2t_1(\cos k_x + \cos k_y) + 2t_2(\cos(k_x+k_y) + \cos(k_x-k_y))\right] a_k^\dagger a_k \\ &\quad = \sum_k \left[-\mu + 2t_1(\cos k_x + \cos k_y) + 4t_2\cos(k_x)\cos(k_y)\right] a_k^\dagger a_k \end{aligned} \quad (3.2)$$

Nearest and next-nearest neighbor $p_x + ip_y$ terms, illustrated in Fig. 3.2, and given explicitly by:

Figure 3.1: Nearest, and next-nearest neighbor t hopping terms

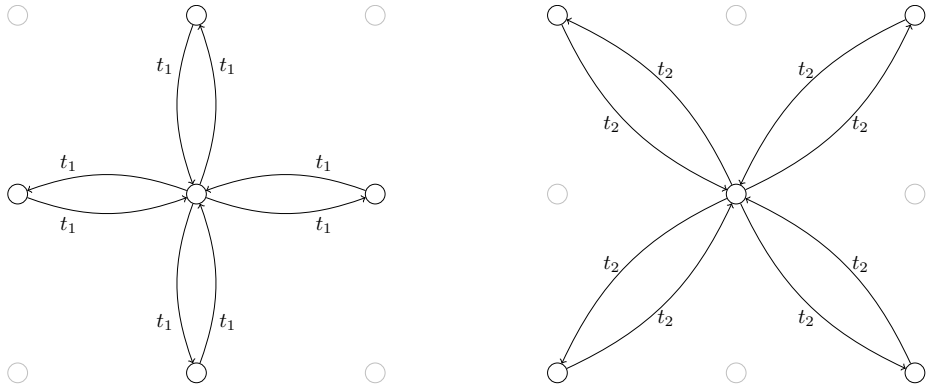

Figure 3.2: Nearest, and next-nearest neighbor $p_x + ip_y$ pairing terms

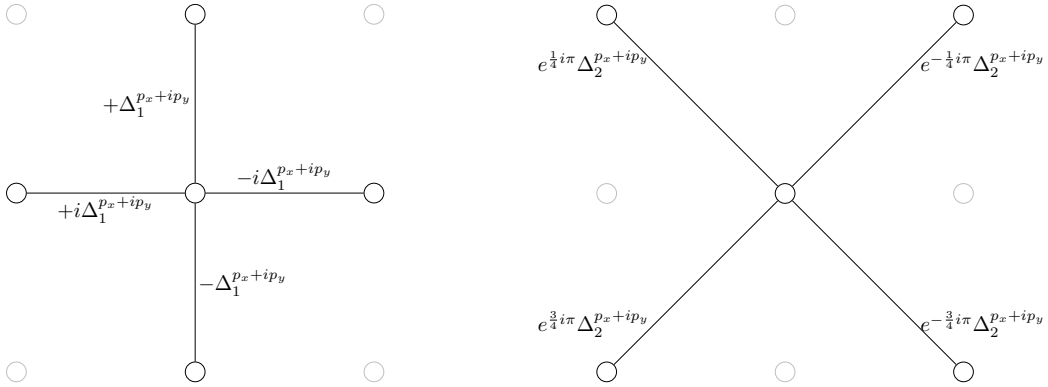

Figure 3.3: Nearest, and next-nearest neighbor $d_{x^2-y^2} + id_{xy}$ pairing terms

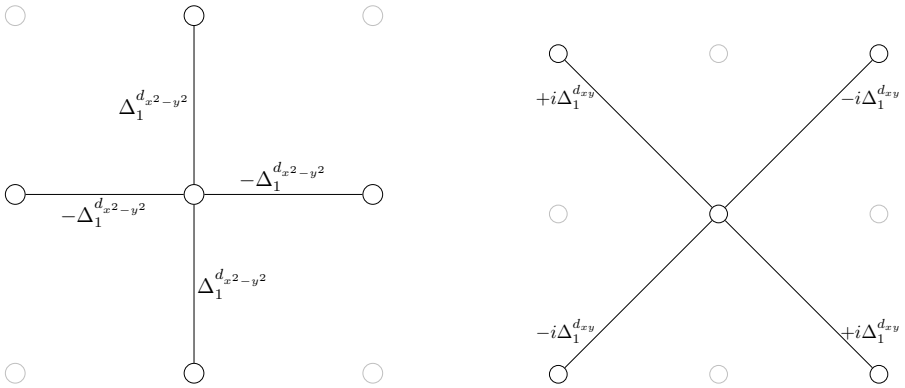

$$\Delta_{ij} = \Delta_1^{p_x+ip_y}\left[i\delta_{i-a\hat{x},j} - i\delta_{i+a\hat{x},j} + \delta_{i-a\hat{y},j} - \delta_{i+a\hat{y},j}\right]$$
$$+ \Delta_2^{p_x+ip_y}\left[e^{\frac{1}{4}i\pi}\delta_{i-a(\hat{x}-\hat{y}),j} + e^{-\frac{3}{4}i\pi}\delta_{i+a(\hat{x}-\hat{y}),j} + e^{\frac{3}{4}i\pi}\delta_{i-a(\hat{x}+\hat{y}),j} + e^{-\frac{1}{4}i\pi}\delta_{i+a(\hat{x}+\hat{y}),j}\right] \tag{3.3}$$

Notice that a chirality is created here: the phase winds counterclockwise, reaching a total phase of 2π after rotating once around the axis. Furthermore, notice that, without both terms in the x and y direction, the chirality symmetry would not be broken. The choice of coefficients may become more clear once a Fourier transform is performed:

$$\begin{aligned}
&\sum \Delta_{ij} c_i^\dagger c_j^\dagger \\
&= \sum_k \left[2\Delta_1^{p_x+ip_y}(\sin k_x + i\sin k_y) + 2\Delta_2^{p_x+ip_y}e^{-\frac{1}{4}i\pi}(\sin(k_x-k_y) + i\sin(k_x+k_y))\right] a_k^\dagger a_{-k}^\dagger \\
&= \sum_k \left[2\Delta_1^{p_x+ip_y}(\sin k_x + i\sin k_y) + 2\sqrt{2}\Delta_2^{p_x+ip_y}(\sin(k_x)\cos(k_y) - i\cos(k_x)\sin(k_y))\right] a_k^\dagger a_{-k}
\end{aligned} \tag{3.4}$$

Next, consider terms from d-wave pairing, illustrated in Fig. 3.3, and explicitly:

$$\Delta_{ij} = \Delta_1^{d_{x^2-y^2}} \left[-\delta_{i-a\hat{x},j} - \delta_{i+a\hat{x},j} + \delta_{i-a\hat{y},j} + \delta_{i+a\hat{y},j}\right] + \Delta_1^{d_{xy}} \left[i\delta_{i-a(\hat{x}-\hat{y}),j} + i\delta_{i+a(\hat{x}-\hat{y}),j} - i\delta_{i-a(\hat{x}+\hat{y}),j} - i\delta_{i+a(\hat{x}+\hat{y}),j}\right] \quad (3.5)$$

Notice that, again, the phase has been chosen such that it winds counterclockwise around the lattice (and does so *twice* giving $\ell = 2$), and again the chirality requires the second longer term. The Fourier transform is therefore

$$\begin{aligned}
&\sum \Delta_{ij} c_i^\dagger c_j^\dagger \\
&= \sum_k \left[2\Delta_1^{d_{x^2-y^2}} (\cos k_x - \cos k_y) + 2i\Delta_1^{d_{xy}} (\cos(k_x + k_y) - \cos(k_x - k_y))\right] a_k^\dagger a_{-k}^\dagger \\
&= \sum_k \left[2\Delta_1^{d_{x^2-y^2}} (\cos k_x - \cos k_y) - 4i\Delta_1^{d_{xy}} \sin(k_x)\sin(k_y)\right] a_k^\dagger a_{-k}^\dagger \quad (3.6)
\end{aligned}$$

3.2 Phase Diagram for phase-locked p-wave

First, we address the phases of the $\ell = 1$, $p_x + ip_y$ pairing, with interactions given by Eq. 3.3. In this form, phases of nearest and next-nearest neighbors are locked (i.e., their phases look like $e^{i\ell\theta+\phi_0}$ with the same ϕ_0). Subject to these restrictions, a standard process identifies the gap closures, as outlined in the introduction, and can be used to identify the phases. In particular, two Fourier transforms must vanish: $\Delta(k)$, the fourier transform of the pairing terms, found above and given by

$$\Re\Delta(k) = 2\sin(k_x)\left[\Delta_1^{p_x+ip_y} + \sqrt{2}\Delta_2^{p_x+ip_y}\cos(k_y)\right]$$

and

$$\Im\Delta(k) = 2\sin(k_y)\left[\Delta_1^{p_x+ip_y} + \sqrt{2}\Delta_2^{p_x+ip_y}\cos(k_x)\right]$$

as well as $\mathbf{h}_\mathbf{k}^z$, the fourier transform of the hopping terms, restated

$$\mathbf{h}_\mathbf{k}^z = -\mu + 2t_1\left[\cos(k_x) + \cos(k_y)\right] + 4t_2\cos(k_x)\cos(k_y)$$

Notice first that zeros of Δ occur at high-symmetry points in the Brillouin zone,

Figure 3.4: $p + ip$ superconducting phases for $\alpha = 0.5$

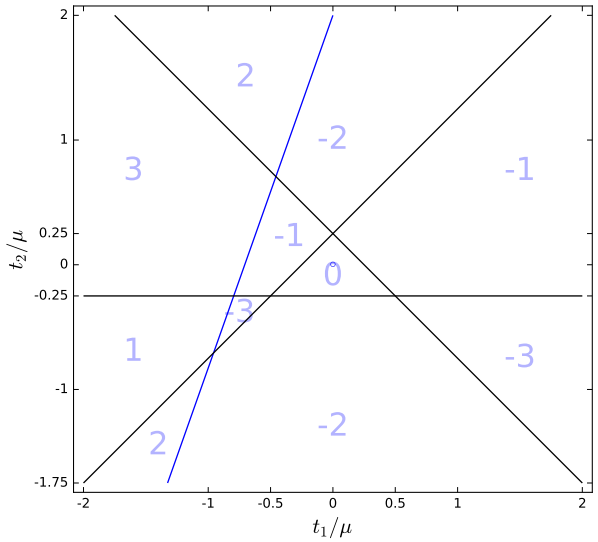

Γ, X, Y and M. Putting $\alpha = \frac{\Delta_1^{p_x+ip_y}}{\Delta_2^{p_x+ip_y}}$, the remaining four zeros of Δ are at

$$|k_x| = |k_y| = \arccos \frac{-\alpha}{\sqrt{2}}$$

which we will refer to collectively simply as $A(\alpha)$. The Chern number is determined by noticing that each zero of $\Delta(k)$ contributes either $+1$ or -1 to the overall Chern number, depending on whether $h_z(k) > 0$ at that point in the Brillouin zone (and details of the zero of Δ). Evaluating h_z at the 8 zeroes of $\Delta(k)$

$$\frac{1}{4\mu}\begin{bmatrix} h_z(\Gamma) \\ h_z(X) \\ h_z(Y) \\ h_z(M) \\ h_z(A(\alpha)) \end{bmatrix} = \begin{bmatrix} \frac{t_1}{\mu} + \frac{t_2}{\mu} - \frac{1}{4} \\ -\frac{t_2}{\mu} - \frac{1}{4} \\ -\frac{t_2}{\mu} - \frac{1}{4} \\ -\frac{t_1}{\mu} + \frac{t_2}{\mu} - \frac{1}{4} \\ -\frac{\alpha}{\sqrt{2}}\frac{t_1}{\mu} + \frac{\alpha^2}{2}\frac{t_2}{\mu} - \frac{1}{4} \end{bmatrix}.$$

Figure 3.5: $d + id$ superconducting phases

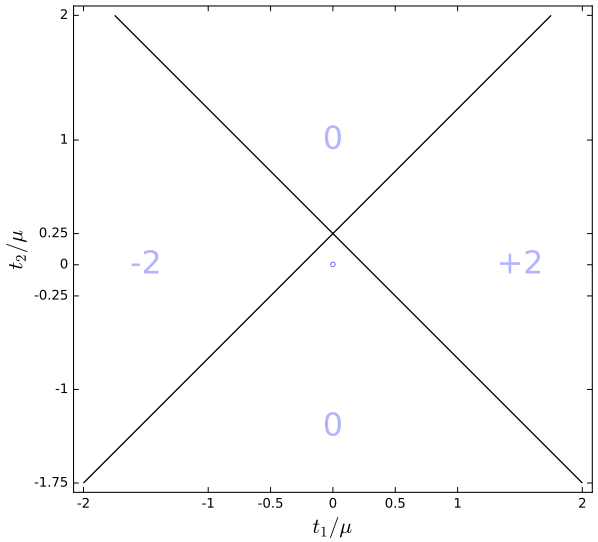

The Chern contributions for each zero when $h_z > 0$ are, respectively

$$\begin{bmatrix} -1 \\ +1 \\ +1 \\ -1 \\ \text{N/A} \end{bmatrix} \text{ if } |\alpha| \geq \sqrt{2}, \text{ and for } |\alpha| < \sqrt{2}, \begin{bmatrix} -1 \\ -1 \\ -1 \\ -1 \\ +1 \end{bmatrix}$$

These phases are summarized in Fig. 3.4.

3.3 Phase diagram for the phase-locked d-wave case

Next, we address the phases of the $\ell = 2$, $d_{x^2-y^2} + id_{xy}$ pairing. The hopping terms are the same as above,

$$h_z(k) = -\mu + 2t_1 \left[\cos(k_x) + \cos(k_y)\right] + 4t_2 \cos(k_x)\cos(k_y)$$

while the Fourier transform of the pairing terms is now

$$\Re\Delta(k) = 2\Delta_1^{d_{x^2-y^2}} \left[\cos(k_x) - \cos(k_y)\right]$$

and

$$\Im\Delta(k) = -4\Delta_1^{d_{xy}} \sin(k_x)\sin(k_y)$$

In this case, it's clear that the only zeros of $\Delta(k)$ are at the *two* high-symmetry points Γ and M. There are, therefore, phase transitions controlled by the more simple diagram

$$\tfrac{1}{4\mu}\begin{bmatrix} h_z(\Gamma) \\ h_z(M) \end{bmatrix} = \begin{bmatrix} \frac{t_1}{\mu} + \frac{t_2}{\mu} - \frac{1}{4} \\ -\frac{t_1}{\mu} + \frac{t_2}{\mu} - \frac{1}{4} \end{bmatrix}.$$

These phases are summarized in Fig. 3.5.

3.4 Phase Diagram for phase-unlocked p-wave

It is also possible to consider the situation where $\Delta_2^{p_x+ip_y}$ is not real. This corresponds to next-nearest neighbor pairing that is not phase-locked to the nearest neighbor pairing. In this section such an order parameter is examined—the phase of $\Delta_2^{p_x+ip_y}$ will be taken to be $e^{\frac{1}{4}i\pi}$ throughout this section.

Again, the bulk band gap is seen to collapse for momenta $\mathbf{k} = (k_x, k_y)$ such that

$$0 = \frac{1}{2\Delta_2^{p_x+ip_y}}\Delta(k) = \alpha\left[\sin(k_x) + i\sin(k_y)\right] + \sin(k_x - k_y) + i\sin(k_x + k_y) \quad (3.7)$$

and

$$0 = \frac{1}{\mu}h(k) = -1 + 2\left(\frac{t_1}{\mu}\right)\left[\cos(k_x) + \cos(k_y)\right] + 4\left(\frac{t_2}{\mu}\right)\cos(k_x)\cos(k_y) \quad (3.8)$$

Again, there are the four zeros of Δ at the high symmetry points (i.e., where $\sin k_x = \sin k_y = 0$). Assuming that the sine terms do not vanish, the remaining four zeros of Δ can be shown to satisfy

$$\begin{aligned} \cot(k_x)^2 &= \frac{\alpha^2}{2-\alpha^2}\left[1 + \sqrt{\frac{4}{4+\alpha^4}}\right] \\ \cot(k_y)^2 &= \frac{\alpha^2}{2-\alpha^2}\left[1 - \sqrt{\frac{4}{4+\alpha^4}}\right] \end{aligned} \quad (3.9)$$

Thus, there are two cases: $\alpha^2 \geq 2$, in which $\Delta(\mathbf{k})$ only vanishes at the four high-symmetry points, and $\alpha^2 < 2$, for which the order parameter vanishes at two additional, α-dependent momenta. A straightforward, if lengthy, consideration of cases of the signs of the $\cos(k_i)$ and $\sin(k_i)$ would allow the cotangent terms to be plotted implicitly, giving an exact solution for the location in the Brillouin zone for each zero. Fortunately, an explicit solution for the momenta of the zeros is not needed, as we will see momentarily.

h at the zeros of Δ

For $\mathbf{k}$ such that $\Delta(\mathbf{k}) = 0$, the band gap closes if and only if $h(\mathbf{k}) = 0$. Furthermore, the phase winding of Δ around its zeros and the sign of $h(\mathbf{k})$ at each zero indicate the Chern number. This well-known result is reviewed in Appendix 1.3. At the high-symmetry points Γ, X, Y, and M,

$$\frac{1}{4\mu}\begin{bmatrix} h(0,0) \\ h(\pm\pi,0) \\ h(0,\pm\pi) \\ h(\pm\pi,\pm\pi) \end{bmatrix} = \begin{bmatrix} t_2/\mu + t_1/\mu - \frac{1}{4} \\ -t_2/\mu - \frac{1}{4} \\ -t_2/\mu - \frac{1}{4} \\ t_2/\mu - t_1/\mu - \frac{1}{4} \end{bmatrix} \tag{3.10}$$

By setting $h(\mathbf{k}) = 0$, we get the three alpha-independent phase transition lines: $t_2/\mu = -1/4$, $t_2/\mu + t_1/\mu = 1/4$, and $t_2/\mu - t_1/\mu = 1/4$. The Chern number changes by 1 when crossing each line (except for the $t_1/\mu = -1/4$ double line, where the change is 2). At the α-dependent zeros of Δ given by Equation (3.9), h is evaluated (a tedious but straightforward considerations of cases):

$$\frac{1}{\mu}h(\mathbf{k}) = -1 - \left(\frac{t_1}{\mu}\right)\alpha(2-\alpha^2) - \left(\frac{t_2}{\mu}\right)\alpha^4 \tag{3.11}$$

The condition that the α-dependent zeros are included or excluded by the Fermi surface (i.e., $h(\mathbf{k}) \lessgtr 0$) is recast by defining

$$\beta = \begin{bmatrix} -\alpha(2-\alpha^2) \\ -\alpha^4 \end{bmatrix} \quad \text{and} \quad \mathbf{t} = \frac{1}{\mu}\begin{bmatrix} t_1 \\ t_2 \end{bmatrix} \tag{3.12}$$

and the above condition can be restated as

$$0 \leq \frac{1}{\mu} h(\mathbf{k}) = -1 + \mathbf{t} \cdot \beta \quad \text{or} \quad \frac{1}{\beta} \leq \mathbf{t} \cdot \hat{\beta} \tag{3.13}$$

I.e., there is a phase transition line, with closest approach to the t_1-t_2 origin given by $Z = \frac{\hat{\beta}}{\beta}$. Plotting these four phase transition lines, identifying the topologically trivial phase where where $(t_1, t_2) = (0, 0)$, and counting the number of lines crossed allows for the creation of phase diagrams for various values of α, such as those in Fig. 3.6.

Figure 3.6: Phase diagrams for phase-unlocked p-wave pairing.

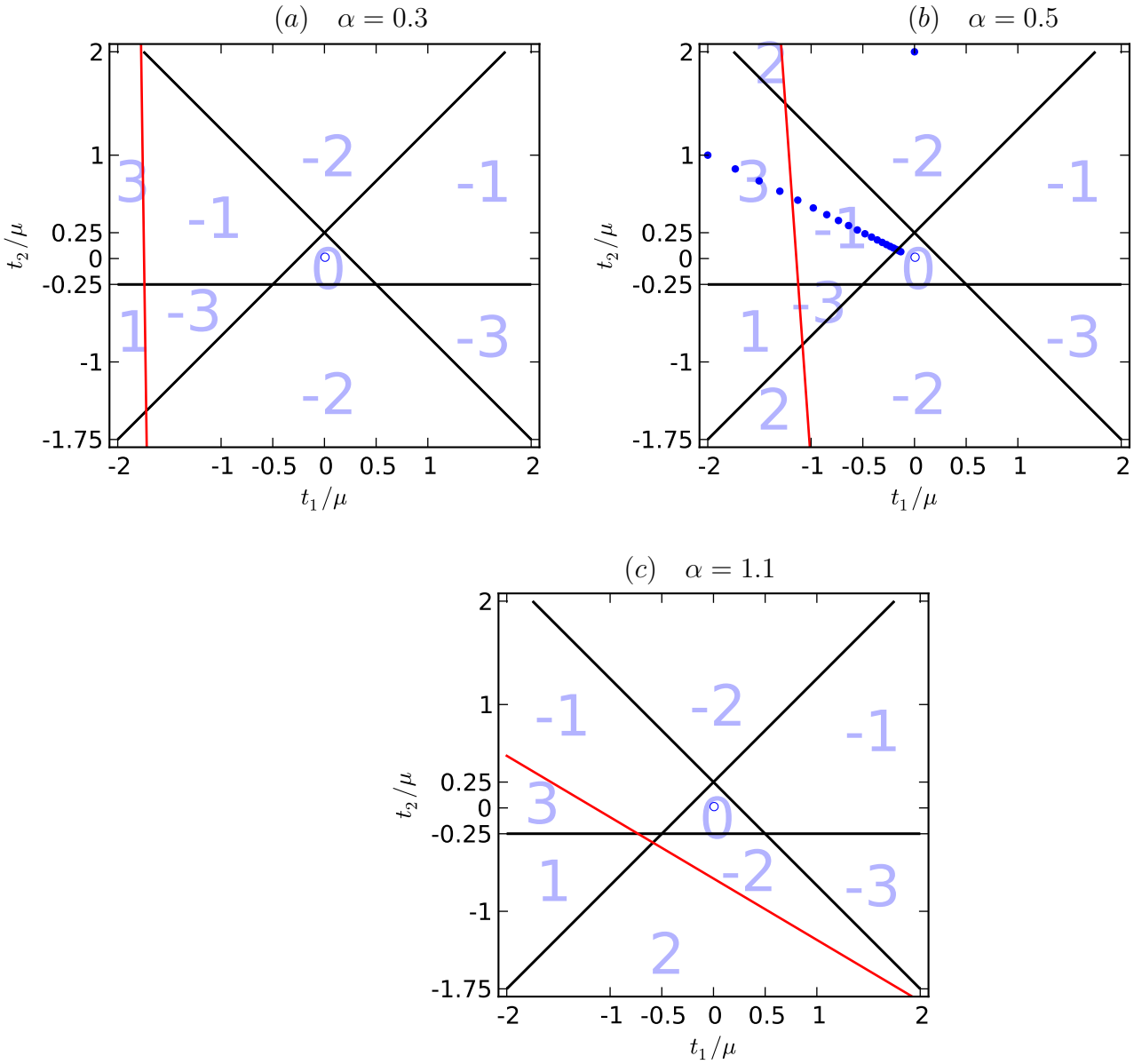

Values of $\alpha = \Delta_1/\Delta_2$, with Chern number for each phase. The dots subfigure (b) indicate values of $t_1/\mu, t_2/\mu$ investigated numerically in Chapter 4.

CHAPTER 4

Numerical Studies of Majorana Fermions near Vortices in Chiral Superconductors

4.1 Majorana Modes and defects

There has been much interest in topological features of various condensed matter systems, in particular Majorana fermions. [MZF12, Kit01, Wil09, MR91, FK08, SLT10, STL10, AOR11, Ali10, LSD10, DSV11, Ali12, RG00, Iva01, Roy10] Majorana fermions satisfy $\gamma^\dagger = \gamma$; that is, they are their own antiparticle. In systems with particle-hole symmetry, their energy is therefore pinned to zero. Consequently, Majorana fermions can only be destroyed by pairing with another and hybridizing into a Dirac fermion.

We focus on chiral p_x+ip_y superconductors. In continuum models with nonzero Chern numbers, zero-energy Majorana fermions develop around defects, such as vortices.[KS91, Ali12, RG00, Iva01, Vol99, CGM64, HK10, Roy10] When the vortices are well-separated, the associated Majorana fermions are protected from local perturbations, which could be useful in quantum computers. Majorana fermions are also expected in lattice models of chiral superconductors; if the gap is of the form $\sin(nk_x) + i\sin(nk_y)$, where n is the range of the interaction, it reduces to $n\partial_x + in\partial_y$ in the continuum limit.

In contrast to the continuum case where the range of the interaction, n, simply rescales the gap function, the range plays a more interesting role on the lattice. Previous work [NCH12] suggested that the inclusion of longer-ranged interactions

leads to novel phases. These longer-ranged interactions in general give rise to larger Chern numbers in a way that can be most easily understood when all interactions are of the same range. When all interactions are of the same range, a number of noninteracting sublattices, $S(n)$, form. For example, in FIG. 4.1, two sublattices form when only next-nearest neighbor terms are present. As separate systems, each sublattice has its own Chern number, either 0 or 1. Therefore, the Chern number for the whole system is either 0 or $S(n)$.

To explore the more complicated case of interactions of different ranges, we study a square lattice with a combination of nearest-neighbor (NN) and next-nearest-neighbor (NNN) hopping (respectively, t_1 and t_2), and $p_x + ip_y$ pairing (respectively, $\Delta_1^{p_x+ip_y}$ and $\Delta_2^{p_x+ip_y}$) terms. The system is kept at chemical potential μ. Both the hopping and pairing terms are illustrated in Fig. 3.1 and Fig. 3.2.

The five parameters t_1, t_2, $\Delta_1^{p_x+ip_y}$, $\Delta_2^{p_x+ip_y}$, and μ constitute a parameter space rich enough to include the well-known BEC and BCS superconducting systems, as well as their two-sublattice versions (i.e., purely NNN interactions). Because the BEC-BCS transition is topological in nature, we search for the surfaces in parameter space where the bulk band gap collapses and topological phase transitions occur.

Our analysis of the system shows that the phase diagram depends only on *three* ratios of parameters: $\alpha = \frac{\Delta_1}{\Delta_2}$ and the scaled hopping terms t_1/μ, t_2/μ. For fixed values of α, all phase transitions are lines in the t_1-t_2 plane. There are four such lines, three of which are independent of α. When a system is tuned to one of these phase transition lines, the gap in the system collapses because a zero of $\Delta(\mathbf{k})$ is crossing the Fermi surface. The lines constitute the phase diagram for a given value of α, as shown in Fig. 3.6. When $|\alpha|^2 \geq 2$, the phase transition lines remain fixed, and $\Delta(\mathbf{k})$ only has zeros at the four high-symmetry points Γ, X, Y, and M because the NNN pairing terms are not strong enough to introduce any zeros into $\Delta(\mathbf{k})$. The topology of the system is unaffected by the weak NNN pairing. When

Figure 4.1: 2D Sublattices

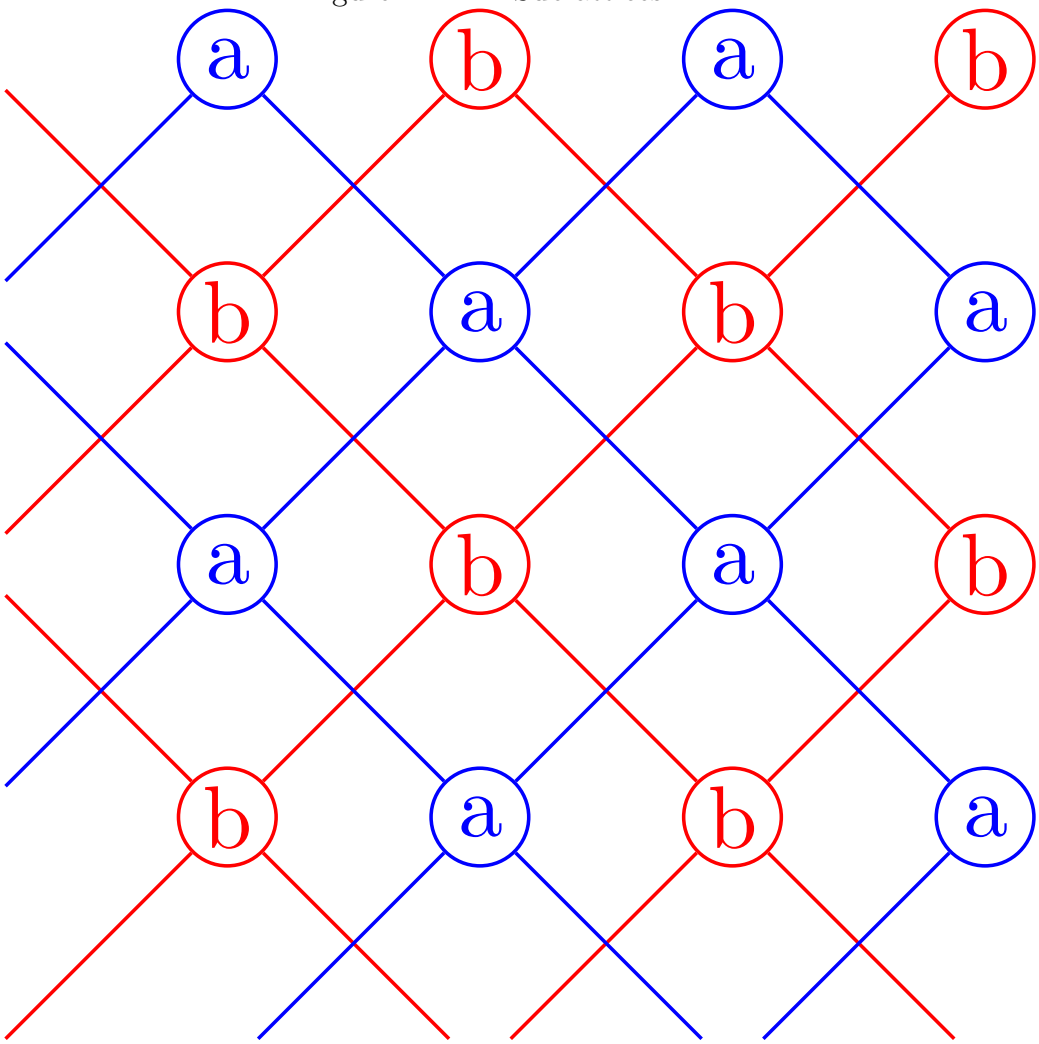

When only next-nearest neighbor interactions are present in a 2 dimensional lattice model, two sublattices form, each responding independently to defects. Pairs of defect modes evolve correspondingly independently. When nearest-neighbor interactions are turned on, the pairs of defect modes persist.

$|\alpha|^2 < 2$, four additional zeros are introduced into $\Delta(\mathbf{k})$, permitting larger Chern numbers. An analytical calculation finds all Chern numbers possible with NN and NNN terms; they range from -3 to $+3$. Chern number ± 4, while conceivably possible with NNN pairing terms, cannot be obtained with just NNN hopping terms for the same reason that Chern number 2 cannot be obtained with just NN pairing and hopping terms. However, the system does take on Chern number 3, which is surprising because purely NNN interactions yield Chern number 2.

The numerical aspect of the present work characterizes the response of the model system to defects in different phases. In particular, we focus on characterizing the low-energy response, i.e., identifying the fundamental excitations of the system. For the numerics, we include three kinds of position-dependent terms into the Hamiltonian: edges, on-site disorder, and magnetic fields in an extreme type-II limit with vortices in the superconducting order parameter. Edges are introduced by adding terms of the form $O_i c_i^\dagger c_i$, where O_i is very large past the edge, confining the states in the low energy spectrum. On-site disorder is added in a similar manner: O_i takes on a value of E_d with probability $\frac{p}{2}$ and $-E_d$ with the same probability, and 0 otherwise. For the magnetic field, we assume a very long magnetic screening length so that the magnetic field is constant, consistent with the sample being two-dimensional. However, the superconducting coherence length ξ is finite, and vortices appear in the superconducting order parameter.

The output of numerical simulations are the energies and wavefunctions of the quasiparticles of the Hamiltonian. The edge modes and vortex core modes are perfectly distinct in the ideal limit of infinite separation. In the realistic case of finite separation, the modes hybridize. The vortex core modes interact with each other in a similar way. The energies of the lowest vortex core modes exhibit exponentially damped oscillations as the vortices are separated, an effect theoretically predicted [CLG09] and numerically observed [MM10] in related systems. The edges hybridize with vortices over longer length scale than the vortices hybridize

with each other.

The hybridization effects also depend on the bulk parameters of the system, i.e., t_1, t_2, $\Delta_1^{p_x+ip_y}$, $\Delta_2^{p_x+ip_y}$, and μ. In particular, as these parameters are tuned to the phase transitions, the edge-vortex length scale diverges. Such tuning is explored in a system with $(\Delta_1^{p_x+ip_y}, \Delta_2^{p_x+ip_y}) = (0.5, 1.0)$ and $t_1 = -2$ (energy is given in terms of the NNN hopping strength, t_2) by adjusting the chemical potential μ, i.e. by moving along the path shown in Fig. 3.6, which crosses several phase transitions. While in the Chern number 3 portion of the phase diagram, we find that the spatial period of vortex-vortex oscillation increase linearly with the chemical potential: $\Lambda \sim 0.8\mu + \text{constant}$. When μ takes on values putting the system too close to the phase transition, edge-vortex hybridization destroys the vortex-vortex oscillatory behavior.

Another issue addressed in the numerical simulation is the number of low-energy modes created around defects. When only NNN interactions are present, one Majorana mode per vortex per sublattice forms. When the NN terms are turned on, the Majorana fermions may hybridize down to zero or one residual zero-energy mode, for even and odd Chern number, respectively [Roy10]. Interestingly, there is some degree of protection of the additional defect mode for the Chern number 2 phase. The numerical simulation reveals two, apparently disorder resistant, zero energy, vortex core modes. The Chern number 3 phase, however, enjoys no such additional modes: only one low-energy vortex-core mode is observed in the numerical simulations.

4.2 Defects and Magnetic Fields

4.2.1 Magnetic Fields: Flux Tubes and Vortices

Here, we explore the response of the superconductor to magnetic fields. We assume we are in an extreme type-II limit: flux tubes form creating real-space vortices in the superconducting order parameter. In the two-dimensional case at hand, the associated response currents are essentially two-dimensional and therefore very weak. The natural simplifying limit is to take the London penetration depth $\lambda \to \infty$ and neglect the response magnetic field. We therefore assume a constant, unaffected, external magnetic field. Notwithstanding the infinite penetration depth, we still keep the superconducting coherence length ξ finite, allowing vortices in the superconducting order parameter. The vortices are therefore localized regions of vanishing superconducting order parameter Δ, without associated magnetic inhomogeneity, which we now describe more precisely.

We are guided by the relation

$$v_s = \frac{1}{2m}\left(\nabla\phi - \frac{2e}{c}\mathbf{A}\right) \tag{4.1}$$

where v_s is the superfluid velocity, ϕ is the phase of the superconducting order parameter, and $\mathbf{A}$ is the vector potential, in London gauge. When far away from a vortex ($r \gg \lambda$), we assume $v_s = 0$ and $\mathbf{B} = 0$. Integrating around the vortex yields

$$2\pi n = \oint \nabla\phi \cdot d\mathbf{l} = \frac{2e}{c}\Phi_m$$

(i.e., the well-known fact that an integer multiple of magnetic flux quanta penetrates through a flux tube). Because the order parameter is nonzero away from vortices, even for $r < \lambda$, the winding is an integer multiple of 2π around each vortex.

With a qualitative description of the behavior of the order parameter (the magnitude falls off near vortices, and the phase winds an integer multiple of 2π

Figure 4.2: Plot of the wavefunction of a vortex mode.

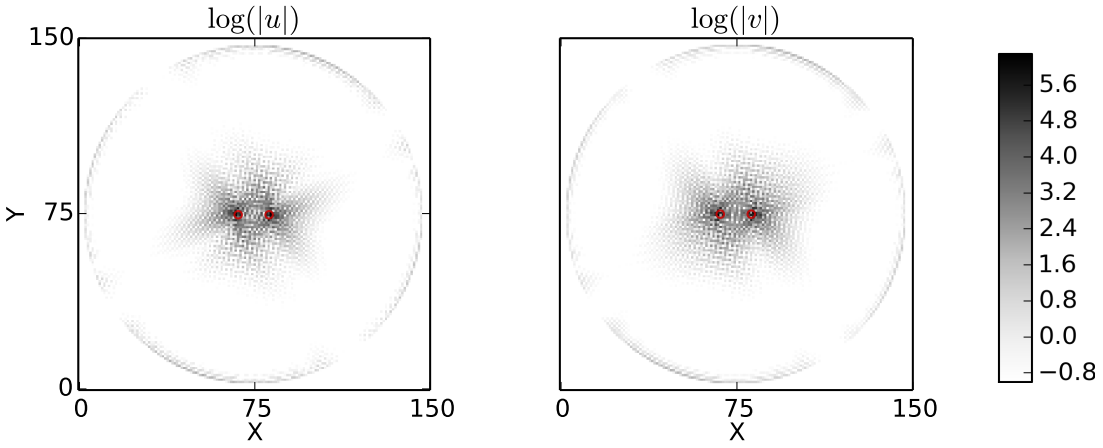

The lattice is 150 by 150, $t_1 = -2$, $\mu = 1$, and $(\Delta_1, \Delta_2) = (0.5, 1.0)$ (energy given in units of t_2). The plots are of the natural logarithm of the probability densities of the $\begin{bmatrix} u \\ v \end{bmatrix}$ parts of the BdG wavefunction. The Hamiltonian includes two vortices of radius $r_V = 1.6$ indicated by red circles, separated by 13.2 in the x-direction. The eigenenergy is in-gap: $E/t_2 \approx 5.3 \times 10^{-3}$.

around each vortex), a quantitative model to perform a numerical simulation must now be established. We use the model [MT06, VM06]

$$\Delta_{jk} = \Delta^{(0)}_{k-j} \mathcal{D}\left(j,k\right) e^{i\phi_{jk}} \tag{4.2}$$

The phase of the order parameter ϕ_{jk} is a geometric mean of the expected phases at j and k:

$$e^{i\theta_{jk}} = \frac{e^{i\phi_k} + e^{i\phi_j}}{\left|e^{i\phi_k} + e^{i\phi_j}\right|} \tag{4.3}$$

(The arithmetic mean of ϕ_i and ϕ_j is insufficient, because the phase for pairing terms crossing any branch cut would be incorrect.) Near the vortex cores, $\mathcal{D}$ falls off as

$$\mathcal{D}(j,k) = \frac{d_{\text{eff}}(j,k)}{\sqrt{d_{\text{eff}}(j,k)^2 + r_V^2}} \tag{4.4}$$

Where the "effective distance" is given by

$$d_{\text{eff}}^{-1}(j,k) = \sum_n \left(\min_{x \text{ between } j \text{ and } k} |x - v_n| \right)^{-1} \tag{4.5}$$

Figure 4.3: Plot of the wavefunction of an edge mode

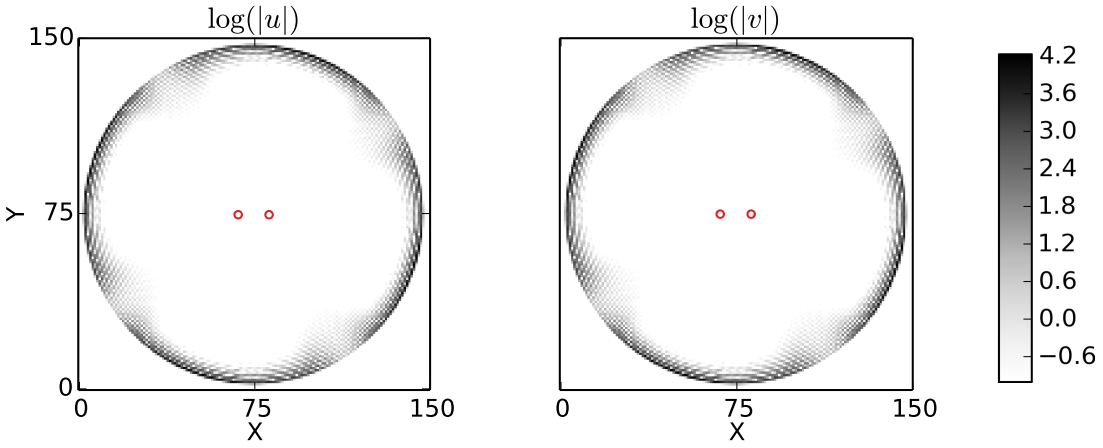

Compare with Fig. 4.2. The eigenenergy is in-gap: $E/t_2 \approx 3.1 \times 10^{-3}$. The state hybridized weakly with the vortices.

x lies on the line connecting j and k. The vortex core radius r_V is a parameter of the model, on the order of the superconducting coherence length. Provided that vortices were separated from each other and the edge by many multiples of r_V, the vortex core size was to only weakly affect the measured properties of the system. To reduce the required lattice sizes for numerical stability, we set $r_V = 1.6$, the same order of magnitude as the coherence length in the cuprates. The hopping terms h_{jk} acquire a Peierls phase due to the magnetic vector potential

$$h_{jk} = h^{(0)}_{k-j} e^{i\frac{e}{c}\int_k^j \mathbf{A}\cdot d\ell}$$

Relation (4.1) expresses $\mathbf{A}$ in London gauge: $\nabla\cdot\mathbf{A} = 0$ and the normal component of $\mathbf{A}\cdot\hat{n}$ becomes the physically meaningful boundary supercurrent. By choosing a gauge where $\mathbf{A}$ vanishes at the center of the sample, the vector potential for a constant magnetic field takes the simple form $\mathbf{A} \propto \rho\hat{\phi}$, where ρ is the distance from the center of the sample. Additionally, for our choice of $\mathbf{A}$, the boundary current vanishes for circular geometry. For non-circular geometries, the approximation will remain valid provided that the edge (and associated currents) are far from the features of interest.

4.2.2 Edges

Square edges can be produced by omitting certain terms in the Hamiltonian, i.e., setting all terms of the form h_{ij} and Δ_{ij} to zero for ij which cross an edge. While intuitive and simple, when two edges are introduced, an artificially "sharp" corner is produced. The low-energy edge modes that develop are strongly concentrated at the artificial corners. One might be concerned that such an unphysical feature might poison the simulation.

A choice of smoother edge removes the unphysically sharp corners, but introduces another problem: there are now lattice sites "outside" of the region of interest. The spectrum will include the unphysical quasiparticle modes outside the edge, complicating the analysis. A more natural approach is to make occupation of states beyond the edge energetically unfavorable. On-site terms $O_i c_i^\dagger c_i$ are added with O_i increasingly large near and beyond the edges of the system. For our purposes, the edge is made very steep and circular, i.e., it goes from 0 inside a circular region of the lattice, to a very large number outside it. The lattice sites with large on-site energies must play no role in the low-energy spectrum of the Hamiltonian.

4.2.3 Disorder

By adjusting the O_i terms, on site disorder is produced, representing quenched impurities on the lattice. The model is

$$O_i = \begin{cases} 0, & \text{with probability } 1-p \\ -E_d, & \text{with probability } p/2 \\ +E_d, & \text{with probability } p/2 \end{cases}$$

When vortices are moved, such as in Fig. 4.7, the same disorder realization is used for each vortex placement.

Figure 4.4: Quasiparticle energies near two vortices

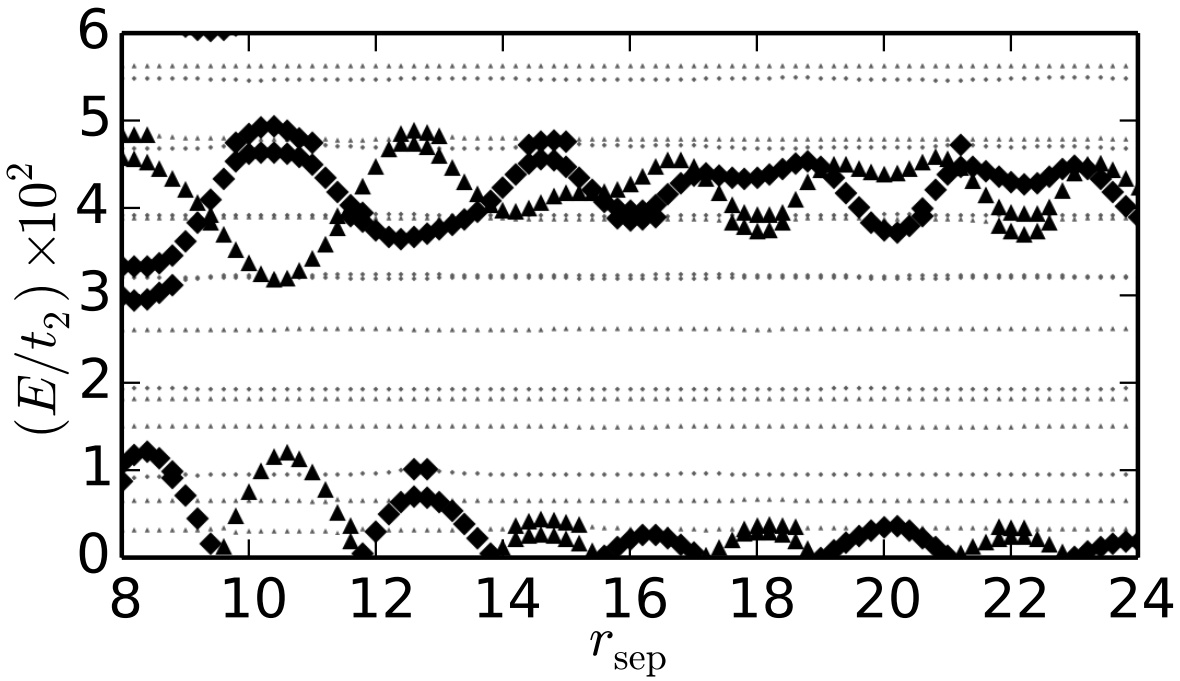

Plot of several lowest quasiparticle energies as the separation between two vortices in the x direction is varied. The lattice was 150 by 150, with a circular edge. The other parameters are $(\Delta_1, \Delta_2) = (0.5, 1.0)$, $\mu = 1$, and $t_1 = -2.0$ (energies are given in terms of t_2). The choice of parameters leads to Chern number 3 and a single zero-energy vortex core mode, as guaranteed for odd Chern numbers, c.f. Fig. 4.5. The shapes of the markers indicate the parity of the state under spatial-inversion symmetry: diamond is even, and triangle is odd (see Appendix A.8). The unimportant edge states are indicated by the smaller, fainter markers.

4.3 Numerical Results

Here, we discuss the results of the numerical diagonalization of the Bogoliubov de-Gennes Hamiltonian for eigenvalues near zero. These mid-gap states arise because of the topological nature of the system. Being deep inside the superconducting gap, these mid-gap states experience strong particle-hole mixing. As lattice sizes and vortex separation are increased, hybridization dies off, quasiparticle energies go to zero, and the particle and hole parts can be made equal, $|u| = |v|$. In our realistic case of finite separation, there will always be nonzero hybridization, and consequential deviation from equality.

We put $(\Delta_1^{p_x+ip_y}, \Delta_2^{p_x+ip_y}) = (0.5, 1.0)$, and always work with energy is in units of the NNN hopping, t_2. Our choice of parameters creates a rich phase diagram while keeping the magnitudes of both NN and NNN pairing terms similar. Several choices of t_1/t_2 were investigated, but all focus on exploring $t_1 < 0$ and $t_2 > 0$, which is similar to the superconducting band of the strontium ruthenates.

The output of the numerical simulation is the low energy spectrum and associated wavefunctions. Both vortex core states, such as Fig. 4.2, and edge states, such as Fig. 4.3, are part of the output. Although presented as distinct in the examples, they can and do hybridize. To distinguish the edge and vortex states automatically, the probability of a state being present within some distance of the edge is found and used to classify a given state as "edge" or not. As seen in, for example, Fig. 4.4 with $r_{\text{sep}} \approx 13$, the edge-vortex hybridization becomes strong enough to cause the third edge modes to hybridize strongly with the vortex modes, resulting in significant occupation away from the edge. In general, however, edge modes, being localized away from the vortices (due to the careful choice of parameters), do not strongly influence the low-energy vortex core modes.

Figure 4.5: Quasiparticle energies near vortices as t_2 is varied

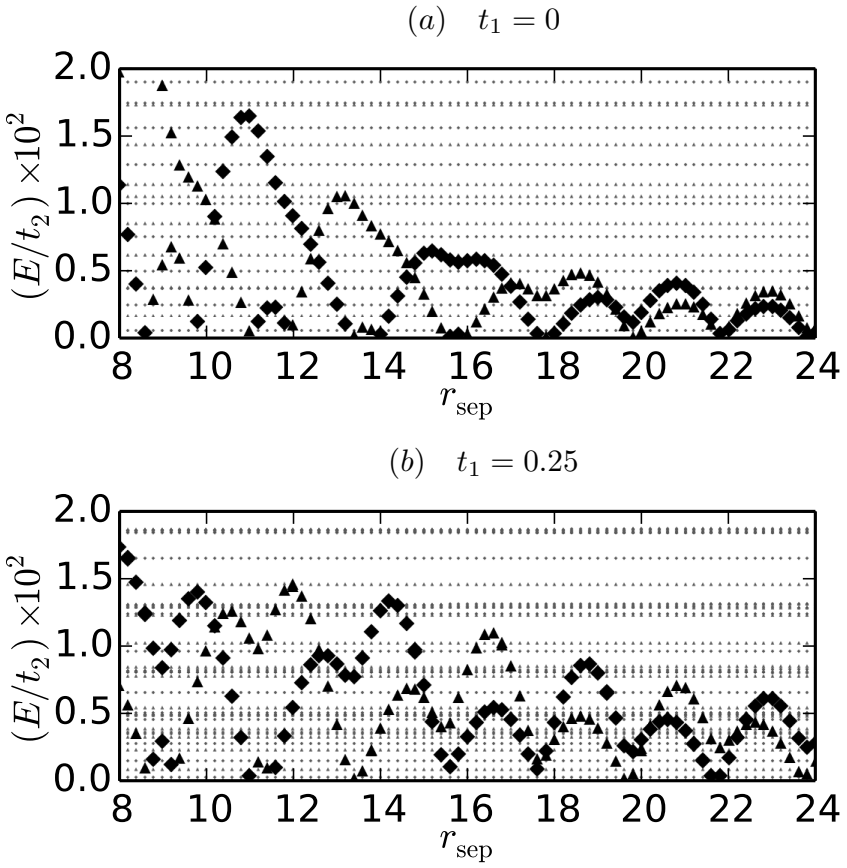

Circular lattice, $(\Delta_1, \Delta_2) = (0.25, 0.5)$, with chemical potential $\mu = 0.5$. Compare with FIG. 4.4. Each subfigure has a different value of t_1, as shown; all energies are given in terms of t_2. The vortex separation r_{sep} is given in terms of lattice spacing. Notice the *two* oscillating low energy excitations, possibly with an exponentially damped envelope. In the limit of large separation of the vortices, these vortex core states could become 0-energy Majorana modes. We suspect that that a significant portion of the Chern number -2 phase enjoys these multiple Majorana modes, suggesting analytical investigation. Resistance to weak disorder is discussed later Fig. 4.7.

Figure 4.6: Spatial Oscillations

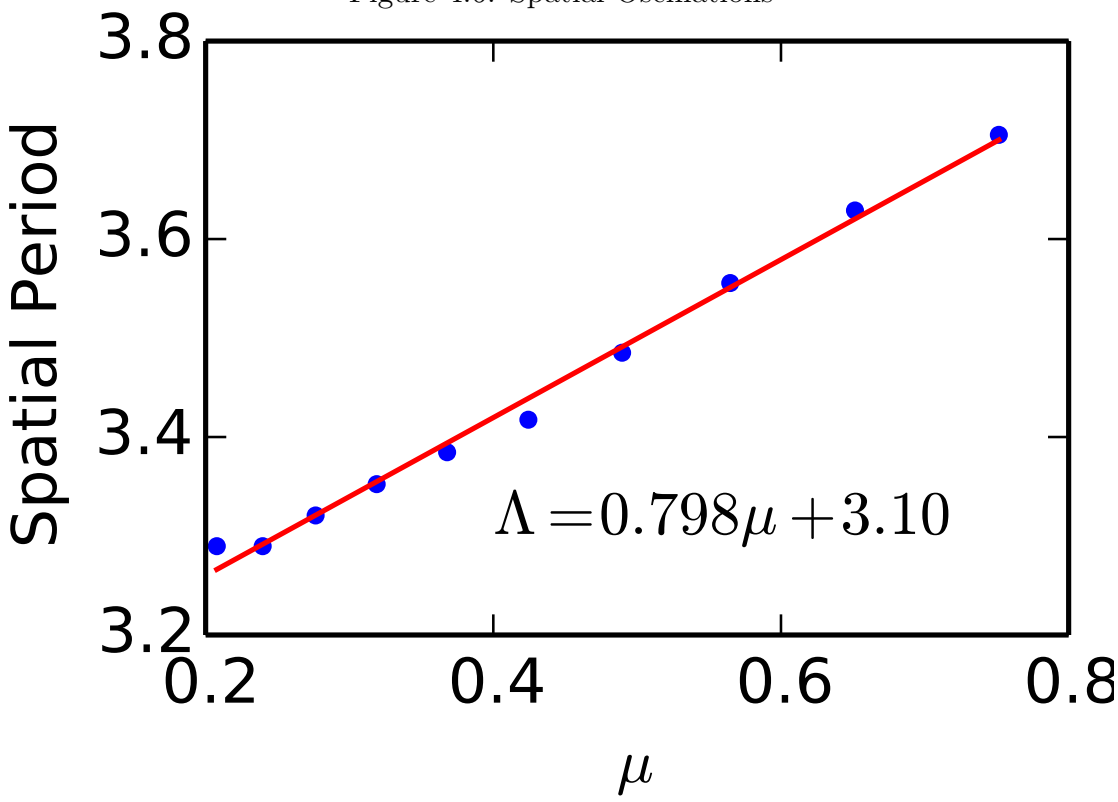

Spatial period of oscillation of vortex mode energy as two vortices are separated in the x direction, as in Fig. 4.4. The spatial period changes as the chemical potential μ is varied (all other parameters are as in the aforementioned figure). For plotted values of μ, the Chern number was 3. Larger values of μ were inaccessible due to edge-vortex hybridization.

4.3.1 Vortex Core Mode Oscillations

When the separation between two magnetic vortices is adjusted, the spectrum shifts, as seen in Fig. 4.4 and Fig. 4.5. Most notably, the energies of the lowest quasiparticles exhibit damped oscillation. The dominant Fourier component of these oscillations is found (and inverted) to give a spatial period. The spatial period Λ is found as a function of the chemical potential μ in FIG. 4.6 for $t_1 = -2$, $\Delta_1 = 0.5$ (energy given in terms of t_2). The only values of μ shown are where the vortex core mode only hybridized weakly with the edge modes. Even small distortions to the oscillations disturb the calculation of the spatial period significantly. Systems close to criticality were therefore not examined. In particular, only points in the Chern number 3 phase were far enough from criticality to be calculated reliably. In that region, Λ was found to depend linearly on μ, with slope close to 0.8. As mentioned before, these oscillations have been analytically [CLG09] and numerically [MM10] investigated before (for slightly different systems) with a period $\sim \frac{2\pi}{k_F}$, due to the oscillations in the vortex mode wavefunctions on the same spatial period.

4.3.2 Majorana Mode Count

For Chern number 3, only one vortex mode exists; see FIG. 4.4. However, for Chern number ± 2, two 0-energy modes develop when two vortices are introduced. Modes in the -2 region near $t_1 = 0$ are examined in FIG. 4.5. The Chern number $+2$ region (with, e.g., $(t_1/\mu, t_2/\mu) = (-1.5, 2)$ in Fig. 3.6) probably also supports an additional vortex mode, but the issue there is complicated by the fact that the system is usually quite close to criticality. I.e., the zeros of $\Delta(k)$ occur where h_k is relatively small, leading to a divergence of correlation lengths. Effective analysis requires that the edge-vortex hybridization be suppressed; much larger systems would have to be simulated.

4.3.3 Disorder

Here, we discuss the results on-site disorder to O_i mentioned earlier. The same simulations with disorder added are shown in FIG. 4.7. For weak disorder, pairs of vortex modes that exist without disorder persist after turning on the weak disorder. In reality, vortices would become pinned to disorder sites. A more detailed calculation would not install vortices at prespecified locations. Despite these caveats, we believe that these additional modes warrant further analytical investigation.

4.4 Conclusion

Chiral p-wave superconductors on a lattice support additional, interesting phases beyond the two well-known (topologically trivial) BEC and (Chern number 1) BCS phases. The Chern number ± 2 phases can be understood intuitively as a pair of weakly interacting sublattices: the defect modes appear to survive variation of parameters as well as the addition of weak disorder. It is expected [Roy10] that some perturbation of the Hamiltonian will hybridize the defect states, though the precise form of the interaction has not been determined. The Chern number 3 phase, on the other hand, does not support any additional modes. The consequences of including NNN interactions in two-dimensional chiral superconductors are worthy of analytical attention.

Figure 4.7: Disorder Modes

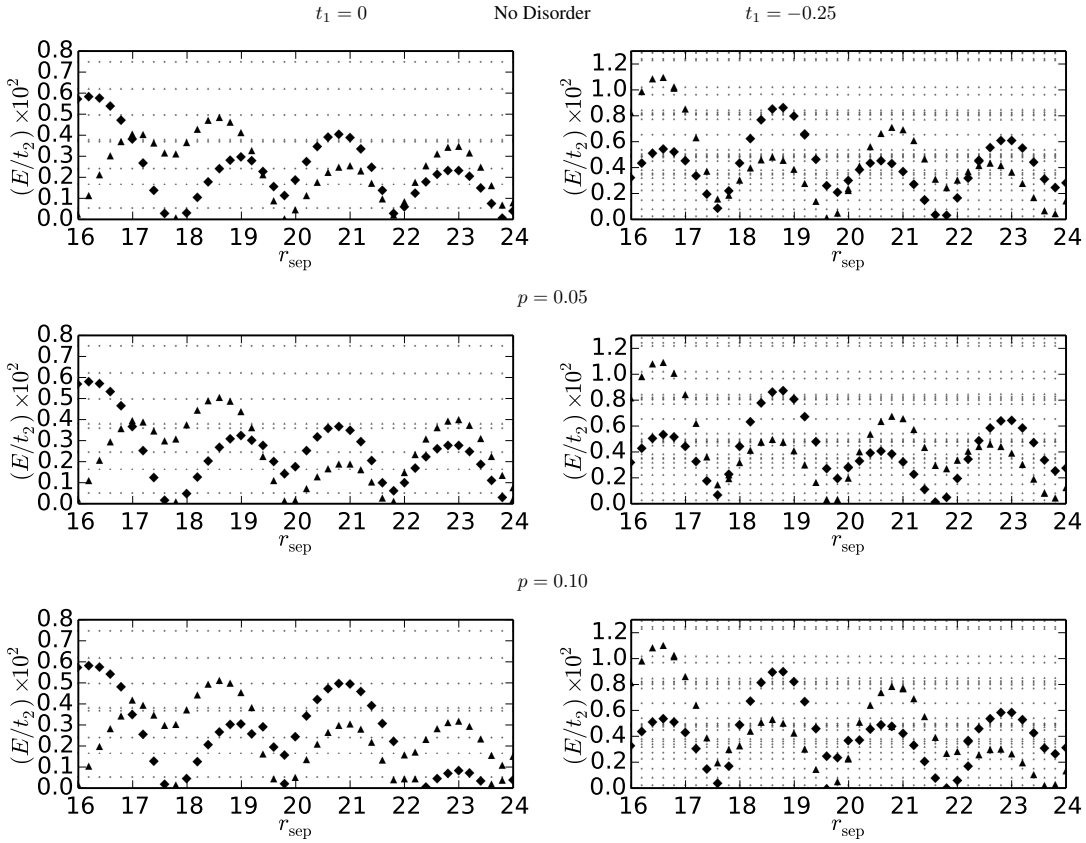

Compare with FIG. 4.5, the choices of parameters is the same same. The focus of these figures is on the disorder, of strength $E_d = \frac{1}{10}$ and probability p. All energies give in terms of t_2. Although disorder destroys inversion symmetry (discussed in Appendix A.8), there is still significant overlap of wavefunctions with their spatial inversion partner. The different markers indicate the sign of the overlap: positive is diamond; negative is triangle; and weak overlap is indicated by a circle. Weak disorder *should not* destroy exponentially damped oscillating behavior if it already exists; no qualitative changes occur when weak disorder is added.

CHAPTER 5

Numerical Studies of Chiral Superconductors with Next-Nearest-Neighbor Terms

5.1 Introduction

Chiral superconductors break time-reversal symmetry, removing any symmetry protection of zero edge currents. Small edge currents can indeed be generated in the self-consistent mean field limit, while experimental evidence remains ambiguous [BMH05]. Given the sundry forms of superconducting pairing potential, one might expect a respective plethora of edge currents. However, at least in the continuum limit, one expects zero edge current in system with greater than $\ell = 1$, or p-wave, superconductivity [TNO15]. Here, we investigate several different forms of edge current possible with $\ell = 1$ and also $\ell = 2$ in the *lattice* case, which we find compatible with previous results when a continuum limit is taken.

5.2 Self-Consistent

The standard, lattice Hamiltonian

$$H = \sum_{ij} t_{ij} c_i^\dagger c_j + \frac{1}{2} \sum_{ij} \Delta_{ij} c_i^\dagger c_j^\dagger + \text{h.c.} \tag{5.1}$$

which we always take to satisfy a self-consistency equation

$$\Delta_{ij} = \sum_{ij} g_{ij} \langle E_0 | \, c_i c_j \, | E_0 \rangle \tag{5.2}$$

where g_{ij} takes different forms depending on the channel of pairing we are interested in investigating. For the work here, a local interaction

$$g_{ij} = g_1 \left[\delta_{i+a\hat{x},j} + \delta_{i-a\hat{x},j} + \delta_{i+a\hat{y},j} + \delta_{i-a\hat{y},j}\right] + g_2 \left[\delta_{i+a(\hat{x}+\hat{y}),j} + \delta_{i-a(\hat{x}+\hat{y}),j} + \delta_{i+a(\hat{x}-\hat{y}),j} + \delta_{i-a(\hat{x}-\hat{y}),j}\right] \quad (5.3)$$

where a is the lattice spacing, was used. This form allows for nearest- and next-nearest neighbor interactions. Depending on the channel of interest, an initial form for the pairing interactions is chosen, $\Delta_{ij}^{(0)}$. Eqn. 5.1 is then solved, and the correlators $\langle E_0 | \, c_i c_j \, | E_0 \rangle$ calculated (see Appendix A.5 and A.6). If Eqn. 5.2 is satisfied to within some tolerance ϵ, the process is complete. If not,

$$\Delta_{ij}^{(n+1)} = \alpha \Delta_{ij}^{(n)} + (1-\alpha) \sum_{ij} g_{ij} \langle c_i c_j \rangle \quad (5.4)$$

is used in the next iterative step. The parameter α is chosen between 0 and 1 to expedite the convergence of Δ to its final value, and can reduce the effect of oscillations in Δ with iteration number n. The final step of this iterative process always uses $\alpha = 1$ to guarantee that a genuine self-consistent Δ is found. Generically, for a sufficiently large system, this process leads to a Δ that is insensitive to the precise location when deep inside the system, as expected. For the purpose of the calculation of currents, the value of this self-consistency cannot be understated. The currents will not be gauge invariant or conserved (see Appendix A.9).

5.3 Currents

Once a particular system is iterated to self-consistency, the correlators can be calculated, (see Appendix A.5 and A.6), which can then be used to find the currents (see Appendix A.9). Plots of edge currents are shown on the following two pages for several different values of parameters. These results demonstrate the aforementioned techniques and illustrate some interesting features of the situation.

Figure 5.1: $d + id$ currents with weak NNN-terms.

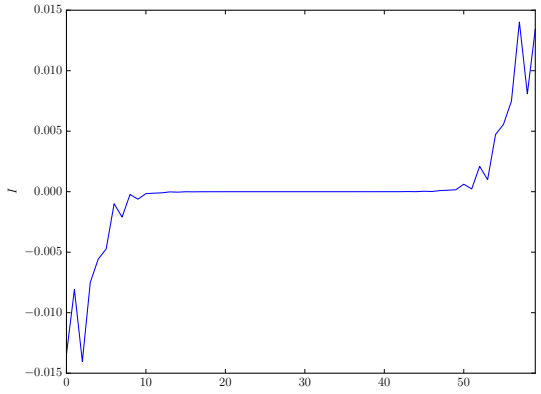

$d_{x^2-y^2} + id_{xy}$ superconductor currents. $t_1 = -1.2$, and $\Delta_1^{d_{x^2-y^2}+id_{xy}}, \Delta_2^{d_{x^2-y^2}+id_{xy}} = 0.8, 0.2$. Total edge current $I_e = 0.1245$ (in units of $e\mu/\hbar$, where the chemical potential $\mu = 1$)

Figure 5.2: $d + id$ currents with very weak NNN-terms.

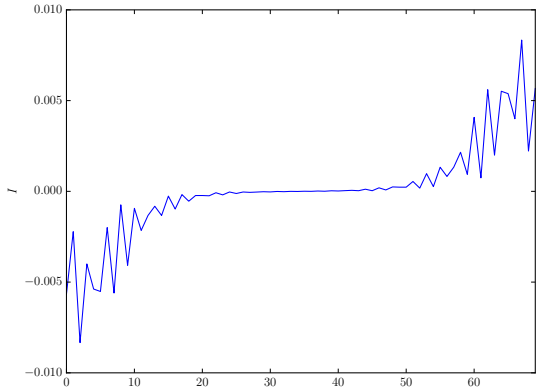

$d_{x^2-y^2} + id_{xy}$ superconductor currents. $t_1 = -1.2$, and $\Delta_1^{d_{x^2-y^2}+id_{xy}}, \Delta_2^{d_{x^2-y^2}+id_{xy}} = 0.8, 0.08$. Total edge current $I_e = 0.0534$ (in units of $e\mu/\hbar$, where the chemical potential $\mu = 1$)

Figure 5.3: $p + ip$ currents with weak NNN-terms, for Chern number -1

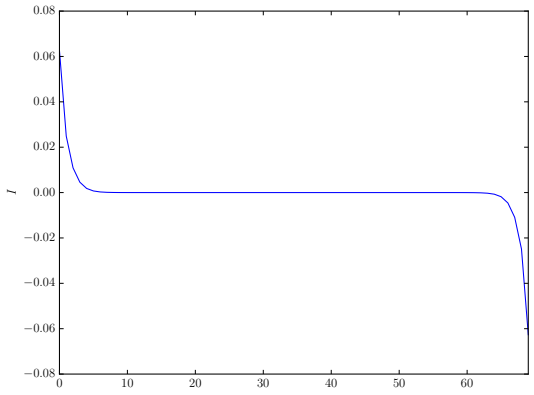

$p_x + ip_y$ superconductor currents. $t_1 = 1.0$, and $\Delta_1^{p_x+ip_y}, \Delta_2^{p_x+ip_y} = 0.6, 0.1$. Total edge current $I_e = 0.106$ (in units of $e\mu/\hbar$, where the chemical potential $\mu = 1$)

Figure 5.4: $p + ip$ currents with very weak NN-terms, for Chern number $+3$

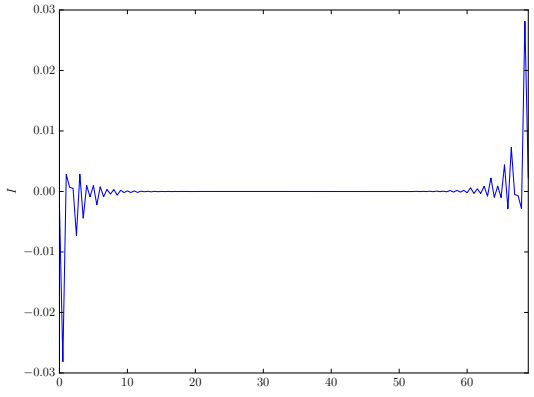

$p_x + ip_y$ superconductor currents. $t_1, t_2 = 0.5, -1.0$, and $\Delta_1^{p_x+ip_y}, \Delta_2^{p_x+ip_y} = 0.6, 0.1$. Total edge current $I_e = 0.037$ (in units of $e\mu/\hbar$, where the chemical potential $\mu = 1$)

The situation is clearly more complicated than simple topology. And, in particular, the edge currents for $d+id$ are certainly not generically zero. One interesting question is then, what precisely is different in the lattice case from the continuum case. Along with the analysis of the various phases for the $p+ip$ superconductor is the content of the paper in preparation.

APPENDIX A

Solving the Bogoliubov-de Gennes Equations

Several routine calculations that were omitted from the body of the text are included here for completeness.

A.1 Supplement to the Introduction

The Hamiltonian is (up to a constant)

$$H = \frac{1}{2}\sum_{k} \begin{bmatrix} (a^\dagger_{\mathbf{k}})^\top & (a_{-\mathbf{k}})^\top \end{bmatrix} \mathcal{H}_{\mathbf{k}} \begin{bmatrix} a_{\mathbf{k}} \\ a^\dagger_{-\mathbf{k}} \end{bmatrix} \tag{A.1}$$

where

$$\mathcal{H}_{\mathbf{k}} = \begin{bmatrix} \xi_{\mathbf{k}} & |d_{\mathbf{k}}|e^{i\phi_{\mathbf{k}}} \\ |d_{\mathbf{k}}|e^{-i\phi_{\mathbf{k}}} & -\xi_{\mathbf{k}} \end{bmatrix} \tag{A.2}$$

which is diagonalized by

$$\mathcal{U}_{\mathbf{k}} = \begin{bmatrix} u_{\mathbf{k}} & \bar{v}_{\mathbf{k}} \\ v_{\mathbf{k}} & \bar{u}_{\mathbf{k}} \end{bmatrix} \tag{A.3}$$

with eigenvalues $E_{\mathbf{k}} = \sqrt{\xi^2_{\mathbf{k}} + |d_{\mathbf{k}}|^2}$ and $-E_{\mathbf{k}}$, and

$$\begin{bmatrix} u_{\mathbf{k}} \\ v_{\mathbf{k}} \end{bmatrix} = \begin{bmatrix} \frac{e^{i\phi_{\mathbf{k}}/2}}{\sqrt{2}}\sqrt{1 - \frac{\xi_{\mathbf{k}}}{\sqrt{\xi^2_{\mathbf{k}}+|d_{\mathbf{k}}|^2}}} \\ \frac{e^{-i\phi_{\mathbf{k}}/2}}{\sqrt{2}}\sqrt{1 + \frac{\xi_{\mathbf{k}}}{\sqrt{\xi^2_{\mathbf{k}}+|d_{\mathbf{k}}|^2}}} \end{bmatrix} \tag{A.4}$$

Notice that

$$H = \frac{1}{2}\sum_k \begin{bmatrix}(a_{\mathbf{k}}^\dagger)^\top & (a_{-\mathbf{k}})^\top\end{bmatrix} \mathcal{U}_{\mathbf{k}}\mathcal{U}_{\mathbf{k}}^\dagger \mathcal{H}_{\mathbf{k}} \mathcal{U}_{\mathbf{k}}\mathcal{U}_{\mathbf{k}}^\dagger \begin{bmatrix} a_{\mathbf{k}} \\ a_{-\mathbf{k}}^\dagger \end{bmatrix}$$

$$= \frac{1}{2}\sum_k \begin{bmatrix}(a_{\mathbf{k}}^\dagger)^\top & (a_{-\mathbf{k}})^\top\end{bmatrix} \mathcal{U}_{\mathbf{k}} \begin{bmatrix} E_{\mathbf{k}} & 0 \\ 0 & -E_{\mathbf{k}} \end{bmatrix} \mathcal{U}_{\mathbf{k}}^\dagger \begin{bmatrix} a_{\mathbf{k}} \\ a_{-\mathbf{k}}^\dagger \end{bmatrix} \quad \text{(A.5)}$$

Multiplying out

$$\begin{bmatrix}(\Psi_{\mathbf{k}}^\dagger)^\top & (\Psi_{\mathbf{k}})^\top\end{bmatrix} := \begin{bmatrix}(a_{\mathbf{k}}^\dagger)^\top & (a_{-\mathbf{k}})^\top\end{bmatrix} \mathcal{U}_{\mathbf{k}} \quad \text{(A.6)}$$

A.2 Real-space Formulation

The introduction worked out the diagonalization of the Bogoliubov-de Gennes equations for superconductors in momentum space. A similar calculation can be performed in real space. Here, an outline of this is given. The tight-binding Hamiltonian of the form

$$H = \sum_{ij} h_{ij} c_i^\dagger c_j + \frac{1}{2}\sum_{ij} \Delta_{ij} c_i^\dagger c_j^\dagger + \text{h.c.} \quad \text{(A.7)}$$

For notational simplicity, put

$$\vec{c} = \begin{bmatrix} c_0 \\ \vdots \\ c_n \end{bmatrix}$$

This Hamiltonian can be written, up to an additive constant, as

$$H = \begin{bmatrix}(\vec{c}^\dagger)^\top & (\vec{c})^\top\end{bmatrix} \overbrace{\frac{1}{2}\begin{bmatrix} h & \Delta \\ \Delta^\dagger & -h^\top \end{bmatrix}}^{\mathcal{H}} \begin{bmatrix} \vec{c} \\ \vec{c}^\dagger \end{bmatrix}$$

To see this:

$$\begin{aligned}
\frac{1}{2}\begin{bmatrix}(\vec{c}^\dagger)^\top & (\vec{c})^\top\end{bmatrix}\begin{bmatrix}h & \Delta \\ \Delta^\dagger & -h^\top\end{bmatrix}\begin{bmatrix}\vec{c} \\ \vec{c}^\dagger\end{bmatrix} &= \frac{1}{2}\begin{bmatrix}(\vec{c}^\dagger)^\top & (\vec{c})^\top\end{bmatrix}\begin{bmatrix}h\vec{c}+\Delta\vec{c}^\dagger \\ \Delta^\dagger\vec{c}-h^\top\vec{c}^\dagger\end{bmatrix} \\
&= \frac{1}{2}\left[(\vec{c}^\dagger)^\top h\vec{c}+(\vec{c}^\dagger)^\top\Delta\vec{c}^\dagger+(\vec{c})^\top\Delta^\dagger\vec{c}-(\vec{c})^\top h^\top\vec{c}^\dagger\right] \\
&= \frac{1}{2}\sum_{ij}c_i^\dagger h_{ij}c_j-\frac{1}{2}\sum_{ij}c_i h_{ji}c_j^\dagger+\frac{1}{2}\sum_{ij}c_i^\dagger\Delta_{ij}c_j^\dagger+\frac{1}{2}\sum_{ij}c_i\Delta_{ij}^\dagger c_j \\
&= \frac{1}{2}\sum_{ij}c_i^\dagger h_{ij}c_j+\frac{1}{2}\sum_{ij}h_{ji}c_j^\dagger c_i+\frac{1}{2}\sum_{ij}c_i^\dagger\Delta_{ij}c_j^\dagger+\frac{1}{2}\sum_{ij}c_i\bar{\Delta}_{ji}c_j+\text{constant} \\
&= \sum_{ij}h_{ij}c_i^\dagger c_j+\frac{1}{2}\sum_{ij}\Delta_{ij}c_i^\dagger c_j^\dagger+\frac{1}{2}\sum_{ij}\bar{\Delta}_{ij}c_j c_i+\text{constant} = H+\text{constant}
\end{aligned}$$

as claimed. Additionally,

$$H^\dagger = \begin{bmatrix}(\vec{c}^\dagger)^\top & (\vec{c})^\top\end{bmatrix}\mathcal{H}^\dagger\begin{bmatrix}\vec{c} \\ \vec{c}^\dagger\end{bmatrix}$$

and

$$\mathcal{H}^\dagger = \frac{1}{2}\begin{bmatrix}\hat{h}^\dagger & \hat{\Delta} \\ \hat{\Delta}^\dagger & -\hat{h}^\top\end{bmatrix}$$

Self-adjointness requires that $h = h^\dagger$ (as we would expect). It follows immediately that $\bar{h} = h^\top$, leading to the slightly more common form

$$\mathcal{H} = \frac{1}{2}\begin{bmatrix}\hat{h} & \hat{\Delta} \\ \hat{\Delta}^\dagger & -\hat{\bar{h}}\end{bmatrix}$$

A.3 Spin Sectors

Taking spin into account, and taking the same simplifying assumptions as in the Introduction, the form of the BdG Hamiltonian simplifies

$$\mathcal{H} = \frac{1}{2}\begin{bmatrix}hI_\mathrm{s} & \Delta\chi \\ \Delta^\dagger\chi^\dagger & -\bar{h}I_\mathrm{s}\end{bmatrix}$$

where the spin sector of $\vec{c}$ has been separated out. I.e., essentially $\vec{c} = \vec{c}_\uparrow \oplus \vec{c}_\downarrow$. The two cases considered are spin-polarized (equivalently to spin-polarized) where

$$\chi = \begin{bmatrix} 1 & 0 \\ 0 & 0 \end{bmatrix}$$

and the sterile, spin-down, Fermions are ignored (leading to the odd-angular momentum pairing). And,

$$\chi = \begin{bmatrix} 0 & 1 \\ -1 & 0 \end{bmatrix}$$

In the even-spin sector (specifically the spin-polarized case), it is clear we can just ignore the spin-down sector entirely (i.e., its essentially just spinless fermions). For the odd spin pairing, the problem still separates into two independent sectors, but both interact via the pairing potential. Specifically, define

$$N_\pm = \frac{1}{\sqrt{2}} \begin{bmatrix} 1 \\ \pm i \end{bmatrix} \quad \text{so that} \quad \chi N_\pm = \pm i N_\pm$$

$$\frac{1}{2} \begin{bmatrix} hI_s & \Delta\chi \\ \Delta^\dagger \chi^\dagger & -\bar{h} I_s \end{bmatrix} \begin{bmatrix} uN_\pm \\ vN_\pm \end{bmatrix} = \frac{1}{2} \begin{bmatrix} h & \pm i\Delta \\ \mp i\Delta^\dagger & -\bar{h} \end{bmatrix} \begin{bmatrix} u \\ v \end{bmatrix} N_\pm$$

(the tensor sum is elided). The two sectors separate, and the only difference is that $\Delta^\top = \Delta$ for the odd spin-pairing case, and $\Delta^\top = -\Delta$ for the even spin-pairing case. It is important to emphasize here that, after this point, one (nontrivial) sector will is all that needs to be considered. If the spin sector needs to be considered, it will be mentioned explicitly.

A.4 Particle-Hole Symmetry

Even after factoring out the redundancy above, the two cases considered here still have a "particle-hole" symmetry left over. Notice that, if

$$\mathcal{S}^\dagger H \mathcal{S} = -H$$

and $H\left|E\right\rangle = E\left|E\right\rangle$, then

$$H[\mathcal{S}\left|E\right\rangle] = (H\mathcal{S})\left|E\right\rangle = (-\mathcal{S}H)\left|E\right\rangle = -\mathcal{S}E\left|E\right\rangle = (-E)[\mathcal{S}\left|E\right\rangle]$$

so that $\mathcal{S}\left|E\right\rangle$ is an energy eigenstate of energy $-E$. To wit, $\mathcal{S}$ converts energy eigenstates into energy eigenstates with negative energy. The exact form depends on the spin pairing (i.e., even or odd). The following exhibits $\mathcal{S}$ explicitly for both cases. Put K to be the complex conjugation operation (with respect to the standard basis). Notice that

$$\begin{aligned}\left\langle e_i\right| KAK\left|\psi\right\rangle = \left\langle e_i\right| \sum_j KA\left|e_j\right\rangle \overline{\left\langle e_j|\psi\right\rangle} \\ = \left\langle e_i\right| \sum_j \sum_{i'} \left|e_{i'}\right\rangle \bar{A}_{i'j} \left\langle e_j|\psi\right\rangle \\ = \sum_j \bar{A}_{ij} \left\langle e_j|\psi\right\rangle = \left\langle e_i\right| \bar{A}\left|\psi\right\rangle \quad \text{(A.8)}\end{aligned}$$

so that $KAK = \bar{A}$. To illustrate the idea, suppose $\psi = \begin{bmatrix} u \\ v \end{bmatrix}$. For the even spin-pairing case, notice that

$$\begin{bmatrix} (\vec{c}^\dagger)^\top & (\vec{c})^\top \end{bmatrix} \psi = \sum_i \left[c_i^\dagger u_i + c_i v_i \right]$$

but also

$$\begin{bmatrix} (\vec{c}^\dagger)^\top & (\vec{c})^\top \end{bmatrix} \sigma_1 K \psi = \begin{bmatrix} (\vec{c}^\dagger)^\top & (\vec{c})^\top \end{bmatrix} \begin{bmatrix} \bar{v} \\ \bar{u} \end{bmatrix} = \sum_i \left[c_i^\dagger \bar{v}_i + c_i \bar{u}_i \right]$$

Roughly, $\sigma_1 K$ corresponds to the adjoint operation. The odd spin-pairing case has a similar interpretation for $\sigma_2 K$.

Notwithstanding the above interpretation, for the odd spin-pairing case

$$\begin{aligned}(\sigma_1^\dagger \mathcal{H} \sigma_1) = \begin{bmatrix} 0 & 1 \\ 1 & 0 \end{bmatrix} \begin{bmatrix} h & \Delta \\ \Delta^\dagger & -\bar{h} \end{bmatrix} \begin{bmatrix} 0 & 1 \\ 1 & 0 \end{bmatrix} = \begin{bmatrix} 0 & 1 \\ 1 & 0 \end{bmatrix} \begin{bmatrix} \Delta & h \\ -\bar{h} & \Delta^\dagger \end{bmatrix} = \begin{bmatrix} -\bar{h} & \Delta^\dagger \\ \Delta & h \end{bmatrix} \\ = - \begin{bmatrix} \bar{h} & -\Delta^\dagger \\ -\Delta & -h \end{bmatrix}\end{aligned}$$

and therefore

$$(K^\dagger \sigma_1^\dagger \mathcal{H} \sigma_1 K) = -\begin{bmatrix} h & \Delta \\ \Delta^\dagger & -\bar{h} \end{bmatrix} = \mathcal{H}$$

because Δ is antisymmetric. A similar result holds for the spin-symmetric case. Consider the + branch:

$$(\sigma_2^\dagger \mathcal{H} \sigma_2) = \begin{bmatrix} 0 & -i \\ i & 0 \end{bmatrix} \begin{bmatrix} h & i\Delta \\ -i\Delta^\dagger & -\bar{h} \end{bmatrix} \begin{bmatrix} 0 & -i \\ i & 0 \end{bmatrix} = \begin{bmatrix} 0 & 1 \\ -1 & 0 \end{bmatrix} \begin{bmatrix} i\Delta & -h \\ -\bar{h} & i\Delta^\dagger \end{bmatrix} = \begin{bmatrix} -\bar{h} & i\Delta^\dagger \\ -i\Delta & h \end{bmatrix}$$
$$= -\begin{bmatrix} \bar{h} & -i\Delta^\dagger \\ i\Delta & -h \end{bmatrix}$$

and therefore

$$(K^\dagger \sigma_2^\dagger \mathcal{H} \sigma_2 K) = -\begin{bmatrix} h & i\Delta \\ -i\Delta^\dagger & -\bar{h} \end{bmatrix} = \mathcal{H}$$

because Δ is symmetric. Hence, for the spin-symmetric case, $\mathcal{S} = \sigma_1 K$ and for the spin-antisymmetric case $\mathcal{S} = \sigma_2 K$.

A.5 The Even Spin-Pairing Sector

For even spin-pairing, the sterile spin species is entirely ignored, and the fermions are treated as spinless. This case is simplest, and treated first for that reason. $\mathcal{H}$ is self-adjoint and can be diagonalized as

$$\mathcal{H}_{\alpha\beta} = \sum_n U_{\alpha n} E_n (U^\dagger)_{n\beta} \tag{A.9}$$

Furthermore, because of the $\mathcal{S}$ symmetry, the unitary matrix U can be taken of the form

$$U = \begin{bmatrix} \bar{Y} & X \\ \bar{X} & Y \end{bmatrix} \tag{A.10}$$

Defining

$$\begin{bmatrix} \Psi \\ \Psi^\dagger \end{bmatrix} = U^\dagger \begin{bmatrix} \vec{c} \\ \vec{c}^\dagger \end{bmatrix} = \begin{bmatrix} Y^\top & X^\top \\ X^\dagger & Y^\dagger \end{bmatrix} \begin{bmatrix} \vec{c} \\ \vec{c}^\dagger \end{bmatrix} = \begin{bmatrix} Y^\top \vec{c} + X^\top \vec{c}^\dagger \\ X^\dagger \vec{c} + \bar{Y}^\dagger \vec{c}^\dagger \end{bmatrix} \tag{A.11}$$

The Hamiltonian takes the form

$$H = \frac{1}{2}\begin{bmatrix}(\vec{c}^\dagger)^\top & (\vec{c})^\top\end{bmatrix} U\Lambda U^\dagger \begin{bmatrix}\vec{c}\\ \vec{c}^\dagger\end{bmatrix} = \frac{1}{2}\sum_i E_i\left[\Psi_i^\dagger\Psi_i - \Psi_i\Psi_i^\dagger\right] = \sum_i E_i\Psi_i^\dagger\Psi_i + \text{const} \tag{A.12}$$

The orthogonality of the eigenvectors of $\mathcal{H}$ (i.e., columns of U) translates into anti-commutation relations for the Ψ operators:

$$\{\Psi_n, \Psi_{n'}\} = \sum_i \left\{Y_{in}c_i + X_{in}c_i^\dagger, Y_{in'}c_i + X_{in'}c_i^\dagger\right\} = 2\sum_i Y_{in}X_{in} = 0 \tag{A.13}$$

and

$$\left\{\Psi_n, \Psi_{n'}^\dagger\right\} = \sum_i \left\{Y_{in}c_i + X_{in}c_i^\dagger, \bar{X}_{in'}c_i + \bar{Y}_{in'}c_i^\dagger\right\} = \sum_i \left[X_{in}\bar{X}_{in'} + Y_{in}\bar{Y}_{in'}\right] = \delta_{nn'} \tag{A.14}$$

So, we have that $\Psi_n^\dagger$ creates an excitation with energy E_n. The inverse transformation is useful (in particular to calculate the correlators). Apply U to the left of Eqn. A.11:

$$\begin{bmatrix}\vec{c}\\ \vec{c}^\dagger\end{bmatrix} = \begin{bmatrix}\bar{Y} & X\\ \bar{X} & Y\end{bmatrix}\begin{bmatrix}\Psi\\ \Psi^\dagger\end{bmatrix} = \begin{bmatrix}\bar{Y}\Psi + X\Psi^\dagger\\ \bar{X}\Psi + Y\Psi^\dagger\end{bmatrix} \tag{A.15}$$

Correlators are then found using the anti-commutation relations

$$\left\langle c_i^\dagger c_j\right\rangle = \sum_{nn'}\left\langle\left(\bar{X}_{in}\Psi_n + Y_{in}\Psi_n^\dagger\right)\left(\bar{Y}_{jn'}\Psi_{n'} + X_{jn'}\Psi_{n'}^\dagger\right)\right\rangle = \sum_n \bar{X}_{in}X_{jn} \tag{A.16}$$

and

$$\left\langle c_i^\dagger c_j^\dagger\right\rangle = \sum_{nn'}\left\langle\left(\bar{X}_{in}\Psi_n + Y_{in}\Psi_n^\dagger\right)\left(\bar{X}_{jn'}\Psi_{n'} + Y_{jn'}\Psi_{n'}^\dagger\right)\right\rangle = \sum_n \bar{X}_{in}Y_{jn} \tag{A.17}$$

A.6 The Odd Spin-Pairing Sector

For the odd spin-pairing case, the reduced $\mathcal{H}'_\pm = \begin{bmatrix}h' & \pm i\Delta'\\ \mp i\Delta'^\dagger & -\bar{h}'\end{bmatrix}$ must be solved. Before beginning, notice that

$$\mathcal{H}'_\pm = \sigma_3\mathcal{H}'_\mp\sigma_3$$

so we just work with $\mathcal{H}' = \mathcal{H}'_+$, and use σ_3 to get access to the other solutions. As in the spin-even case,

$$\mathcal{H}'_{\alpha\beta} = \sum_n U'_{\alpha n} E_n (U'^{\dagger})_{n\beta}$$

with unitary matrix U' that can, because of $\mathcal{S}$ symmetry, be taken of the form

$$U' = \begin{bmatrix} \bar{Y} & X \\ -\bar{X} & Y \end{bmatrix}$$

The full unitary matrix diagonalizing $\mathcal{H}$ is taken as (where the tensor products are elided)

$$U = \begin{bmatrix} \bar{Y}N_+ & \bar{Y}N_- & XN_+ & -XN_- \\ -\bar{X}N_+ & \bar{X}N_- & YN_+ & YN_- \end{bmatrix}$$

Again, define

$$\begin{bmatrix} \Psi_+ \\ \Psi_- \\ \Psi_-^\dagger \\ \Psi_+^\dagger \end{bmatrix} = U^\dagger \begin{bmatrix} \vec{c} \\ \vec{c}^\dagger \end{bmatrix}$$

The calculation of the Hamiltonian and anticommutators proceeds in essentially the same way as above. In particular, since N_+ and N_- are orthogonal, the $+$ and $-$ sectors contribute separately. This routine calculation is omitted. The inverse transformation yields

$$\begin{bmatrix} \vec{c} \\ \vec{c}^\dagger \end{bmatrix} = U \begin{bmatrix} \Psi_+ \\ \Psi_- \\ \Psi_-^\dagger \\ \Psi_+^\dagger \end{bmatrix} = \begin{bmatrix} \bar{Y}N_+\Psi_+ + \bar{Y}N_-\Psi_- + XN_+\Psi_-^\dagger - XN_-\Psi_+^\dagger \\ -\bar{X}N_+\Psi_+ + \bar{X}N_-\Psi_- + YN_+\Psi_-^\dagger + YN_-\Psi_+^\dagger \end{bmatrix}$$

The correlators can then be found using the anti-commutation relations

$$\left\langle c_{i\uparrow}^\dagger c_{j\uparrow}^\dagger \right\rangle = \sum_{nn'} \left\langle \left(-\bar{X}_{in}\Psi_{+,n} + \bar{X}_{in}\Psi_{-,n}\right) \left(Y_{jn'}\Psi_{-,n'}^\dagger + Y_{jn'}\Psi_{+,n'}^\dagger\right) \right\rangle = 0 \quad \text{(A.18)}$$

and

$$\left\langle c^\dagger_{i\uparrow} c^\dagger_{j\downarrow} \right\rangle = \sum_{nn'} \left\langle \left(-\bar{X}_{in}\Psi_{+,n} + \bar{X}_{in}\Psi_{-,n}\right)\left(Y_{jn'}\Psi^\dagger_{-,n'} - Y_{jn'}\Psi^\dagger_{+,n'}\right)\right\rangle = -2\sum_n \bar{X}_{in}Y_{jn} \tag{A.19}$$

and

$$\left\langle c^\dagger_{i\uparrow} c_{j\uparrow} \right\rangle = \sum_{nn'} \left\langle \left(-\bar{X}_{in}\Psi_{+,n} + \bar{X}_{in}\Psi_{-,n}\right)\left(X_{jn'}\Psi^\dagger_{-,n'} - X_{jn'}\Psi^\dagger_{+,n'}\right)\right\rangle = -2\sum_n \bar{X}_{in}X_{jn} \tag{A.20}$$

and

$$\left\langle c^\dagger_{i\uparrow} c_{j\downarrow} \right\rangle = \sum_{nn'} \left\langle \left(-\bar{X}_{in}\Psi_{+,n} + \bar{X}_{in}\Psi_{-,n}\right)\left(X_{jn'}\Psi^\dagger_{-,n'} + X_{jn'}\Psi^\dagger_{+,n'}\right)\right\rangle = 0 \tag{A.21}$$

(terms that immediately vanish, such as $\psi\,|0\rangle$, are elided for readability).

A.7 Efficient Calculation for Spin Symmetric

As seen earlier, solving the quadratic Hamiltonian amounts to diagonalizing a matrix

$$H = \begin{bmatrix} A & B \\ -\bar{B} & -\bar{A} \end{bmatrix}$$

where $A^\dagger = A$ and $B^\top = -B$. Because $\tau_x K H K \tau_x = -H$, this task is easier than a general $4n^2$ matrix. To see this, notice that

$$H^2 = \begin{bmatrix} A & B \\ -\bar{B} & -\bar{A} \end{bmatrix}\begin{bmatrix} A & B \\ -\bar{B} & -\bar{A} \end{bmatrix} = \begin{bmatrix} A^2 - B\bar{B} & AB - B\bar{A} \\ -\bar{B}A + \bar{A}\bar{B} & -\bar{B}B + \bar{A}^2 \end{bmatrix} = \begin{bmatrix} C & D \\ \bar{D} & \bar{C} \end{bmatrix}$$

where

$$C^\dagger = A^\dagger A^\dagger - \bar{B}^\dagger B^\dagger = A^2 - B^\top \bar{B}^\top = C$$

and

$$D^\top = B^\top A^\top - \bar{A}^\top B^\top = -B\bar{A} + AB = D$$

It's clear that $\tau_x K H^2 K \tau_x = H^2$; the pairs of eigenstates of H are now pairs of *degenerate* eigenstates. Roughly, we diagonalize along the subspace of eigenstates of $K\tau_x$,

Real H

To illustrate the point simply, if $H = \bar{H}$, we can ignore complex conjugation (since the eigenstates can be chosen real), and require that they take the form $\begin{bmatrix} u \\ \pm u \end{bmatrix}$. To wit,

$$H^2 \begin{bmatrix} u \\ \pm u \end{bmatrix} = \begin{bmatrix} Cu \pm Du \\ Du \pm Cu \end{bmatrix} = \begin{bmatrix} (C \pm D)u \\ \pm(C \pm D)u \end{bmatrix}$$

Demanding that this be an eigenstate, we see that

$$(C \pm D)u = E^2 u$$

The eigenvalues of the operator $T_\pm = C \pm D$ are therefore the square of the energies and the eigenvectors $u_\pm(E)$ of $T_\pm$ with energy E^2 corresponds precisely with the eigenvectors $\mu_\pm(E)$ of H^2,

$$H^2 \begin{bmatrix} u_\pm(E) \\ \pm u_\pm(E) \end{bmatrix} = E^2 \begin{bmatrix} u_\pm(E) \\ \pm u_\pm(E) \end{bmatrix} = E^2 \mu_\pm(E)$$

Moreover, $\mu_\pm(E)$ are necessarily linear combinations of the eigenstates of energy $\pm E$, $\phi_\pm(E)$ of H:

$$\mu_\pm(E) = \alpha_\pm(E)\phi_+(E) + \beta_\pm(E)\phi_-(E)$$

We know that $\tau_x \phi_\pm(E) = \phi_\mp(E)$, and $\tau_x \mu_\pm(E) = \pm\mu_\pm(E)$, so, applying $\pm\tau_x$ to both sides,

$$\mu_\pm(E) = \pm\beta_\pm(E)\phi_+(E) \pm \alpha_\pm(E)\phi_-(E)$$

to obtain $\beta_\pm(E) = \pm\alpha_\pm(E)$, or, using normalization,

$$\mu_\pm(E) = \alpha_\pm(E)\left[\phi_+(E) \pm \phi_-(E)\right] = \frac{1}{\sqrt{2}}\left[\phi_+(E) \pm \phi_-(E)\right]$$

Or,

$$\phi_\pm(E) = \frac{1}{\sqrt{2}}\left[\mu_+(E) \pm \mu_-(E)\right] = \frac{1}{\sqrt{2}} \begin{bmatrix} u_+(E) \pm u_-(E) \\ u_+(E) \mp u_-(E) \end{bmatrix}$$

Giving us a direct method to calculate the eigenvectors by diagonalizing two n^2 matrices rather than one $4n^2$ matrix.

General H

We treat n-dimensional complex vectors as $2n$-dimensional real vectors:

$$u \to \begin{bmatrix} \Re u \\ \Im u \end{bmatrix}$$

and n by n complex matrices and $2n$ by $2n$ real matrices:

$$X \to \begin{bmatrix} \Re X & -\Im X \\ \Im X & \Re X \end{bmatrix}$$

Notice that the complex conjugation is a matrix in this representation of complex numbers:

$$K \to \begin{bmatrix} I_n & 0 \\ 0 & -I_n \end{bmatrix}$$

Thusly equipped, we remark that it makes sense to ask for eigenstates of $K\tau_x$. In particular

$$K\tau_x \begin{bmatrix} u \\ \pm\bar{u} \end{bmatrix} = K \begin{bmatrix} \pm\bar{u} \\ u \end{bmatrix} = \pm \begin{bmatrix} u \\ \pm\bar{u} \end{bmatrix}$$

We essentially repeat the work in the real case now:

$$H^2 \begin{bmatrix} u \\ \pm\bar{u} \end{bmatrix} = \begin{bmatrix} (C \pm DK)u \\ \pm K(C \pm DK)u \end{bmatrix}$$

and we find the (complex) n by n equation that needs to be solved. We remark that this equation is not complex-linear; we must solve it in the sense we outlined above:

$$\begin{aligned} C \pm DK \to \begin{bmatrix} C_R & -C_I \\ C_I & C_R \end{bmatrix} \pm \begin{bmatrix} D_R & -D_I \\ D_I & D_R \end{bmatrix} \begin{bmatrix} I_n & 0 \\ 0 & -I_n \end{bmatrix} &= \begin{bmatrix} C_R & -C_I \\ C_I & C_R \end{bmatrix} \pm \begin{bmatrix} D_R & D_I \\ D_I & -D_R \end{bmatrix} \\ &= \begin{bmatrix} C_R \pm D_R & -C_I \pm D_I \\ C_I \pm D_I & C_R \mp D_R \end{bmatrix} \end{aligned}$$

The condition that $D^\top = D$ converts directly to $D_R^\top = D_R$ and $D_I^\top = D_I$, while $C^\dagger = C$ gives $C_R^\top = C_R$ and $C_I^\top = -C_I$. Notice that

$$\begin{bmatrix} C_R \pm D_R & -C_I \pm D_I \\ C_I \pm D_I & C_R \mp D_R \end{bmatrix}^\top = \begin{bmatrix} C_R \pm D_R & C_I^\top \pm D_I \\ -C_I^\top \pm D_I & C_R \mp D_R \end{bmatrix}$$

So that this matrix is real and symmetric. This matrix therefore has real eigenvalues, and the complex equation has eigenvectors with possibly complex eigenvalues

$$C \pm DK = \lambda_\pm u_\pm$$

However, notice that

$$(C - DK)(iu_+) = i(C + DK)u_+ = \lambda_+(iu_+)$$

Notice, however, that multiplying u by i takes us from

$$\begin{bmatrix} u \\ \bar{u} \end{bmatrix} \to \begin{bmatrix} iu \\ -i\bar{u} \end{bmatrix}$$

The above remark tells us that, when we consider complex linear combinations, we can ignore one of these two equations—i.e., we get all the required data by looking at complex linear combinations of the eigenvectors produced from just $C + DK$. It much computationally easier to diagonalize H on each subspace. In short: instead of diagonalizing a $2n \times 2n$ complex matrix, we diagonalize a $2n \times 2n$ real matrix, and then diagonalize each eigenspace separately.

A.8 Inversion Symmetry Simplifications

The overarching strategy demonstrated above is to diagonalize the smallest possible space. For the work performed here, our desire was to see the behavior of a single edge of a cylinder, presumably shielded from other distant edges by the intervening superconductor bulk. To accomplish this, we have chosen a Hamiltonian with spatial inversion symmetry. The invervening bulk should shield the edge of interest from any other effects far away from it.

Having chosen this simplified Hamiltonian, we can make a number of remarks that will simplify the numerical calculations. To do this, we must establish a little bit of notation, restated here from prior work. Let $\mathcal{I}$ perform a spatial inversion of a wavefunction. I.e., if $\begin{bmatrix} u \\ v \end{bmatrix}$ is a Nambu spinor, then $\mathcal{I}u$ inverts the particle part of that wavefunction. Notice that $(\mathcal{I}h)_{ij} = h_{-i,-j}$. Next, put $\mathscr{I} = \tau_3 \otimes \mathcal{I}$ (τ_3 acts on the space of Nambu spinors). It is easy to see that $\mathscr{I}^2 = 1$ and $\mathscr{I}^\dagger = \mathscr{I}$, so the eigenvalues of $\mathscr{I}$ are ± 1. The inversion symmetry's action on the Hamiltonian as follows:

$$\begin{aligned} \mathscr{I}^\dagger \mathcal{H}_{ij} \mathscr{I} &= \mathcal{I}^\dagger \tau_3^\dagger \mathcal{H}_{ij} \tau_3 \mathcal{I} \\ &= \mathcal{I}^\dagger \begin{bmatrix} h_{ij} & -\Delta_{ij} \\ -\bar{\Delta}_{ji} & -\bar{h}_{ij} \end{bmatrix} \mathcal{I} = \begin{bmatrix} h_{-i-j} & -\Delta_{-i-j} \\ -\bar{\Delta}_{-j-i} & -\bar{h}_{-i-j} \end{bmatrix} \\ &= \begin{bmatrix} h_{ij} & \Delta_{ij} \\ \bar{\Delta}_{ji} & -h_{ij} \end{bmatrix} = \mathcal{H}_{ij} \end{aligned} \quad \text{(A.22)}$$

Thus, the inversion symmetry $\mathscr{I}$ relates quasiparticles of the form (u_i, v_i) to $(u_{-i}, -v_{-i})$. For appropriate energy eigenstates, $\psi = \pm \mathscr{I}\psi$ and the subparts u and v therefore have separate (and opposite) inversion symmetries given by $\mathcal{I}u = \pm u$ and $\mathcal{I}v = \mp v$. These eigenvalues can be changed using the Bogoliubov-de Gennes particle-hole symmetry (i.e., $\Xi = \tau_1 \otimes K$, where K is complex conjugation); the symmetry-related negative-energy pair has opposite $\mathscr{I}$ eigenvalue:

$$\Xi \mathscr{I} = \tau_1 K \tau_3 \mathscr{I} = -i\tau_2 \mathscr{I} = -\mathscr{I}\Xi \quad \text{(A.23)}$$

Next notice that both $\begin{bmatrix} u \\ v \end{bmatrix}$ and $\begin{bmatrix} \mathcal{I}u \\ -\mathcal{I}v \end{bmatrix}$ are eigenstates of H with the same eigenvalue. It therefore follows that both

$$\begin{bmatrix} u \pm \mathcal{I}u \\ v \mp \mathcal{I}v \end{bmatrix}$$

are also eigenvectors of H. Moreover, these two solutions can be related by Bogoliubov-de Gennes particle hole interchange. One may therefore restrict attention to the particle part has even symmetry, and the hole part has odd symmetry (or vice-versa). To exploit this, consider a representation of the linear space such that the spatial inversion operator $\mathcal{I}$ acts by

$$\mathcal{I}\begin{bmatrix} a \\ b \end{bmatrix} = \begin{bmatrix} b \\ a \end{bmatrix}$$

(e.g., the top spot refers to the left side of the system, indexed left to right, and the bottom spot refers to the right side, indexed right to left). Define h_0 and h_1 by

$$h\begin{bmatrix} a \\ b \end{bmatrix} = \begin{bmatrix} h_0 a + h_1 b \\ \cdots \end{bmatrix}$$

and likewise for Δ:

$$\Delta\begin{bmatrix} a \\ b \end{bmatrix} = \begin{bmatrix} \Delta_0 a + \Delta_1 b \\ \cdots \end{bmatrix}$$

Next, notice that

$$h\begin{bmatrix} a \\ b \end{bmatrix} = h\mathcal{I}\begin{bmatrix} b \\ a \end{bmatrix} = \mathcal{I}h\begin{bmatrix} b \\ a \end{bmatrix} = \begin{bmatrix} \cdots \\ h_0 b + h_1 a \end{bmatrix}$$

and, similarly,

$$\Delta\begin{bmatrix} a \\ b \end{bmatrix} = \Delta\mathcal{I}\begin{bmatrix} b \\ a \end{bmatrix} = -\mathcal{I}\Delta\begin{bmatrix} b \\ a \end{bmatrix} = \begin{bmatrix} \cdots \\ -\Delta_0 b - \Delta_1 a \end{bmatrix}$$

Giving a more general form

$$h\begin{bmatrix} a \\ b \end{bmatrix} = \begin{bmatrix} h_0 a + h_1 b \\ h_0 b + h_1 a \end{bmatrix}$$

and likewise for Δ:

$$\Delta\begin{bmatrix} a \\ b \end{bmatrix} = \begin{bmatrix} \Delta_0 a + \Delta_1 b \\ -\Delta_0 b - \Delta_1 a \end{bmatrix}$$

It is clear that only one of these components needs to be kept track of when considering symmetric u and antisymmetric v. Plugging these expressions back into H provides a simpler Hamiltonian to diagonalize.

In the case where disorder is present, the symmetry $\mathcal{I}$ is clearly broken by the inhomogenous terms. Nonetheless, the overlap $\langle\psi|\mathcal{I}\psi\rangle$ is still meaningful: if positive, we can still identify ψ as "symmetric"-like or otherwise. Numerically, it is sometimes helpful to display this diagnostic, e.g. in Fig. 4.7 the sign of the overlap is plotted as the shape of the symbol.

A.9 Currents in BdG Hamiltonian

The continuity equation takes the form

$$\operatorname{div}\mathbf{j} + \frac{d\rho}{dt} = 0$$

The Heisenberg equation of motion allows us to solve for the divergence of the current:

$$\operatorname{div}\mathbf{j} = -\frac{d\rho}{dt} = \frac{1}{i\hbar}[H,\rho]$$

For a quadratic Hamiltonian on the lattice, $\rho_i = c_i^\dagger c_i$ and

$$H = \sum_{ij} h_{ij}c_i^\dagger c_j + \frac{1}{2}\sum_{ij}\Delta_{ij}c_i^\dagger c_j^\dagger + \text{h.c.} = \sum_{ij} h_{ij}c_i^\dagger c_j + \frac{1}{2}\sum_{ij}\Delta_{ij}c_i^\dagger c_j^\dagger - \frac{1}{2}\sum_{ij}\bar{\Delta}_{ij}c_i c_j$$

because $\Delta_{ij} = -\Delta_{ji}$. Therefore,

$$\begin{aligned}
[H,\rho_n] &= \sum_{ij} h_{ij}\left[c_i^\dagger c_j, \rho_n\right] + \frac{1}{2}\sum_{ij}\Delta_{ij}\left[c_i^\dagger c_j^\dagger, \rho_n\right] - \frac{1}{2}\sum_{ij}\bar{\Delta}_{ij}\left[c_i c_j, \rho_n\right] \\
&= \sum_{ij} h_{ij}\left(\delta_{jn} - \delta_{in}\right)c_i^\dagger c_j - \frac{1}{2}\sum_{ij}\Delta_{ij}\left(\delta_{jn} + \delta_{in}\right)c_i^\dagger c_j^\dagger - \frac{1}{2}\sum_{ij}\bar{\Delta}_{ij}\left(\delta_{ni} + \delta_{jn}\right)c_i c_j \\
&= \sum_{i} h_{in}c_i^\dagger c_n - \sum_{j} h_{nj}c_n^\dagger c_j - \frac{1}{2}\left(\sum_i \Delta_{in}c_i^\dagger c_n^\dagger + \sum_j \Delta_{nj}c_n^\dagger c_j^\dagger + \sum_j \bar{\Delta}_{nj}c_n c_j + \sum_i \bar{\Delta}_{in}c_i c_n\right) \\
&= \sum_i \left(h_{in}c_i^\dagger c_n - \bar{h}_{in}c_n^\dagger c_i\right) - \frac{1}{2}\sum_i \left(\Delta_{in}c_i^\dagger c_n^\dagger - \Delta_{in}c_n^\dagger c_i^\dagger - \bar{\Delta}_{in}c_n c_i + \bar{\Delta}_{in}c_i c_n\right) \\
&= \sum_i \left(h_{in}c_i^\dagger c_n - \bar{h}_{in}c_n^\dagger c_i\right) - \sum_i \left(\Delta_{in}c_i^\dagger c_n^\dagger - \bar{\Delta}_{in}c_n c_i\right)
\end{aligned}$$

The expectation value of this operator in a state ψ is therefore

$$\begin{aligned}\langle[H,\rho_n]\rangle_\psi &= \sum_i \left(h_{in} \left\langle c_i^\dagger c_n \right\rangle_\psi - \bar{h}_{in} \left\langle c_n^\dagger c_i \right\rangle_\psi \right) - \sum_i \left(\Delta_{in} \left\langle c_i^\dagger c_n^\dagger \right\rangle_\psi - \bar{\Delta}_{in} \left\langle c_n c_i \right\rangle_\psi \right) \\ &= \sum_i \left(h_{in} \left\langle c_i^\dagger c_n \right\rangle_\psi - \overline{h_{in} \left\langle c_i^\dagger c_n \right\rangle_\psi} \right) - \sum_i \left(\Delta_{in} \left\langle c_i^\dagger c_n^\dagger \right\rangle_\psi - \overline{\Delta_{in} \left\langle c_i c_n \right\rangle_\psi} \right) \\ &= 2i \left[\sum_i \Im \left(h_{in} \left\langle c_i^\dagger c_n \right\rangle_\psi \right) - \sum_i \Im \left(\Delta_{in} \left\langle c_i^\dagger c_n^\dagger \right\rangle_\psi \right) \right]\end{aligned}$$

Therefore,

$$\operatorname{div} \mathbf{j}(n) = \frac{2}{\hbar} \left[\sum_i \Im \left(h_{in} \left\langle c_i^\dagger c_n \right\rangle_\psi \right) - \sum_i \Im \left(\Delta_{in} \left\langle c_i^\dagger c_n^\dagger \right\rangle_\psi \right) \right] \tag{A.24}$$

If we define the "normal" current from site n to site i by

$$\mathbf{j}(n \to i)_{\text{normal}} = \frac{2}{\hbar} \Im \left(h_{in} \left\langle c_i^\dagger c_n \right\rangle_\psi \right)$$

then the divergence of this current (defined simply as the sum over all outgoing sites i) matches the first term in Eqn. A.24. The $c^\dagger c^\dagger$ and cc terms give rise to another source (and sink) of particles, with the second term of Eqn. A.24. This term can be interpreted as the pair *breaking* rate, since it results in a reduction of the divergence, or an increase of the probability of finding a particle at site n. The field

$$P_{\text{pair breaking}}(i,j) = P_{\text{pair breaking}}(j,i) = \Im \left(\Delta_{ij} \left\langle c_i^\dagger c_j^\dagger \right\rangle_\psi \right)$$

captures the rate of breaking of pairs in the superfluid condensate, leaving unpaired particles at lattice sites i and j.

$$\operatorname{div} \mathbf{j}(n) = \operatorname{div} \mathbf{j}(n \to i)_{\text{normal}} + \sum_i P_{\text{pair breaking}}(i,n)$$

In the next section, the "pair breaking" current is shown to vanish.

Conservation

Assume the Δ_{ij} terms arise from a mean field theory with self-consistent equations

$$\Delta_{ij} = \sum_{kl} V_{ijkl} \left\langle c_k c_l \right\rangle$$

Moreover, assume that these are due to density-density interactions, so that $V_{ijkl} = \delta_{ik}\delta_{jl}g_{ij}$ with $g_{ij} = g_{ji}$ real, so that

$$\Delta_{ij} = g_{ij} \langle c_i c_j \rangle$$

Notice that the original terms are of the form $g_{ij}c_i^\dagger c_j^\dagger c_i c_j$ and will never generate a two-particle current. The self-consistent approximation actually maintains that property in the mean-field theory:

$$\Delta_{ij} \left\langle c_i^\dagger c_j^\dagger \right\rangle = g_{ij} \langle c_i c_j \rangle \left\langle c_i^\dagger c_j^\dagger \right\rangle$$

Notice that the above is real. Therefore,

$$P_{\text{pair breaking}}(i,n) = \Im\left(\Delta_{ij} \left\langle c_i^\dagger c_j^\dagger \right\rangle\right) = 0$$

Consider also the fully interacting Hamiltonian:

$$H = \sum_{ij} h_{ij} c_i^\dagger c_j + \sum_{ij} g_{ijkl} c_i^\dagger c_j^\dagger c_k c_l$$

To find the current we will need to calculate

$$\begin{aligned}
\left[\sum_{ijkl} g_{ijkl} c_i^\dagger c_j^\dagger c_k c_l, \rho\right] &= \sum_{ijkl} g_{ijkl} \left[c_i^\dagger c_j^\dagger c_k c_l, \rho\right] = \sum_{ijkl} g_{ijkl}(\delta_{nk} + \delta_{ln} + \delta_{nj} + \delta_{in}) c_i^\dagger c_j^\dagger c_k c_l \\
&= \sum_{ijk} g_{ijkn} c_i^\dagger c_j^\dagger c_k c_n + \sum_{ijl} g_{ijnl} c_i^\dagger c_j^\dagger c_n c_l + \sum_{ikl} g_{inkl} c_i^\dagger c_n^\dagger c_k c_l + \sum_{jkl} g_{njkl} c_n^\dagger c_j^\dagger c_k c_l \\
&= \sum_{ijk} g_{ijkn} c_i^\dagger c_j^\dagger c_k c_n - \sum_{ijk} g_{ijnk} c_i^\dagger c_j^\dagger c_k c_n + \sum_{ikl} g_{inkl} c_i^\dagger c_n^\dagger c_k c_l - \sum_{ikl} g_{nikl} c_i^\dagger c_n^\dagger c_k c_l \\
&= \sum_{ijk} \left[g_{ijkn} - g_{ijnk}\right] c_i^\dagger c_j^\dagger c_k c_n + \sum_{ikl} \left[g_{inkl} - g_{nikl}\right] c_i^\dagger c_n^\dagger c_k c_l
\end{aligned}$$

Using the results from the previous section, we find a divergence due to a "normal" current

$$\mathbf{j}(n \to i)_{\text{normal}} = \frac{2}{\hbar} \Im\left(h_{in} \left\langle c_i^\dagger c_n \right\rangle_\psi\right)$$

as expected.

APPENDIX B

The Ground State of the Ising Model

The Ising model,

$$H = -\sum_{ij} J_{ij} s_i s_j, \tag{B.1}$$

was solved in one dimension by Ising himself in his thesis [Isi24], by Onsager in two dimensions [Ons44], and is well studied in three [RY93] and four dimensions. Above its upper critical dimension of 4, the Ising model's critical behavior is modeled exactly by mean field theory.

For the purposes of the present work, a random field h_i is added, to give the random-field Ising model Hamiltonian

$$H = -\sum_{ij} J_{ij} s_i s_j - \sum_{i} h_i s_i. \tag{B.2}$$

The purpose of this section is to describe the technique to identify the ground state of this classical Hamiltonian. The technique employed was introduced by Picard and Ratliff [PR75], and restates the Ising problem in terms of the *minimal cut* through a network flow model. Via a theorem (the "maximum-flow minimum-cut" theorem) due to Ford and Fulkerson [FF56], this minimum cut is equivalent to the maximal flow through the same network. The complete chain of logic will be reproduced here for completeness.

B.1 Brief Introduction to Network Flows

Consider a directed, weighted graph. The vertices of the graph are precisely the set V, and the adjacency matrix $c_{v,v'}$ (for all $v, v' \in V$) is nonnegative and referred to as the "capacity;" $c_{v,v'} = 0$ indicates there is no edge connecting vertices v to v'. An interpretation for the the weight $c_{v,v'} > 0$ will be provided momentarily. Two subsets of vertices, the sources $S \subset V$, and sink, $T \subset V$, are also given. For simplicity, we assume that $c_{v,v'} = 0$ if $v' \in S$ or $v \in T$.

First, we introduce the notion of a "flow," a function $f : V \times V \to \mathbb{R}$—and should be informally visualized as representing the amount of some fictional "fluid" being transported between vertices along the edges. The quantity

$$F(v) = \overbrace{\sum_{v' \in V} f_{v,v'}}^{\text{outflow from vertex } v} - \overbrace{\sum_{v' \in V} f_{v',v}}^{\text{inflow to vertex } v} = \sum_{v' \in V} [f_{v,v'} - f_{v',v}] \tag{B.3}$$

is called the the net flow from a vertex. A flow must satisfy two conditions:

1. $0 \leq f_{v,v'} \leq c_{v,v'}$, where $v, v' \in V$—interpreted as the flow along the edge v, v' is limited by the "capacity" of that edge.

2. For all $v \in V - (S \cup T)$, $F(v) = 0$. The condition is visualized as constraining the flow to conserve the "fluid" at all nodes besides the sources and sinks.

The "value" of the flow represents the volume of the fictional fluid passing through the network. It is the total outflow of the sources, or the total inflow to the sinks. These two quantities are the same:

$$\begin{aligned} 0 = \sum_{v,v' \in V} f_{v,v'} - \sum_{v,v' \in V} f_{v',v} = \sum_{v \in V} \left[\sum_{v' \in V} [f_{v,v'} - f_{v',v}] \right] = \sum_{v \in V} F(v) \\ = \sum_{v \in S} F(v) + \sum_{v \in T} F(v) + \sum_{v \in V - (S \cup T)} F(v) \end{aligned} \tag{B.4}$$

Because the last term vanishes, the value of a flow is defined to be the common value

$$\mathrm{val}_f = \sum_{v \in S} F(v) = -\sum_{v \in T} F(v). \tag{B.5}$$

Another concept needed is called a "cut," a partition of the vertices of a network into two sets, V_S and V_T, with $S \subset V_S$ and $T \subset V_T$. The value of the cut is defined as

$$\mathrm{cut}_c(V_S, V_T) = \sum_{v \in V_S} \sum_{v' \in V_T} c_{v,v'} \tag{B.6}$$

and represents the sum of the capacities connecting nodes on either side of the partition of the network. Intuitively, the flow must pass from the source to the sink through any cut, so any cut must bound any flow:

$$\begin{aligned} \mathrm{val}_f = \frac{1}{2}\left[\sum_{v \in S} F(v) - \sum_{v \in T} F(v)\right] &= \frac{1}{2}\left[\sum_{v \in V_S} F(v) - \sum_{v \in V_T} F(v)\right] \\ &= \frac{1}{2}\left[\sum_{v \in V_S} \sum_{v' \in V} [f_{v,v'} - f_{v',v}] - \sum_{v \in V_T} \sum_{v' \in V} [f_{v,v'} - f_{v',v}]\right] \\ &= \frac{1}{2}\left[\sum_{v \in V_S} \sum_{v' \in V} - \sum_{v \in V_T} \sum_{v' \in V}\right] [f_{v,v'} - f_{v',v}] \end{aligned} \tag{B.7}$$

The reader is implored to indulge this non-standard summation notation. Notwithstanding,

$$\begin{aligned} \mathrm{val}_f = \frac{1}{2}\left[\sum_{v \in V_S} \sum_{v' \in V_S} + \sum_{v \in V_S} \sum_{v' \in V_T} - \sum_{v \in V_T} \sum_{v' \in V_S} - \sum_{v \in V_T} \sum_{v' \in V_T}\right] [f_{v,v'} - f_{v',v}] \\ = \sum_{v \in V_S, v' \in V_T} [f_{v,v'} - f_{v',v}] \leq \sum_{v \in V_S, v' \in V_T} f_{v,v'} \leq \mathrm{cut}_c(V_S, V_T) \end{aligned} \tag{B.8}$$

Indeed, the intuition is born out by this direct evaluation—and moreover it is clear that the *minimum* among cuts must be a bound on the *maximum* flow. A natural question is then, "is it always possible to saturate this bound?" Indeed, it can—and this is known as the maximum-flow minimum-cut theorem.

A sketch of an argument is provided. Let a maximal flow f be given, and consider the "residual" network flow model with the same vertices, source, and

sink, and with capacities

$$c'_{v,v'} = c_{v,v'} - f_{v,v'} \tag{B.9}$$

The maximum flow through this residual graph must be 0, and moreover, by simplying summing over the edges in a cut

$$\mathrm{cut}_{c'}(V_S, V_T) = \mathrm{cut}_c(V_S, V_T) - \mathrm{val}_f \tag{B.10}$$

Notice that, by this remark, we need only find a cut with value 0. However, if there is at least one path from S to T in the residual graph, a flow exists on the residual graph, so there must be no such path. But that means that S and T are not connected in the residual graph. Therefore, we must have a partition of the graph into $V_S \supset S$ and $V_T \supset T$, with no edges connecting the partitions. That partition is therefore a cut with value 0, and we have the claim.

This technique leads naturally to the Ford-Fulkerson algorithm [FF56]: find a path from the source to the sink, and saturate it, by increasing the flows along each leg. Repeat using the residual graph, until no such path exists. This technique has the unfortunate feature of not terminating for all graphs. However, in the special case that all capacities are rational numbers, all capacities can be made integers by multiplying by a large enough integer. Then, each step of saturating a particular path from source to sink reduces the value $\sum_{v,v' \in V} c_{v,v'}$ by 1. The algorithm must therefore terminate. Most numerical implementations on computers are only capable of representing rational numbers, so this non-termination issue is not a direct problem.

These features of network flow theory are sufficient background for the remainder of this section.

B.2 From Ising Model to Network Flow

Originally presented by Picard and Ratliff [PR75], the disordered Ising Hamiltonian

$$H = -\sum_{ij} J_{ij} s_i s_j - \sum_i h_i s_i \tag{B.11}$$

can be restated in terms of a minimal cut, provided that $J_{ji} = J_{ij} \geq 0$. First, consider a graph with vertices given by each lattice site, and an additional source s and sink t vertices. The underlying idea is to have a spin configuration correspond to a cut of the network. The capacities are chosen so that the value of a cut is (up to a constant) the energy of that configuration. Put

$$c_{i,j} = 4J_{ij} \tag{B.12}$$

As a convention, if a vertex is on the source side of the cut, say it is up. Therefore,

$$c_{s,i} = \begin{cases} 2h_i, & h_i \geq 0 \\ 0, & h_i < 0 \end{cases} \tag{B.13}$$

and

$$c_{i,t} = \begin{cases} -2h_i, & h_i \leq 0 \\ 0, & h_i > 0 \end{cases} \tag{B.14}$$

The value of a cut (U, D) is then

$$\text{cut}_c(V_S, V_T) = \sum_{i \in U, j \in D} 4J_{ij} - \sum_{i \in U, h_i < 0} 2h_i + \sum_{i \in D, h_i > 0} 2h_i \tag{B.15}$$

If we add $-\sum_{ij} J_{ij}$ to the portion resembling the spin-spin interaction,

$$\begin{aligned} &\sum_{i \in U, j \in D} 4J_{ij} - \sum_{ij} J_{ij} \\ &\qquad = \sum_{i \in U, j \in D} 3J_{ij} - \sum_{i \in D, j \in U} J_{ij} - \sum_{i \in U, j \in U} J_{ij} - \sum_{i \in D, j \in D} J_{ij} \\ &\qquad = -\sum_{ij} J_{ij} \sigma_i \sigma_j \end{aligned} \tag{B.16}$$

Similarly, if we add $-\sum_i |h_i|$ to the portion resembling the field interaction

$$
\begin{aligned}
-\sum_{i\in U,h_i<0} 2h_i + \sum_{i\in D,h_i>0} 2h_i + \sum_{h_i<0} h_i - \sum_{h_i>0} h_i = \\
-\sum_{i\in U,h_i<0} 2h_i + \sum_{i\in U,h_i<0} h_i - \sum_{i\in U,h_i>0} h_i + \sum_{i\in D,h_i>0} 2h_i + \sum_{i\in D,h_i<0} h_i - \sum_{i\in D,h_i>0} h_i \\
= -\sum_{i\in U} h_i + \sum_{i\in D} h_i = -\sum_i \sigma_i h_i \quad \text{(B.17)}
\end{aligned}
$$

I.e.,

$$H = \mathrm{cut}_c(V_S, V_T) - \sum_{ij} J_{ij} - \sum_i |h_i| \quad \text{(B.18)}$$

The exact form of the adjacency matrix can be adjusted slightly [HR02] to improve the performance of the maximum-flow algorithm, but is not particularly interesting from a physics perspective.

References

[ACS14] Andrea Allais, Debanjan Chowdhury, and Subir Sachdev. "Connecting high-field quantum oscillations to zero-field electron spectral functions in the underdoped cuprates." *Nat Commun*, **5**:5771, 2014.

[Ali10] Jason Alicea. "Majorana fermions in a tunable semiconductor device." *Phys. Rev. B*, **81**:125318, Mar 2010.

[Ali12] Jason Alicea. "New directions in the pursuit of Majorana fermions in solid state systems." *Reports on Progress in Physics*, **75**(7):076501, Jul 2012.

[AOR11] Jason Alicea, Yuval Oreg, Gil Refael, Felix von Oppen, and Matthew P. A. Fisher. "Non-Abelian statistics and topological quantum information processing in 1D wire networks." *Nature Physics*, **7**(5):412–417, Feb 2011.

[ASM12] A. J. Achkar, R. Sutarto, X. Mao, F. He, A. Frano, S. Blanco-Canosa, M. Le Tacon, G. Ghiringhelli, L. Braicovich, M. Minola, M. Moretti Sala, C. Mazzoli, Ruixing Liang, D. A. Bonn, W. N. Hardy, B. Keimer, G. A. Sawatzky, and D. G. Hawthorn. "Distinct Charge Orders in the Planes and Chains of Ortho-III-Ordered YBa_{2}Cu_{3}O_{6+δ} Superconductors Identified by Resonant Elastic X-ray Scattering." *Phys. Rev. Lett.*, **109**(16):167001, Oct 2012.

[ASW14] Elihu Abrahams, Jörg Schmalian, and Peter Wölfle. "Strong-coupling theory of heavy-fermion criticality." *Phys. Rev. B*, **90**:045105, 2014.

[AZ97] Alexander Altland and Martin R. Zirnbauer. "Nonstandard symmetry classes in mesoscopic normal-superconducting hybrid structures." *Phys. Rev. B*, **55**:1142–1161, Jan 1997.

[BCS57] J. Bardeen, L. N. Cooper, and J. R. Schrieffer. "Theory of Superconductivity." *Phys. Rev.*, **108**(5):1175–1204, Dec 1957.

[Ber84] M. V. Berry. "Quantal Phase Factors Accompanying Adiabatic Changes." *Proceedings of the Royal Society A: Mathematical, Physical and Engineering Sciences*, **392**(1802):45–57, Mar 1984.

[Bin83] K. Binder. "Random-field induced interface widths in Ising systems." *Zeitschrift für Physik B Condensed Matter*, **50**(4):343–352, 1983.

[BMH05] Per G. Björnsson, Yoshiteru Maeno, Martin E. Huber, and Kathryn A. Moler. "Scanning magnetic imaging of Sr 2 Ru O 4." *Phys. Rev. B*, **72**(1), Jul 2005.

[Bog58] N. N. Bogoliubov. *Nuovo Cimento*, **7**:794, 1958.

[CBH12] J. Chang, E. Blackburn, A. T. Holmes, N. B. Christensen, J. Larsen, J. Mesot, Ruixing Liang, D. A. Bonn, W. N. Hardy, A. Watenphul, M. v. Zimmermann, E. M. Forgan, and S. M. Hayden. "Direct observation of competition between superconductivity and charge density wave order in YBa2Cu3O6.67." *Nature Physics*, **8**(12):871–876, Oct 2012.

[CGM64] C. Caroli, P.G. De Gennes, and J. Matricon. "Bound Fermion states on a vortex line in a type II superconductor." *Physics Letters*, **9**(4):307 – 309, 1964.

[Cha08] S. Chakravarty. "Physics - From complexity to simplicity." *Science*, **319**:735–736, 2008.

[CK08] Sudip Chakravarty and Hae-Young Kee. "Fermi pockets and quantum oscillations of the Hall coefficient in high-temperature superconductors." *Proc. Natl. Acad. Sci. USA*, **105**:8835–8839, 2008.

[CLG09] Meng Cheng, Roman Lutchyn, Victor Galitski, and S. Das Sarma. "Splitting of Majorana-Fermion Modes due to Intervortex Tunneling in a px+ipy Superconductor." *Physical Review Letters*, **103**:107001, Aug 2009.

[DBC15] N. Doiron-Leyraud, S. Badoux, S. René de Cotret, S. Lepault, D. LeBoeuf, F. Laliberté, E. Hassinger, B. J. Ramshaw, D. A. Bonn, W. N. Hardy, R. Liang, J.-H.. Park, D. Vignolles, B. Vignolle, L. Taillefer, and C. Proust. "Evidence for a small hole pocket in the Fermi surface of underdoped YBa2Cu3Oy." *Nature Communications*, **6**:6034, Jan 2015.

[DGJ08] Ivailo Dimov, Pallab Goswami, Xun Jia, and Sudip Chakravarty. "Competing order, Fermi surface reconstruction, and quantum oscillations in underdoped high-temperature superconductors." *Phys. Rev. B*, **78**(13):134529, Oct 2008.

[DPL07] Nicolas Doiron-Leyraud, Cyril Proust, David LeBoeuf, Julien Levallois, Jean-Baptiste Bonnemaison, Ruixing Liang, D. A. Bonn, W. N. Hardy, and Louis Taillefer. "Quantum oscillations and the Fermi surface in an underdoped high-Tc superconductor." *Nature*, **447**(7144):565–568, May 2007.

[DSV11] Wade DeGottardi, Diptiman Sen, and Smitha Vishveshwara. "Topological phases, Majorana modes and quench dynamics in a spin ladder system." *New Journal of Physics*, **13**(6):065028, Jun 2011.

[EWC12] Jonghyoun Eun, Zhiqiang Wang, and Sudip Chakravarty. "Quantum oscillations in $YBa_2Cu_3O_{6+\delta}$ from period-8 d-density wave order." *Proc. Natl. Acad. Sci. USA*, **109**:13198–13203, 2012.

[FF56] L. R. Ford and D. R. Fulkerson. "Maximal flow through a network." *Canad. J. Math.*, **8**(0):399–404, Jan 1956.

[FK08] Liang Fu and C. L. Kane. "Superconducting Proximity Effect and Majorana Fermions at the Surface of a Topological Insulator." *Phys. Rev. Lett.*, **100**:096407, Mar 2008.

[GJN15] S. Gerber, H. Jang, H. Nojiri, S. Matsuzawa, H. Yasumura, D. A. Bonn, R. Liang, W. N. Hardy, Z. Islam, A. Mehta, S. Song, M. Sikorski, D. Stefanescu, Y. Feng, S. A. Kivelson, T. P. Devereaux, Z.-X. Shen, C.-C. Kao, W.-S. Lee, D. Zhu, and J.-S. Lee. "Three-dimensional charge density wave order in YBa2Cu3O6.67 at high magnetic fields." *Science*, Nov 2015.

[GK77] V. L Ginzburg and D. A Kirzhnits, editors. *High-Temperature Superconductivity.* Consultants Bureau, 1977.

[GLD15] G. Grissonnanche, F. Laliberte, S. Dufour-Beausejour, A. Riopel, S. Badoux, M. Caouette-Mansour, M. Matusiak, A. Juneau-Fecteau, P. Bourgeois-Hope, O. Cyr-Choiniere, J. C. Baglo, B. J. Ramshaw, R. Liang, D. A. Bonn, W. N. Hardy, S. Kramer, D. LeBoeuf, D. Graf, N. Doiron-Leyraud, and Louis Taillefer. "Onset field for Fermi-surface reconstruction in the cuprate superconductor YBCO." *arXiv*, **1508.05486**, Aug 2015.

[GLM12] G. Ghiringhelli, M. Le Tacon, M. Minola, S. Blanco-Canosa, C. Mazzoli, N. B. Brookes, G. M. De Luca, A. Frano, D. G. Hawthorn, F. He, T. Loew, M. M. Sala, D. C. Peets, M. Salluzzo, E. Schierle, R. Sutarto, G. A. Sawatzky, E. Weschke, B. Keimer, and L. Braicovich. "Long-Range Incommensurate Charge Fluctuations in (Y,Nd)Ba2Cu3O6+x." *Science*, **337**(6096):821–825, Jul 2012.

[HK10] M. Z. Hasan and C. L. Kane. "*Colloquium* : Topological insulators." *Rev. Mod. Phys.*, **82**:3045–3067, Nov 2010.

[HMV14] Changtao Hou, D. E. MacLaughlin, and C. M. Varma. "Zeeman modulated spin echo in orthorhombic symmetry." *Phys. Rev. B*, **89**(23):235108, Jun 2014.

[Hof02] J. E. Hoffman. "A Four Unit Cell Periodic Pattern of Quasi-Particle States Surrounding Vortex Cores in Bi2Sr2CaCu2O8+delta." *Science*, **295**(5554):466–469, Jan 2002.

[HR02] Alexander K. Hartmann and Heiko Rieger. *Optimization Algorithms in Physics*. Wiley-VCH, 2002.

[Isi24] Ernst Ising. *Beitrag zur Theorie des Ferro- und Paramagnetismus*. PhD thesis, Hamburg, 1924.

[Iva01] D. A. Ivanov. "Non-Abelian Statistics of Half-Quantum Vortices in p-Wave Superconductors." *Phys. Rev. Lett.*, **86**:268–271, Jan 2001.

[JVA08] Cyril Jaudet, David Vignolles, Alain Audouard, Julien Levallois, D. LeBoeuf, Nicolas Doiron-Leyraud, B. Vignolle, M. Nardone, A. Zitouni, Ruixing Liang, D. A. Bonn, W. N. Hardy, Louis Taillefer, and Cyril Proust. "de Haas–van Alphen Oscillations in the Underdoped High-Temperature Superconductor YBa 2 Cu 3 O 6.5." *Phys. Rev. Lett.*, **100**(18):187005, May 2008.

[Kit01] A Yu Kitaev. "Unpaired Majorana fermions in quantum wires." *Physics-Uspekhi*, **44**(10S):131, 2001.

[KS91] N. B. Kopnin and M. M. Salomaa. "Mutual friction in superfluid ^{3}He: Effects of bound states in the vortex core." *Phys. Rev. B*, **44**:9667–9677, Nov 1991.

[KTF07] Y. Kohsaka, C. Taylor, K. Fujita, A. Schmidt, C. Lupien, T. Hanaguri, M. Azuma, M. Takano, H. Eisaki, H. Takagi, S. Uchida, and J. C. Davis. "An Intrinsic Bond-Centered Electronic Glass with Unidirectional Domains in Underdoped Cuprates." *Science*, **315**(5817):1380–1385, Mar 2007.

[Lau14] R. B. Laughlin. "Hartree-Fock computation of the high-T_c cuprate phase diagram." *Phys. Rev. B*, **89**:035134, 2014.

[LDL07] David LeBoeuf, Nicolas Doiron-Leyraud, Julien Levallois, R. Daou, J.-B. Bonnemaison, N. E. Hussey, L. Balicas, B. J. Ramshaw, Ruixing Liang, D. A. Bonn, W. N. Hardy, S. Adachi, Cyril Proust, and Louis Taillefer. "Electron pockets in the Fermi surface of hole-doped high-Tc superconductors." *Nature*, **450**(7169):533–536, Nov 2007.

[Leg75] Anthony J. Leggett. "A theoretical description of the new phases of liquid ^{3}He." *Rev. Mod. Phys.*, **47**:331–414, Apr 1975.

[LKH12] David LeBoeuf, S. Krämer, W. N. Hardy, Ruixing Liang, D. A. Bonn, and Cyril Proust. "Thermodynamic phase diagram of static charge order in underdoped YBa2Cu3Oy." *Nature Physics*, **9**(2):79–83, Dec 2012.

[LSD10] Roman M. Lutchyn, Jay D. Sau, and S. Das Sarma. "Majorana Fermions and a Topological Phase Transition in Semiconductor-Superconductor Heterostructures." *Phys. Rev. Lett.*, **105**:077001, Aug 2010.

[MDH02] H. A. Mook, Pengcheng Dai, S. M. Hayden, A. Hiess, J. W. Lynn, S. H. Lee, and F. Doğan. "Magnetic order in $YBa_2Cu_3O_{6+x}$ superconductors." *Phys. Rev. B*, **66**(14):144513, 2002.

[MDH04] H. A. Mook, Pengcheng Dai, S. M. Hayden, A. Hiess, S. H. Lee, and F. Doğan. "Polarized neutron measurement of magnetic order in YBa2Cu3O6.45." *Phys. Rev. B*, **69**(13):134509, 2004.

[MF02] A. Alan Middleton and Daniel S. Fisher. "Three-dimensional random-field Ising magnet: Interfaces, scaling, and the nature of states." *Phys. Rev. B*, **65**:134411, Mar 2002.

[MHR14] Akash V. Maharaj, Pavan Hosur, and S. Raghu. "Crisscrossed stripe order from interlayer tunneling in hole-doped cuprates." *Phys. Rev. B*, **90**:125108, 2014.

[MM10] T. Mizushima and K. Machida. "Splitting and oscillation of Majorana zero modes in the p-wave BCS-BEC evolution with plural vortices." *Phys. Rev. A*, **82**:023624, Aug 2010.

[MR91] Gregory Moore and Nicholas Read. "Nonabelions in the fractional quantum hall effect." *Nuclear Physics B*, **360**(2-3):362–396, Aug 1991.

[MT06] Ashot Melikyan and Zlatko Tešanović. "Mixed state of a lattice d-wave superconductor." *Phys. Rev. B*, **74**(14):144501, Oct 2006.

[MZF12] V. Mourik, K. Zuo, S. M. Frolov, S. R. Plissard, E. P. A. M. Bakkers, and L. P. Kouwenhoven. "Signatures of Majorana Fermions in Hybrid Superconductor-Semiconductor Nanowire Devices." *Science*, **336**(6084):1003–1007, 2012.

[Nak03] M. Nakahara. *Geometry, Topology and Physics.* 2003. Bristol, UK: Hilger (1990) 505 p. (Graduate student series in physics).

[Nay00] Chetan Nayak. "Density-wave states of nonzero angular momentum." *Phys. Rev. B*, **62**:4880–4889, Aug 2000.

[NCH12] Yuezhen Niu, Suk Bum Chung, Chen-Hsuan Hsu, Ipsita Mandal, S. Raghu, and Sudip Chakravarty. "Majorana zero modes in a quantum Ising chain with longer-ranged interactions." *Phys. Rev. B*, **85**:035110, Jan 2012.

[NTK14] L. Nie, G. Tarjus, and S. A. Kivelson. "Quenched disorder and vestigial nematicity in the pseudogap regime of the cuprates." *Proc. Natl. Acad. Sci. USA*, **111**(22):7980–7985, May 2014.

[Ons44] Lars Onsager. "Crystal Statistics. I. A Two-Dimensional Model with an Order-Disorder Transition." *Phys. Rev.*, **65**:117–149, Feb 1944.

[PR75] J. C. Picard and H. D. Ratliff. "Minimum cuts and related problems." *Networks*, **5**(4):357–370, Oct 1975.

[RG00] N. Read and Dmitry Green. "Paired states of fermions in two dimensions with breaking of parity and time-reversal symmetries and the fractional quantum Hall effect." *Phys. Rev. B*, **61**:10267–10297, Apr 2000.

[Roy10] Rahul Roy. "Topological Majorana and Dirac Zero Modes in Superconducting Vortex Cores." *Phys. Rev. Lett.*, **105**:186401, Oct 2010.

[RY93] H. Rieger and A. P. Young. "Critical exponents of the three-dimensional random field Ising model." *J. Phys. A: Math. Gen.*, **26**:5279–5284, May 1993.

[Sac11] Subir Sachdev. *Quantum Phase Transitions*. Cambridge University Press, 2011.

[SC09] David Schwab and Sudip Chakravarty. "Glassy states in fermionic systems with strong disorder and interactions." *Phys. Rev. B*, **79**:125102, 2009.

[SGM11] S. Strässle, B. Graneli, M. Mali, J. Roos, and H. Keller. "Absence of Orbital Currents in Superconducting $YBa_2Cu_4O_8$ Using a Zeeman-Perturbed Nuclear-Quadrupole-Resonance Technique." *Phys. Rev. Lett.*, **106**:097003, 2011.

[SHB14] Suchitra E. Sebastian, N. Harrison, F. F. Balakirev, M. M. Altarawneh, P. A. Goddard, Ruixing Liang, D. A. Bonn, W. N. Hardy, and G. G. Lonzarich. "Normal-state nodal electronic structure in underdoped high-T_c copper oxides." *Nature*, **511**:61–64, 2014.

[SLT10] Jay D. Sau, Roman M. Lutchyn, Sumanta Tewari, and S. Das Sarma. "Generic New Platform for Topological Quantum Computation Using Semiconductor Heterostructures." *Phys. Rev. Lett.*, **104**:040502, Jan 2010.

[STL10] Jay D. Sau, Sumanta Tewari, Roman M. Lutchyn, Tudor D. Stanescu, and S. Das Sarma. "Non-Abelian quantum order in spin-orbit-coupled semiconductors: Search for topological Majorana particles in solid-state systems." *Phys. Rev. B*, **82**:214509, Dec 2010.

[THZ15] B. S. Tan, N. Harrison, Z. Zhu, F. Balakirev, B. J. Ramshaw, A. Srivastava, S. A. Sabok, B. Dabrowski, G. G. Lonzarich, and Suchitra E. Sebastian. "Fragile charge order in the nonsuperconducting ground state of the underdoped high-temperature superconductors." *Proc. Natl. Acad. Sci. USA*, **112**(31):9568–9572, Jul 2015.

[Tin96] Michael Tinkham. *Introduction to Superconductivity.* McGraw-Hill, 1996.

[TKN82] D. J. Thouless, M. Kohmoto, M. P. Nightingale, and M. den Nijs. "Quantized Hall Conductance in a Two-Dimensional Periodic Potential." *Phys. Rev. Lett.*, **49**:405–408, Aug 1982.

[TLT14] W. Tabis, Y. Li, M. Le Tacon, L. Braicovich, A. Kreyssig, M. Minola, G. Dellea, E. Weschke, M. J. Veit, M. Ramazanoglu, A. I. Goldman, T. Schmitt, G. Ghiringhelli, N. Barišić, M. K. Chan, C. J. Dorow, G. Yu, X. Zhao, B. Keimer, and M. Greven. "Charge order and its connection with Fermi-liquid charge transport in a pristine high-Tc cuprate." *Nature Communications*, **5**:5875, Dec 2014.

[TNO15] Yasuhiro Tada, Wenxing Nie, and Masaki Oshikawa. "Orbital Angular Momentum and Spectral Flow in Two-Dimensional Chiral Superfluids." *Phys. Rev. Lett.*, **114**(19), May 2015.

[Val58] J. Valatin. **7**:843, 1958.

[VM06] Oskar Vafek and Ashot Melikyan. "Index Theoretic Characterization of d-Wave Superconductors in the Vortex State." *Physical Review Letters*, **96**(16):167005, Apr 2006.

[Vol99] G.E. Volovik. "Fermion zero modes on vortices in chiral superconductors." *Journal of Experimental and Theoretical Physics Letters*, **70**(9):609–614, 1999.

[Wil09] Frank Wilczek. "Majorana returns." *Nat Phys*, **5**(9):614–618, Sep 2009.

[WMK11] Tao Wu, Hadrien Mayaffre, Steffen Krämer, Mladen Horvatić, Claude Berthier, W. N. Hardy, Ruixing Liang, D. A. Bonn, and Marc-Henri Julien. "Magnetic-field-induced charge-stripe order in the high-temperature superconductor YBa2Cu3Oy." *Nature*, **477**(7363):191–194, Sep 2011.

[You98] A. P. Young, editor. *Spin Glasses and Random Fields.* World Scientific, Singapore, 1998.

[ZMK15] Yi Zhang, Akash V. Maharaj, and Steven Kivelson. "Disruption of quantum oscillations by an incommensurate charge density wave." *Phys. Rev. B*, **91**(8):085105, Feb 2015.